FINAL REPORT

VEHICLE-SCALE INVESTIGATION OF A FLUORINE JET-PUMP LIQUID HYDROGEN TANK PRESSURIZATION SYSTEM

by

E. C. CADY AND D. W. KENDLE

MCDONNELL DOUGLAS ASTRONAUTICS COMPANY
HUNTINGTON BEACH, CALIFORNIA

PREPARED FOR
NATIONAL AERONAUTICS AND SPACE ADMINISTRATION
28 FEBRUARY 1972
CONTRACT NAS3-14381

NASA Lewis Research Center
Cleveland, Ohio
Erwin A. Edelman, Project Manager
CHEMICAL AND NUCLEAR ROCKET PROCUREMENT SECTION

PREFACE

This report was prepared by McDonnell Douglas Astronautics Company under Contract NAS3-14381. The contract is administered by the National Aeronautics and Space Administration, Lewis Research Center, Chemical and Nuclear Rocket Procurement Section, Cleveland, Ohio. The NASA Project Manager for the contract is Mr. Erwin A. Edelman. This is the final report on the contract, and it summarizes the technical effort from 1 July 1971 to 31 January 1972.

ABSTRACT

A comprehensive analytical and experimental program was performed to evaluate the performance of a unique fluorine-hydrogen jet-pump injector for main tank injection (MTI) pressurization of a liquid hydrogen (LH_2) tank. The injector performance during pressurization and LH_2 expulsion was determined by a series of seven tests of a full-scale injector and MTI pressure control system in a $28.3m^3$ ($1,000$ ft^3) flight-weight LH_2 tank. Although the injector did not effectively jet-pump LH_2 continuously, it showed improved pressurization performance compared to straight-pipe injectors tested under the same conditions in a previous program. The MTI computer code was modified to allow performance prediction for the jet-pump injector.

SUMMARY

A comprehensive analytical and experimental program was performed to evaluate the performance of a unique two-stage supersonic jet-pump injector, developed by North American Rockwell-Rocketdyne (NAR) for main tank injection (MTI) pressurization of large-scale liquid hydrogen (LH_2) tanks. The injector first stage uses the injectant gaseous fluorine (GF_2) to pump sufficient hydrogen (design O/F ratio of 800:1) to heat the GF_2 prior to entering the second stage. In the second stage, the heated GF_2 is expanded through a supersonic nozzle to a low pressure which is used to pump LH_2 from the tank into a downstream combustion zone at a design O/F ratio of 1.8:1. The resultant hot hydrogen at 1555 °K (2800 °R) is used to pressurize the LH_2 tank. The injector was tested in a 28.3-m^3 (1,000-ft^3) flight-weight LH_2 tank used in a previous program under Contract NAS3-13306 to evaluate straight-pipe and diffuser-type MTI injectors. Seven tests were performed at varied LH_2 outflow rates and with ullage volumes from 3 m^3 (106 ft^3) to 26.9 m^3 (950 ft^3). Prepressurization, constant-pressure hold, and LH_2 expulsion at controlled tank pressures of 30 x 10^4 N/m^2 (43 psia) and 18 x 10^4 N/m^2 (26 psia) were demonstrated. The injector second stage LH_2 pumping annulus was damaged by overheating caused by its inability to pump LH_2 with large initial ullages and with cyclic operation. Nevertheless, the injector demonstrated improved pressurization performance (less GH_2 usage and lower ullage temperature) compared to straight-pipe injectors tested previously. Analytical correlation of the data indicated that the performance gain was due to first stage GF_2 heating and second stage GH_2 pumping which gave greater injectant jet penetration and ullage mixing. Modifications were made to the MTI computer code to allow jet-pump injector performance prediction.

CONTENTS

FIGURES

TABLES

SYMBOLS

a	Acceleration
A	Area
C_p	Specific heat at constant pressure
C	Constant
d	Jet exit diameter, characteristic dimension
f	Injector on-time fraction
f_m	Ullage mixing fraction
h	Heat transfer coefficient
K	Thermal conductivity
$\dot{m}$	Mass flowrate
P	Pressure
$\dot{q}$	Heat flux
R	Universal gas constant
t	Time
T	Temperature
U	Velocity
V	Observed forced-convection velocity
W	Molecular weight
X	Distance on the vertical axis
Δ	Increment
ρ	Density
μ	Viscosity

Subscripts

b	Buoyancy
c	Combustion
C	Jet velocity core
fo	Forced
F	Flame
F_2	Fluorine

g	Gas
H_2	Hydrogen
HF	Hydrogen fluoride
if	interface
in	injector exit plane
j	Injectant jet flow
L	Liquid
m	Maximum
M	Turbulent mixing
mix	Ullage mixing
p	Jet penetration
r	Reaction
u	Ullage
o	Initial

INTRODUCTION

For space vehicles using cryogenic propellants, particularly those that require multiburn operation, tank pressurization can contribute significantly to the weight, complexity, and cost of the propulsion feed system. A tank pressurization concept called the main tank injection (MTI) technique can reduce the weight and complexity of the system. In the MTI technique, a hypergolic reactant is injected into a propellant tank and the heat released is used to pressurize the tank. This technique has resulted in considerable improvement in performance and cost, especially for advanced hydrogen-fueled upper stages.

From July 1966 through April 1968, McDonnell Douglas Astronautics Company (MDAC) conducted an MTI pressurization research program under NASA Contract NAS3-7963 to determine, analytically and experimentally, the feasibility, limitations, and operating characteristics of small-scale fluorine-hydrogen MTI pressurization (Reference 1). After the system feasibility and characteristics had been established, MDAC conducted a comprehensive program to devise an analytical method to predict MTI performance for liquid hydrogen-fueled space vehicles of any size and to develop and demonstrate a full-scale flight-type MTI pressurization system. This program was conducted from July 1969 through June 1970 under NASA Contract NAS3-13306.

In Task I of this program, a computer code was developed from an analytical technique to predict the performance and behavior of MTI pressurization of a liquid hydrogen (LH_2) tank through ullage injection of gaseous fluorine (GF_2). This code, designated H819, included routines to account for injection jet penetration, ullage mixing, and tank wall and LH_2 interface heat (and mass) transfer using the most

1

advanced one-dimensional nodal techniques. In Task II, a large-scale test apparatus, including MTI injectors, tank pressure control system, and instrumentation, was designed for installation in a 28.3-m^3 ($1,000\text{-ft}^3$) flight-weight Thor tank. In Task III, the MTI injection system was test-fired to assure proper durability and performance and then installed in the 28.3-m^3 ($1,000\text{-ft}^3$) LH_2 tank. A series of 17 tests was performed at ullage volumes from 5 to 90 percent, LH_2 outflow rates from 2.3 to 6.8 kg/sec (5 to 15 lb/sec), and tank pressures of 17×10^4 and 30×10^4 N/m^2 (25 and 43 psia), utilizing both straight-pipe and diffuser-type injectors. Tank prepressurization, constant pressure hold at no outflow, and constant pressure expulsion modes were demonstrated with tank pressure maintained constant to within 0.7×10^4 N/m^2 (1 psia). In Task IV, the data from these tests were analyzed and correlated with the H819 computer code, and empirical factors in the code were determined. The H819 code was then used to predict the performance of an MTI pressurization system designed for an advanced Centaur-type vehicle.

It was found from the MTI tests conducted under Contract NAS3-13306 and reported in Reference 2 that when tank pressurization and expulsion was performed with a nearly full tank (~5-percent ullage), the GF_2 jet penetrated the LH_2 interface and evaporated sufficient LH_2 to keep the ullage temperatures low. As the interface receded during outflow, the LH_2 evaporation ceased and the ullage temperatures rose rapidly. The higher ullage temperatures led to greater tank wall heat transfer losses, thus to increased GF_2 demand and consumption. It appeared that if controlled ullage mass addition were to occur throughout the expulsion, lower temperatures and reduced fluorine usage could be realized.

Concurrent with the NAS3-13306 work by MDAC, North American Rockwell-Rocketdyne (NAR) was conducting a program under NASA Contract NAS3-13328 to develop an MTI injector which uses the GF_2

inflow to jet-pump LH_2 from the tank, vaporizes the LH_2, and delivers a controlled flow of hot H_2 into the ullage, regardless of interface location. The NAR injector was hot-fired for short durations under Contract NAS3-13328 (Reference 3) and performed well enough to justify pressurization testing in the same 28.3-m^3 $(1,000\text{-ft}^3)$ tank used for the MDAC tests under Contract NAS3-13306.

This report describes a program in which the work performed under Contract NAS3-13306 was continued under Contract NAS3-14381. Essentially, the same test apparatus was used to evaluate the performance of the advanced MTI injector developed by NAR under Contract NAS3-13328. The tank pressurization performance of the injector was compared with the straight-pipe injector performance from Contract NAS3-13306, and the MTI computer code (H819) was modified to allow injector performance prediction.

PRESSURIZATION SYSTEM DESIGN

INJECTOR DESIGN

The design details of the NAR injector are described in Reference 3. The overall injector configuration is shown in Figure 1. The injector operates nominally in this way. GF_2 enters the first stage venturi, a converging-diverging nozzle. The low static GF_2 pressure in the venturi throat pulls H_2 from the vicinity of the second stage venturi, vaporizes and heats the H_2 in a heat exchanger, and pumps it through the center tube of the first stage venturi where it combusts with the GF_2 at an O/F ratio of about 800:1. With ambient temperature GF_2 inlet conditions, this O/F ratio results in a GF_2 temperature of about $555°K$ $(1,000°R)$ entering the second stage. This hot GF_2 is again expanded through a converging-diverging nozzle in the second stage venturi to a Mach number of 1.6, which results in a static GF_2 pressure at the second stage exit of about 16 percent of the GF_2 inlet pressure. This low static pressure provides a pressure differential across the annulus at the second stage for pumping LH_2 from the tank into the injector. It is clear that the GF_2 inlet pressure must be controlled so that the second stage static pressure is less than the LH_2 pressure, to provide pumping action. It was found during the Contract NAS3-13328 work that the optimum GF_2 inlet pressure should be 2.25 times the LH_2 pressure (tank pressure).

It was determined from results of the NAS3-13306 MTI tests (Reference 2) that during test No.'s 2, 4, 8, and 10, tank pressure collapse occurred late in the tests because of insufficient GF_2 flow. Analysis of the data indicated that at a tank pressure of 30×10^4 N/m^2 (43 psia), LH_2 outflow rates from 5.2 to 6.7 kg/sec (11.5 to 14.8 lb/sec), and ullage temperatures from $165°K$ to $299°K$ ($298°R$ to $538°R$),

5

MOUNTING
FLANGE

STATIC
PRESSURE
TAP

LH₂
PUMPING
ZONE

TI 2

TI 3

HEAT
EXCHANGER

FIRST STAGE
VENTURI

TI 1

SECOND STAGE
VENTURI

HYDROGEN
INLET AND
TL9

MOUNTED WITHIN TANK

EXTERIOR TO TANK

FLUORINE
INLET
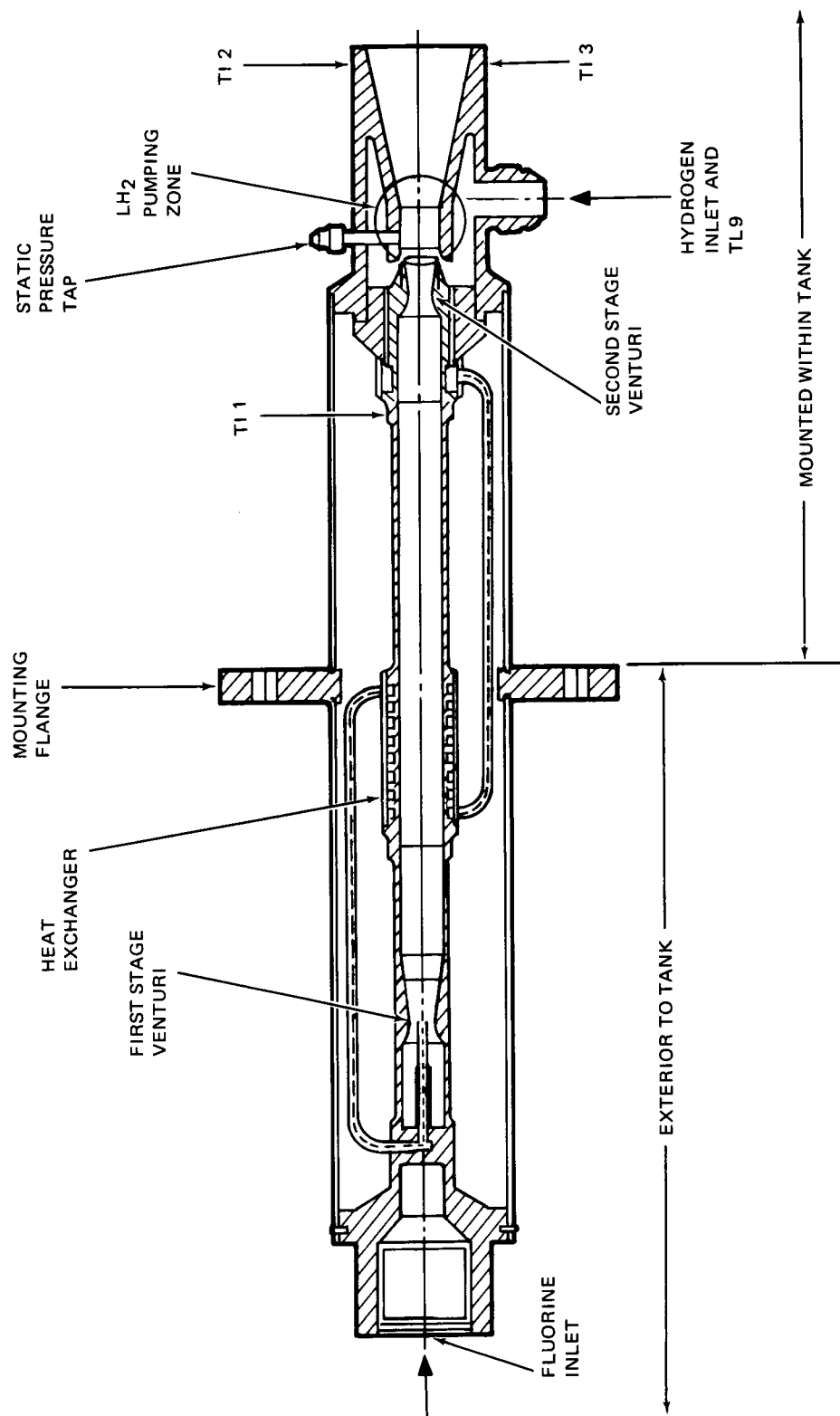
Figure 1. NAR Injector Configuration

a GF_2 flow rate from 0.018 to 0.027 kg/sec (0.04 to 0.06 lb/sec) was required to maintain tank pressure. The flow characteristics of the injector developed under Contract NAS3-13328 are shown in Figure 2. GF_2 inlet pressures in excess of 207×10^4 N/m^2 (300 psia) would be required with this injector to obtain the requisite GF_2 flow rate; therefore, a new scaled-up GF_2 injector was obtained from NAR for testing in the $28.3\text{-}m^3$ ($1,000\text{-}ft^3$) test tank.

The new injector design was established by using scale factors to create a higher flow rate version of the NAS3-13328 injector. The design fluorine flow rate was conservatively set at 0.0317 kg/sec (0.07 lb/sec) at 294°K (530°R), with an inlet pressure of 62×10^4 N/m^2 (90 psia). Flow rate is controlled by the first stage sonic venturi of the injector. An effective throat area of 1.89×10^{-5} m^2 (0.0288 in.^{2}) was determined using a flow coefficient of 0.98. The resulting diametral scale factor for the first stage is 2.11:1. This factor was used throughout the injector for diameter dimensions, except for the second sonic venturi contour where a value of 2.16:1 was used to accommodate anticipated changes in operational temperatures, i.e., the larger injector passages, having less boundary layer effect, were predicted to operate at a slightly higher temperature.

A length scale factor of 2:1 was used in the design. This value was a simplification to facilitate scaling dimensions. The final configuration and dimensional details of the as-built injector are shown in Figure 3 (NAR Drawing AP 71-180). The injector detail parts exposed to GF_2 were fabricated from nickel 200 material (which has excellent resistance to hot GF_2) using electric discharge machining for the critical dimensions. These details prior to assembly are shown in Figure 4. The detail parts were welded together with all seams exposed to fluorine welded by the electron beam process. Hydrogen jacket welds

7
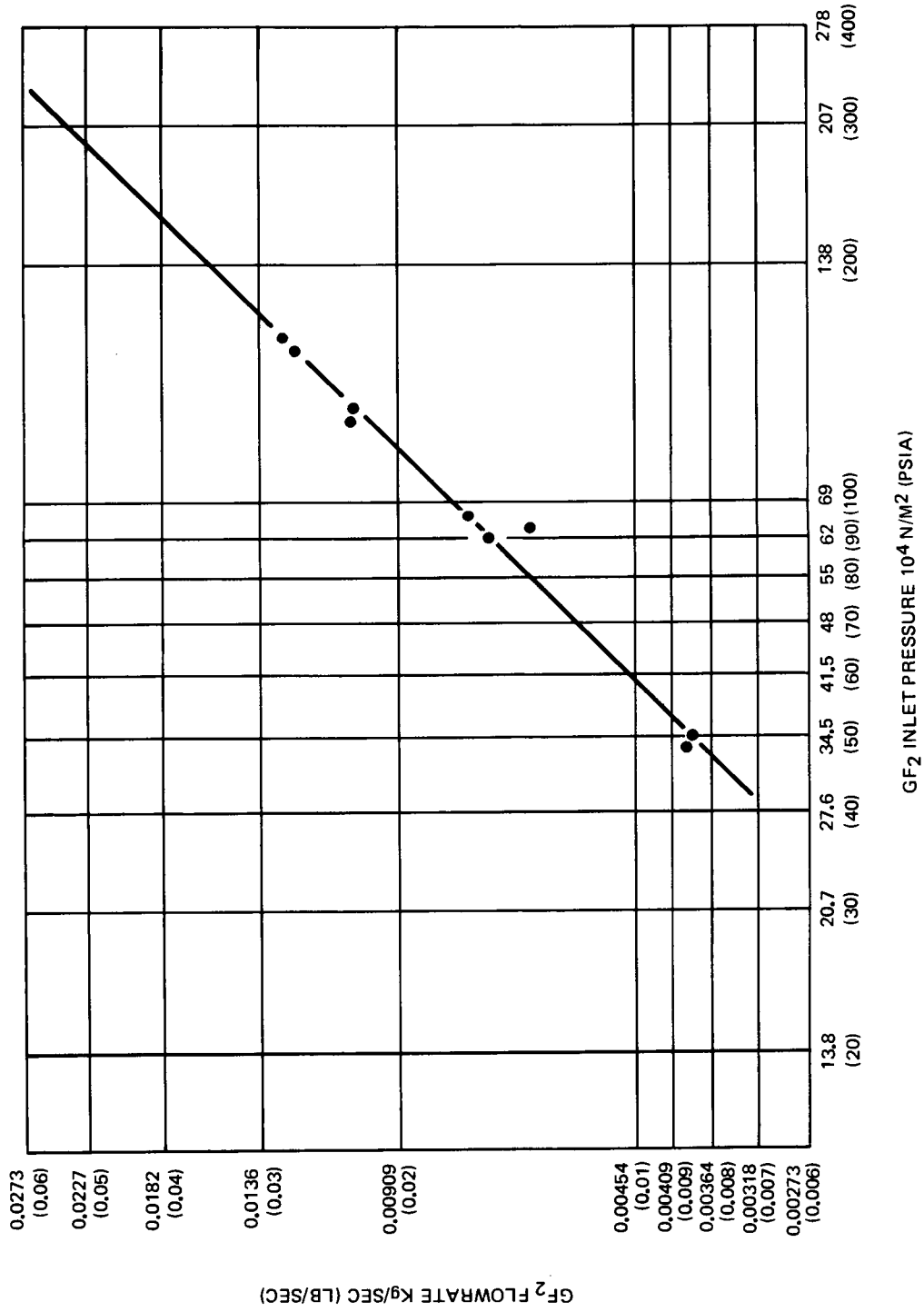
Figure 2. NAS3-13328 Injector Flow Characteristics

8
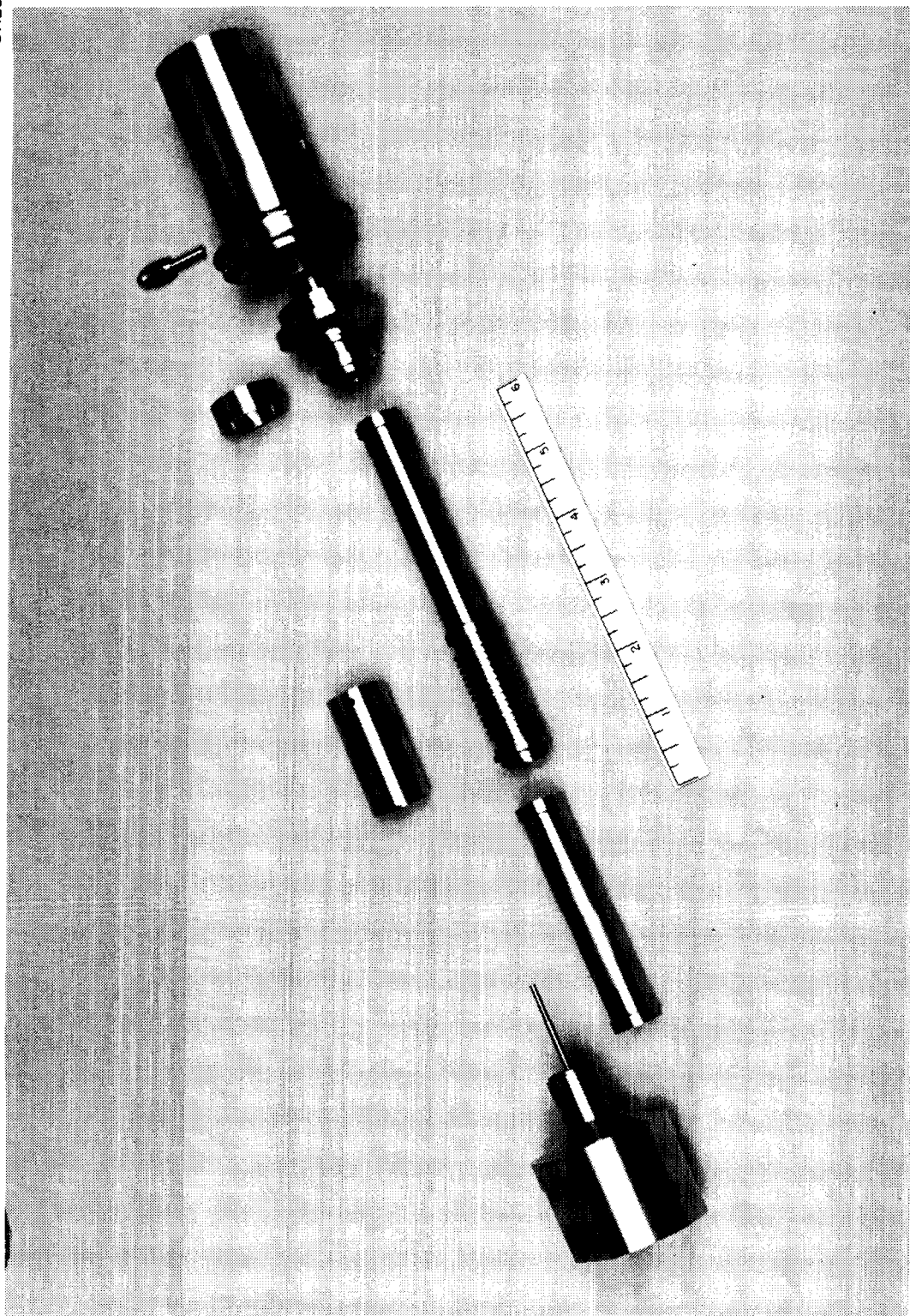
Figure 4. NAR Injector Detail Parts

11

and external welds in the stainless steel outer shell were made using tungsten inert gas (TIG). The small tubes for hydrogen circulation were attached with a fluorine-compatible braze alloy (gold-nickel-palladium alloy, Palniro No. 7). The completed injector is shown in Figure 5.

The injector configuration was somewhat different from the NAS3-13328 injector in order to adapt the new injector for installation on the Thor test tank. The injector was mounted to an existing flange on the test tank, firing vertically downward. The first stage was situated outside the tank (to reduce thermal effects on first stage performance) while the second stage was situated inside the tank. The second stage nozzle has an annular slot in it to reduce heat transfer across the nozzle to the incoming LH_2 flow. At the GF_2 inlet, the -023 tube is pinned and free to slide relative to the -003 body thus allowing for thermal expansion of the injector during firing. The injector was designed so the interior of the injector can be purged with helium to prevent cryopumping of air and freezing on the cold second stage. As shown in Figure 1, the injector was instrumented with chromel-alumel thermocouples (TI 1, 2, and 3) external to the first and second stages. The first stage thermocouple wire was routed through a hole in the -015 nozzle diffuser body and the hole was sealed shut with epoxy on assembly. A static pressure tap was provided in the pumping region downstream of the second stage.

Following assembly, the injector was flow-checked with GN_2. The computed GF_2 flow characteristic of the injector is shown in Figure 6. The H_2 pumping characteristics for the NAS3-13328 injector, from Reference 3, are shown in Figure 7 (the scaled-up injector should have identical LH_2 flow characteristics). The theoretical performance line shown is at a constant GF_2/LH_2 pressure ratio of 2.25:1. After the GN_2 flow calibration, the injector was passivated with GF_2 by NAR and delivered to MDAC for test.

Figure 5. Assembled NAR Injector

13

NOTE: GF_2 Temperature 294°K (530°R)

Line and Shaded Point are Design Values

Open Points are Test Data
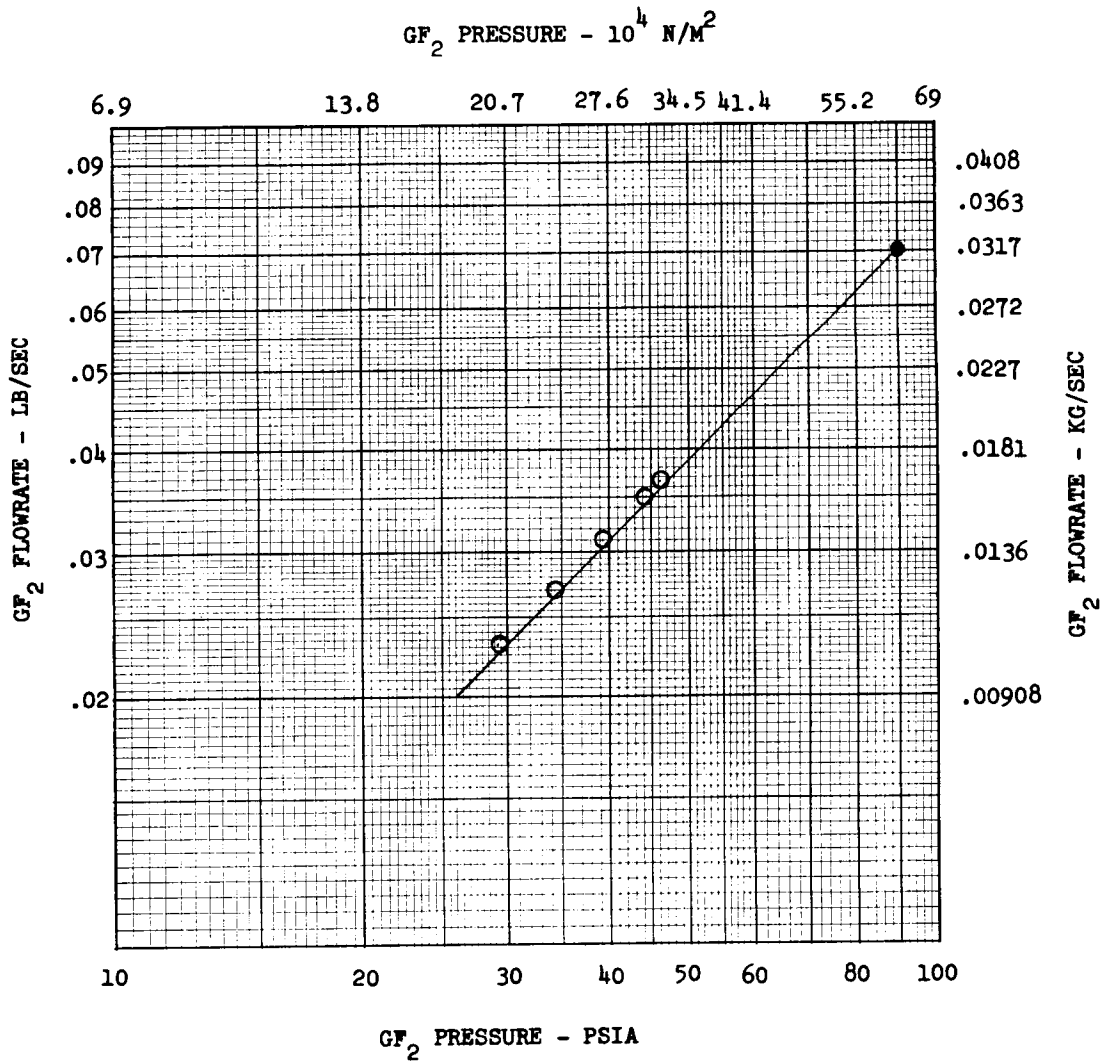
Figure 6. Enlarged NAR Injector Flow Calibration

14
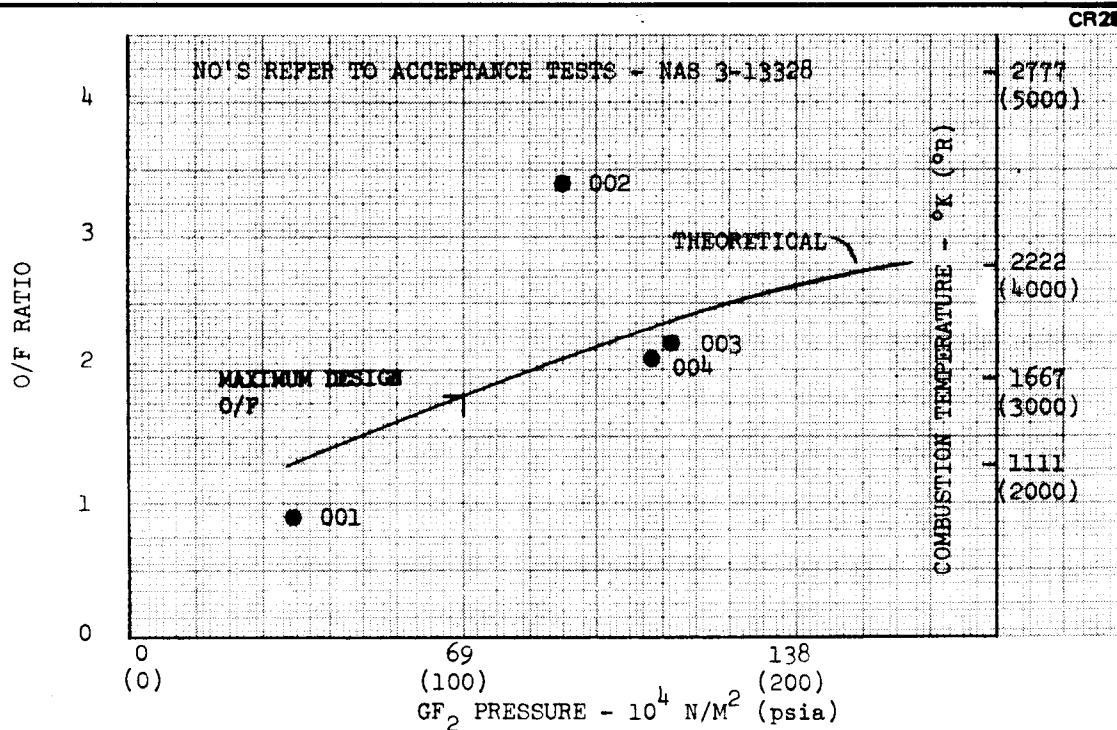
Figure 7. NAR Injector Pumping Characteristics

EXPERIMENTAL SYSTEM DESIGN

The basic experimental system design (test tank, test facility, instrumentation, etc.) was essentially the same as used for the NAS3-13306 tests (see Reference 2), and is described in detail in this section. Modifications of the MTI system to adapt it to the NAR injector are described in the following section, MTI System Modifications.

Test Tank System

The large-scale flight-weight test tank was a Thor missile oxidizer tank made of 2014-T6 aluminum, internal waffle-pattern milled to a minimum wall thickness of 0.00127 m (0.050 in.). The tank had a 2.43-m (95.5-in.) inside diameter, a 5.8-m (228-in.) long cylindrical section, and 0.427-m (16.8-in.) high spherical segment end domes. An insulation system of closed-cell polyurethane foam (Permafoam type CPR385D) with a density of 32 kg/m^3 (2 lb/ft^3) and a thermal

15

conductivity of 2,075 Joule/m-sec-°K (0.16 Btu/hr-°R-ft^2/in.) was installed. Assuming an external foam temperature of 272°K (30°F), 0.0635 m (2-1/2 in.) of this foam was calculated to limit the heat flux into the Thor tank to about 94.6 watt/m^2 (30 Btu/hr-ft^2).

The thick foam insulation had become badly cracked from the tank expansion and thermal stresses induced by the MTI pressurization cycles during previous testing. The apparent heat flux to the tank had increased during the NAS3-13306 test program from 2.11 x 10^3 watt (2 Btu/sec) to 1.054 x 10^4 watt (10 Btu/sec) due to insulation deterioration. The insulation was repaired for the current program by potting the cracks, mechanically fastening the foam to the tank with steel banding straps, enclosing the insulation in a polyethylene purge bag, and purging the insulation with helium. This resulted in no further insulation deterioration and reduced the heat flux to a value of 5.27 x 10^3 watt (5 Btu/sec), which corresponds to 94.6 watt/m^2 (30 Btu/hr-ft^2), as determined by tank self-pressurization tests preceding each hot test.

Test Facility System

The Thor test tank installed at the Alpha Complex—Test Stand 1 at the Sacramento Test Center (STC) is shown in Figure 8. The Alpha Complex is shown schematically in Figure 9, which also indicates the facility capacities for purge and pressurization gases. The test facility, described in detail in Reference 2, is quite complex. The important subsystems making up the facility are described below.

The GF$_2$ supply system was unchanged from the previous program. The baseline GF$_2$ plumbing was selected to be 0.0254-m (1-in.) diameter tubing routed from three manifolded GF$_2$ gas cylinders through a prevalve to the injector complex. GHe and GN$_2$ purge valves were also installed. The GF$_2$ cylinder hand valves can be remotely opened.

CR25
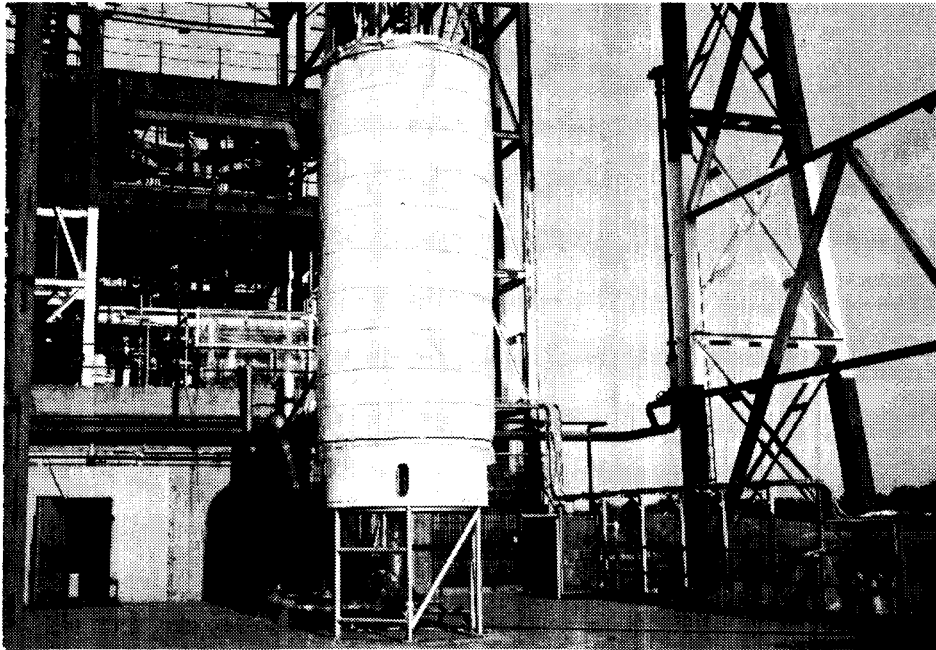
Figure 8. Test Tank Installed at Alpha Test Stand

The LH_2 was filled and emptied from the tank bottom through the main LH_2 outflow valve, a 0.1524-m (6-in.) diameter Annin valve with a Domotor operator. This valve could be set at any position from full-open to closed and was used to control the LH_2 outflow rate to preset values. The LH_2 flow was dumped through the facility LH_2 valve complex (sled) and out the 0.1524-m (6-in.) diameter facility vent line, where it was burned. The tank GH_2 vent valve was also located in the vicinity of the LH_2 valve sled, with the result that the tank vent line was about 23 m (75 ft) long. The tank vent line can be seen in the side view of the Thor tank in Figure 10. The vent line was supported by the vertical beam which also provided support for all plumbing lines and wiring to the top of the tank; the pressure switches were also mounted at the top of the beam (see MTI system design in the next section). This large vent line contributed 0.566 m^3 (20 ft^3) to the tank ullage volume, the effects of which are compensated for in

17

1 LIQUID HYDROGEN
90,000 GAL AT 80 PSIG

2 LIQUID OXYGEN/LIQUID
NITROGEN
13,500 GAL AT 110 PSIG
28,000 GAL AT 50 PSIG
1,200 GPM

3 LIQUID OXYGEN/LIQUID
NITROGEN
13,500 GAL AT 110 PSIG
14,000 GAL AT 50 PSIG
1,200 GPM

4 LIQUID HYDROGEN/GASEOUS
HYDROGEN PUMP VAPORIZOR
40,000 SCF/HR AT 2,500 PSIG

5 GASEOUS HYDROGEN
150,000 SCF AT 2,500 PSIG

TEST STAND 1

TEST TANK

BLOCKHOUSE
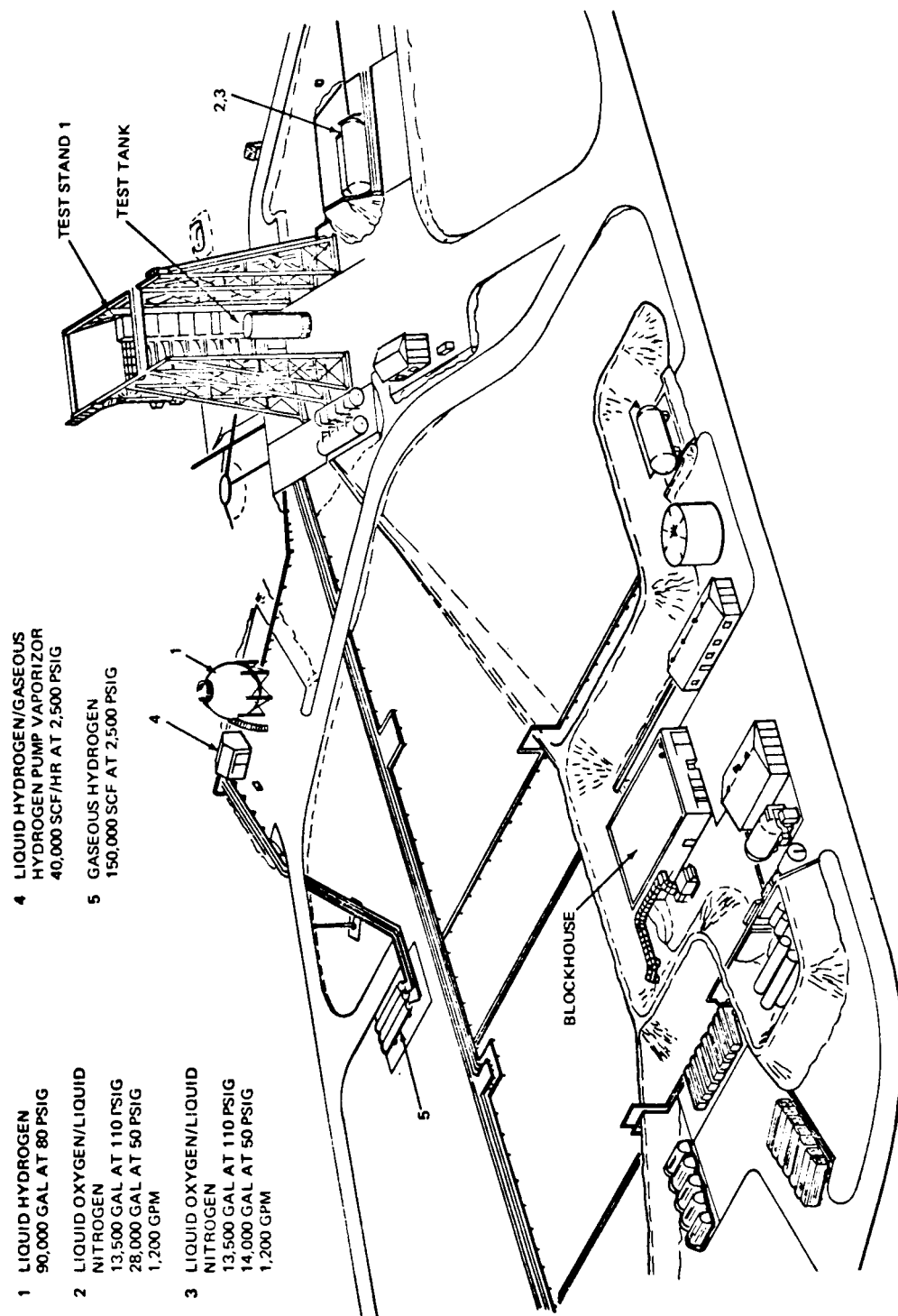
Figure 9. Alpha Complex

18
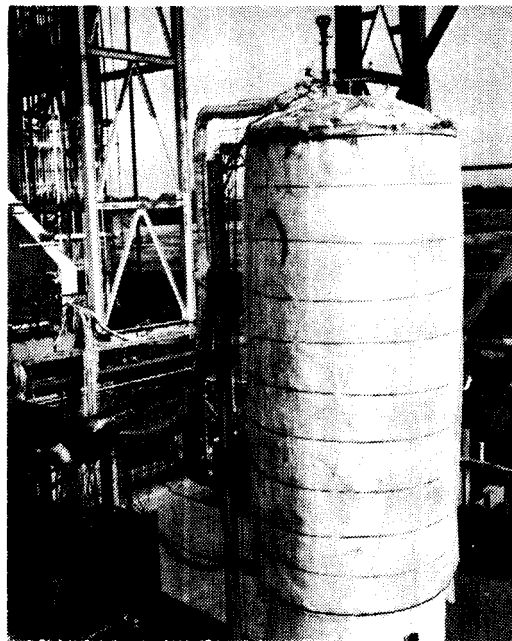
Figure 10. Side View of Test Tank

the analysis of the experimental results. All cryogenic H_2 lines were batted, wrapped, and helium-purged to resist cryopumping. Helium pressurization through a diffuser for LH_2 offloading was available if the situation required.

The extremely complex subsystem which was used to sample for HF in the effluent LH_2 in the NAS3-13306 tests was eliminated for this program. No HF sampling was performed.

The previous work indicated that HF would plate out on the internal tank surfaces. Although frozen HF is not particularly reactive, following MTI pressurization the tank ullage and walls could be warm enough to cause the HF to liquify (or the tank could warm up between test days). Liquid anhydrous HF is quite corrosive and could attack the tank material, instrumentation, wiring, etc. A GN_2 hot purge

19

system was used to purge out and completely warm up the tank to remove HF between test days. The tank was warmed up to about 311°K (100°F). As HF boils at about 292°K (65°F), the warming proved quite successful in eliminating the corrosive effects of HF.

Instrumentation System

The instrumentation and data acquisition equipment used in the test program was basically that used for the previous NAS3-13306 tests, except for some failed temperature transducers which were not replaced. The previous tests utilized several tank-wall-mounted heat flux and temperature sensors at each of several axial locations in the tank to provide data on radial nonuniformities in the ullage gas. No significant nonuniformities were found (see Reference 2), and further, several of the fluxmeters were damaged by overheating. It was therefore decided to provide at least one fluxmeter/wall gas temperature installation at each principal axial location, but not to replace thermal instrumentation beyond that. The location of all thermal sensors (to be used in measuring the temperatures of the ullage gas, LH_2, and tank wall, as well as the local heat flux) is shown in Figure 11, which is an exploded view from inside the tank. The instruments to measure ullage gas (TU) and liquid temperature (TL) were mounted on a vertical probe situated at the half-radius of the tank. These platinum resistance sensors were Thermal Systems, Inc., type 1080-1 (1,380 Ω at 273°K [32°F]), and were situated at 0.305-m (1-ft) intervals on the probe. Essentially, every third sensor was set to measure LH_2 temperature. These generally coincided with the location of the level sensors, and at the basic tank levels of 95, 50 and 10 percent (stations 384, 492, and 588), the LH_2 temperature platinum sensors provided the reference temperature for the thermopile installations. Seven-element thermopile assemblies were situated on the vertical probe above stations 384, 492, and 588 to determine the initial conditions at the interface (as shown in Figure 12). The thermopile assemblies were

NOTE: SHADED POINTS INDICATE
LEVEL SENSOR LOCATIONS
(PERCENT TANK LEVEL SHOWN).
NUMBERS INDICATE STATIONS
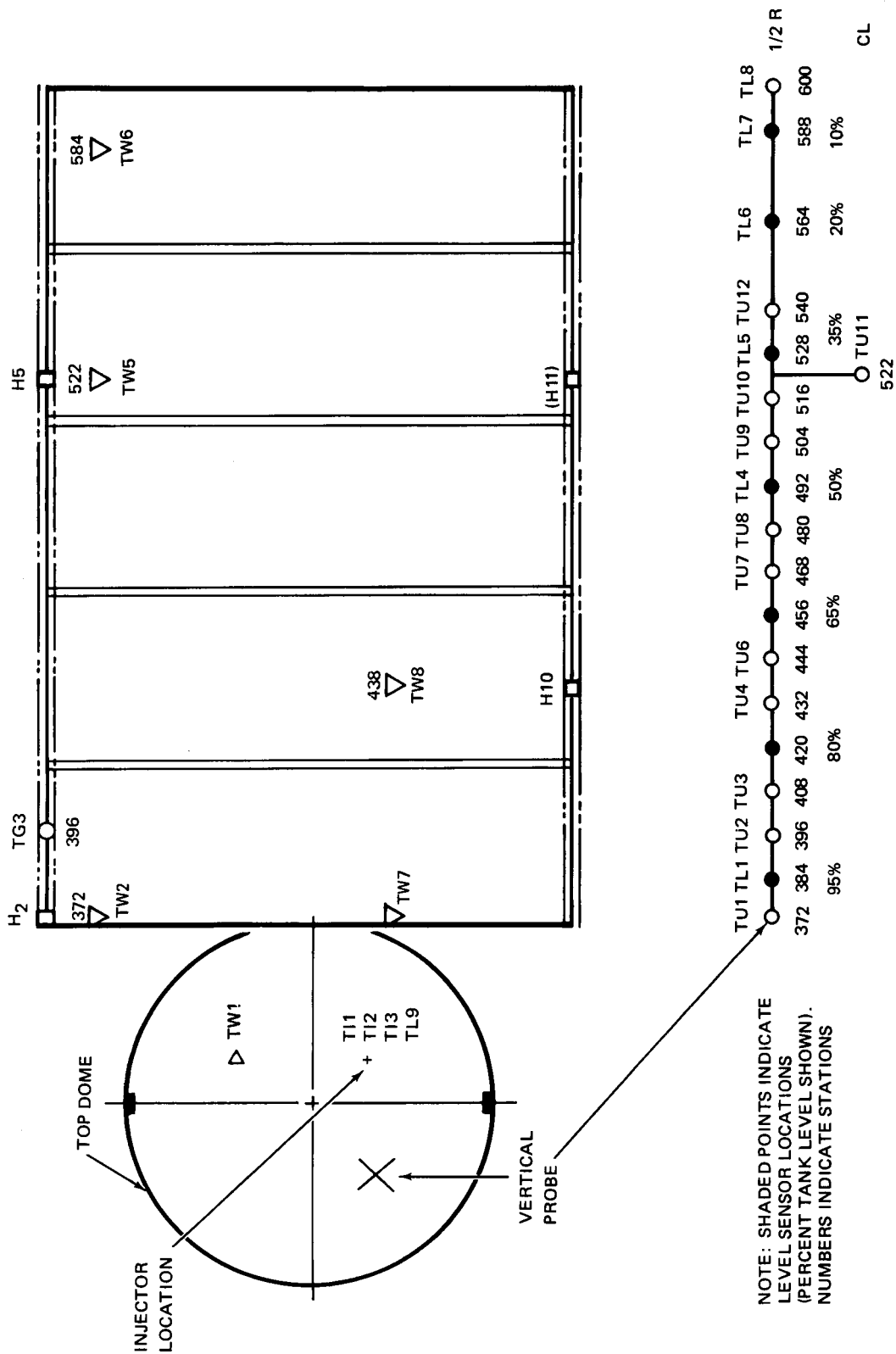
Figure 11. Test Tank Instrumentation Location and Nomenclature

21
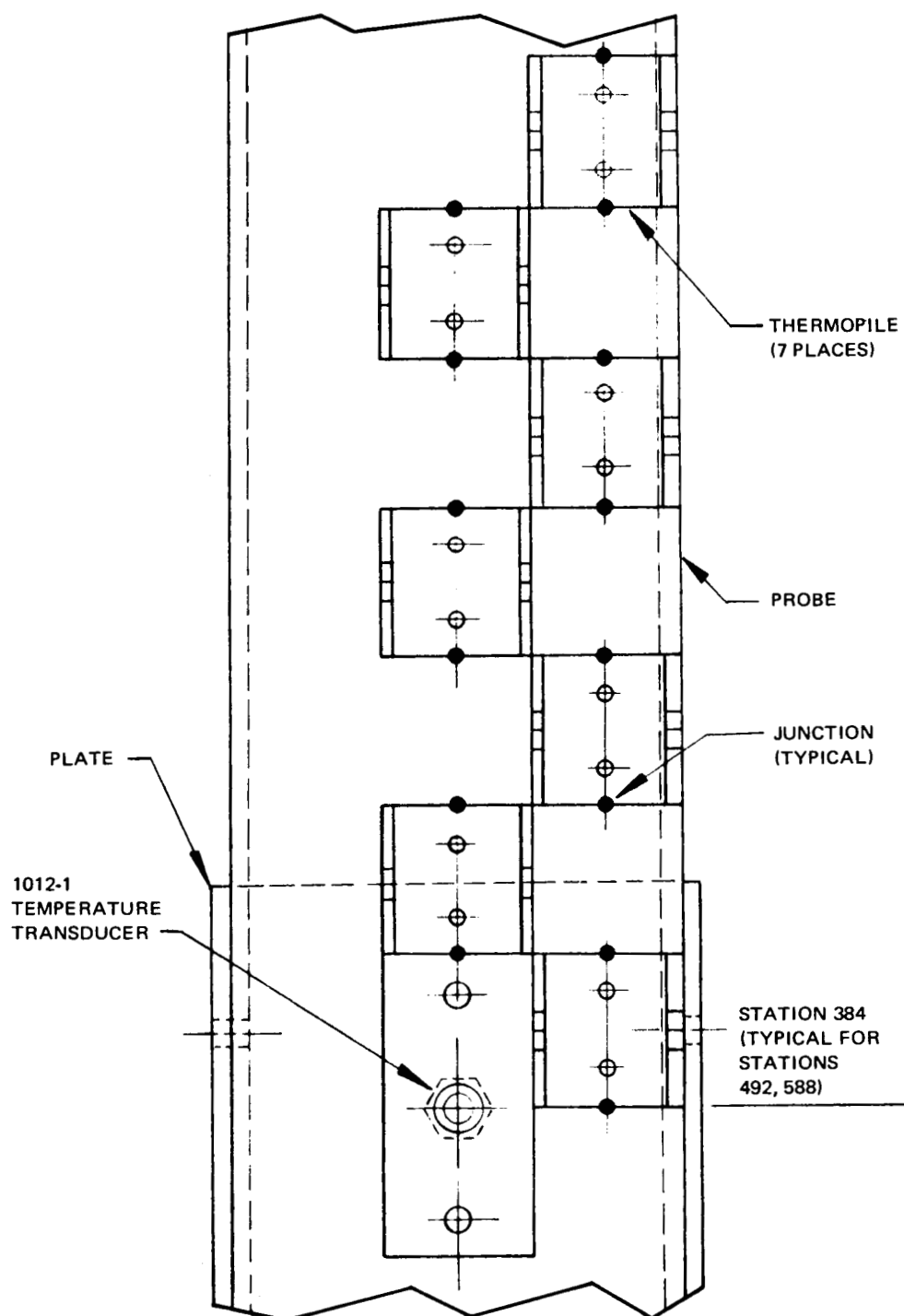
Figure 12. Thermopile Assembly

configured as shown in Figure 13. Each thermopile element had six chromel-constantan junctions (three at one level and three at a level 0.0254 m [1 in.] below) and two null junctions of copper-chromel. The lower junctions of each element were level with the upper junctions of the element below, with the lower junctions of the lowest element level with the LH_2 temperature sensor at that station. The thermopiles measure the temperature difference between the junction levels 0.0254 m (1 in.) apart. Level sensors were also situated on the vertical probe. These were Ohmite Little Devil 1KΩ resistors, overdriven to heat up (and change resistance) rapidly when the surrounding medium changed from LH_2 to gas. Two level sensors were situated 0.0254 m (1 in.) apart at the basic liquid fill levels (95+, 95, 50+, 50, 10+, and 10 percent). The initial liquid level was kept between these sensors which were 0.0254 m (1 in.) apart. These sensors, plus level sensors at 80, 65, 35, and 20-percent liquid levels, were used for LH_2 outflow rate measurement. This technique was used successfully on the previous test program.

The tank wall temperatures (TW) were measured at six (out of the original eight) locations, as shown in Figure 11. The platinum resistance sensors used were Thermal Systems, Inc. type 5001-19 (500Ω at 273°K [32°F]) which were bonded to the outside of the tank wall under the foam insulation.

The heat flux and local heat transfer coefficients inside the tank were measured using commercially fabricated thermal flux meters. This meter, made by International Thermal Instrument Company, is a polyimide glass plate with plated thermopiles on each surface.

The thermopiles would directly measure the ΔT across the plate and produce a multimillivolt signal proportional to heat flux. These devices were completely compatible with the cryogenic environment

*DIMENSIONS
IN INCHES

WIRING SCHEMATIC

CU — COPPER
CR — CHROMEL
CN — CONSTANTAN
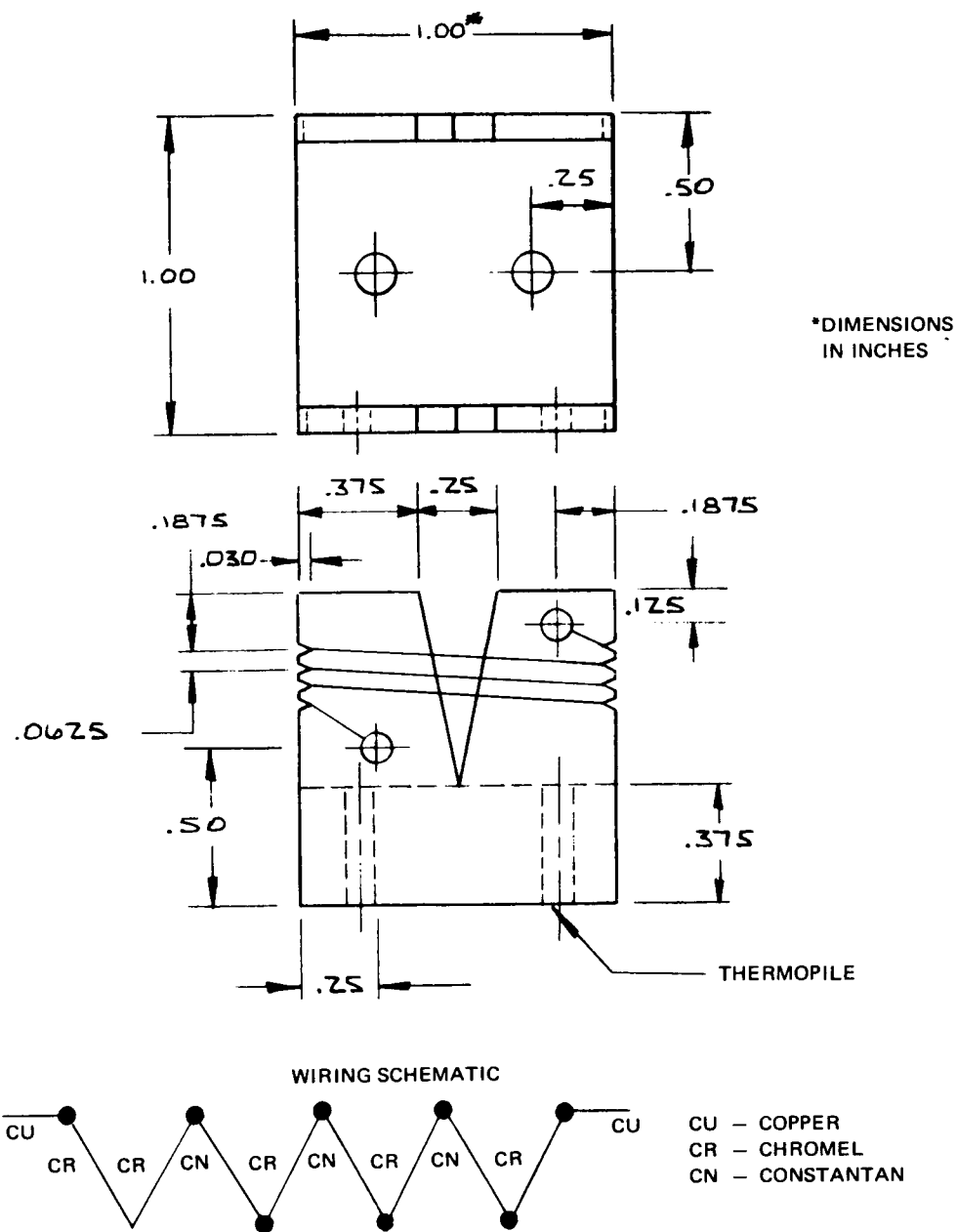
THERMOPILE

Figure 13. Thermopile Element Detail

24

and have been used on many LH_2 research programs. The instruments are individually calibrated to an accuracy of 1 percent. They were supplied clad with stainless steel to protect the glass from HF attack.

These fluxmeters gave consistent data in the previous test program. A typical fluxmeter installation is shown in Figure 14. The fluxmeters were bonded to the aluminum channel with a thin coating of Dow-Corning 731 RTV Silastic. The fluxmeter surface temperature was measured with a Thermal Systems, Inc. type 5001-19 platinum resistance sensor bonded to the front of the fluxmeter with Minnesota Mining and Manufacturing Co. EC3515 epoxy. The gas temperature in the vicinity of the fluxmeter was measured with a Thermal Systems, Inc. type 1012-1 platinum resistance sensor. These also provided a comparison with the gas temperature measured at the vertical probe at the tank half-radius. The local heat transfer coefficient was determined by dividing the heat flux by the temperature difference between the gas and fluxmeter. The fluxmeters were situated in the tank as shown by the H nomenclature in Figure 11.

Figure 15 shows a view looking upward inside the Thor tank prior to testing and indicates the relative position of the instrumentation in the tank. The NAR injector is installed at right center; note the vacuum jacketed LH_2 feedline leading to the injector (see MTI system modifications in the next section). The injector thermocouple wires are visible. The injector thermocouples were chromel-alumel with the reference junction situated at the bottom of the tank where it was immersed in LH_2 during testing.

The fluxmeter output and all other temperatures were recorded on either Leeds and Northrup Speedomax H (Model 1022) strip charts, on Minneapolis-Honeywell Electronic 17 (Model 1070) strip charts, or on
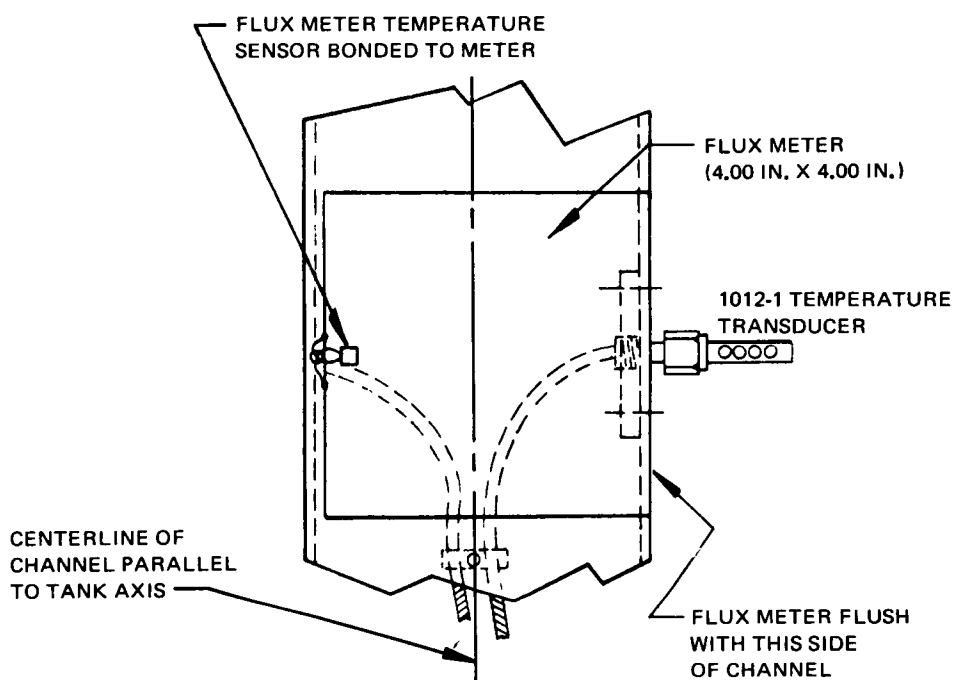
Figure 14. Fluxmeter Installation
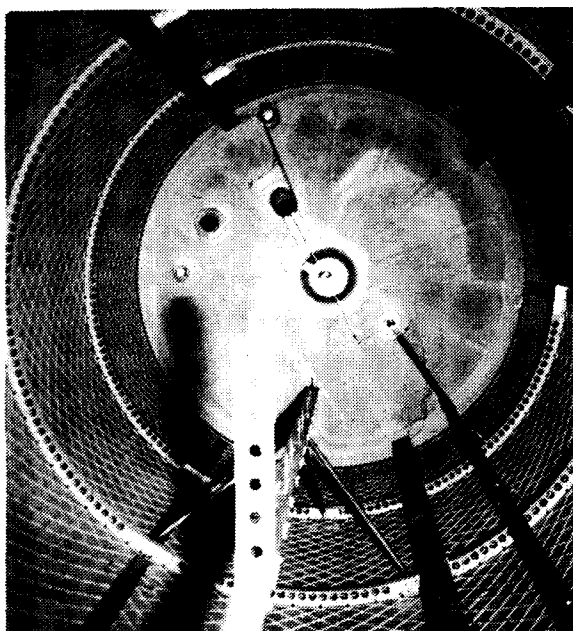
Figure 15. Interior View of Test Tank

the Applied Electronics type 340-700 Pulse Duration Modulation (PDM) system. Sufficient parameters were recorded continuously on the strip charts to evaluate test results without performing the complete automated data reduction built into the PDM system. The temperature data on strip charts included two fluxmeter installations (also recorded on PDM), three tank wall temperatures, and essentially every other ullage temperature sensor on the vertical probe.

The complete temperature-related instrumentation list, showing location, function, working range, and data acquisition method, is shown in Table 1. Timing pulses were supplied by an Astrodata Model DA112-38 Time Code Generator. The relay energize signals from the MTI control system were recorded on a Sanborn Model 125 Event Recorder.

All system pressures were measured with strain-gage-type pressure transducers. The test tank ullage pressure was measured with two fully redundant Owens Labs type PS-254-3A10-TA (0-345 x 10^3 N/m^2 [0-50 psia]) pressure transducers. The GF$_2$ flow rate was determined by the regulated GF$_2$ pressure to the critical-flow injector (see Figure 6). The GF$_2$ pressure upstream of the injector was measured with a Statham PA347-TC-100-350 (0-6.9 x 10^5 N/m^2 [0-100 psia]) transducer. A backup GF$_2$ flow rate measurement was made with a calibrated orifice (0.00635-m [0.25-in.] diameter) in the GF$_2$ flow line just upstream of the injector valve. The GF$_2$ pressure upstream of the orifice (essentially GF$_2$ cylinder pressure) was measured with a Statham type PA822-500 (0-3450 x 10^3 N/m^2 [0-500 psia]) transducer and the pressure drop across the orifice with a Statham type PM280-TC-±5-350 (±34.5 x 10^3 N/m^2 [±5 psia]) transducer. The GF$_2$ temperature upstream of the orifice was measured with a Thermal Systems, Inc. type 1080-1 platinum sensor. The static pressure in the injector second stage was measured with a Statham PA285-TC-50-350

Table 1

INSTRUMENTATION DATA (Page 1 of 4)

No.	P/N	Station Location	Function (T = Temp)	Range °K(°R)	Data
H2		372	Heat Trans Coef		
TG2	TS1 1012-1		Ullage Gas T	20-556 (36-1,000)	S/C &
TQ2	TS1 5001-19		Flux Meter T	20-556 (36-1,000)	PDM
Q2	1 T1 "A"		Flux		
(H3)		396	(Heat Trans Coef)		
TG3	TS1 1012-1		Ullage Gas T	20-556 (36-1,000)	PDM
H5		522	Heat Trans Coef		
TG5	TS1 1012-1		Ullage Gas T	20-556 (36-1,000)	PDM
TQ5	TS1 5001-19		Flux Meter T	20-556 (36-1,000)	
Q5	1 T1 "A"		Flux		
H10		438	Heat Trans Coef		
TG10	TS1 1012-1		Ullage Gas T	20-556 (36-1,000)	S/C &
TQ10	TS1 5001-19		Flux Meter T	20-556 (36-1,000)	PDM
Q10	1 T1 "A"		Flux		
(H11)		522	(Heat Trans Coef)		
TG11	TS1 1012-1		Ullage Gas T	20-556 (36-1,000)	PDM
Q11	1 T1 "A"		Flux		
TW1	TS1 5001-19	Top Dome	Tank Wall T	20-389 (36-700)	S/C
TW2	TS1 5001-19	372	Tank Wall T	20-389 (36-700)	PDM
TW5	TS1 5001-19	522	Tank Wall T	20-389 (36-700)	S/C
TW6	TS1 5001-19	584	Tank Wall T	20-389 (36-700)	PDM
TW7	TS1 5001-19	372	Tank Wall T	20-389 (36-700)	PDM
TW8	TS1 5001-19	438	Tank Wall T	20-389 (36-700)	PDM
TU1	TS1 1080-1	372-1/2 R	Ullage Gas T	20-556 (36-1,000)	S/C
TU2	TS1 1080-1	396-1/2 R	Ullage Gas T	20-556 (36-1,000)	S/C
TU3	TS1 1080-1	408-1/2 R	Ullage Gas T	20-556 (36-1,000)	PDM
TU4	TS1 1080-1	432-1/2 R	Ullage Gas T	20-556 (36-1,000)	S/C

Table 1

INSTRUMENTATION DATA (Page 2 of 4)

No.	P/N	Station Location	Function (T = Temp)	Range °K(°R)	Data
TU6	TS1 1080-1	444-1/2 R	Ullage Gas T	20-556 (36-1,000)	PDM
TU7	TS1 1080-1	468-1/2 R	Ullage Gas T	20-556 (36-1,000)	S/C
TU8	TS1 1080-1	480-1/2 R	Ullage Gas T	20-556 (36-1,000)	PDM
TU9	TS1 1080-1	504-1/2 R	Ullage Gas T	20-556 (36-1,000)	S/C
TU10	TS1 1080-1	516-1/2 R	Ullage Gas T	20-556 (36-1,000)	PDM
TU11	TS1 1080-1	522-CL	Ullage Gas T	20-556 (36-1,000)	S/C
TU12	TS1 1012-1	540-1/2 R	Ullage Gas T	20-556 (36-1,000)	S/C
TL1	TS1 1012-1	384-1/2 R	Liquid T	20-33 (36-60)	PDM
TL4	TS1 1012-1	492-1/2 R	Liquid T	(36-60)	PDM
TL5	TS1 1080-1	528-1/2 R	Liquid T	(36-60)	PDM
TL6	TS1 1080-1	564-1/2 R	Liquid T	(36-60)	PDM
TL7	TS1 1012-1	588-1/2 R	Liquid T	(36-60)	PDM
TL8	TS1 1012-1	600-1/2 R	Liquid T	20-33 (36-60)	S/C
TL9	7882210-505	Injector LH$_2$ Line	LH$_2$ Supply T	20-89 (36-160)	S/C
TP11	MDAC Thermopile	384-1/2 R	Interface T		PDM
TP12	MDAC Thermopile	383-1/2 R	Interface T		PDM
TP13	MDAC Thermopile	382-1/2 R	Interface T		PDM
TP14	MDAC Thermopile	381-1/2 R	Interface T		PDM
TP15	MDAC Thermopile	380-1/2 R	Interface T		PDM

Table 1

INSTRUMENTATION DATA (Page 3 of 4)

No.	P/N	Station Location	Function (T = Temp)	Range °K(°R)	Data
TP16	MDAC Thermopile	379-1/2 R	Interface T		PDM
TP17	MDAC Thermopile	378-1/2 R	Interface T		PDM
TP21	MDAC Thermopile	492-1/2 R	Interface T		PDM
TP22	MDAC Thermopile	491-1/2 R	Interface T		PDM
TP23	MDAC Thermopile	490-1/2 R	Interface T		PDM
TP24	MDAC Thermopile	489-1/2 R	Interface T		PDM
TP25	MDAC Thermopile	488-1/2 R	Interface T		PDM
TP26	MDAC Thermopile	487-1/2 R	Interface T		PDM
TP27	MDAC Thermopile	486-1/2 R	Interface T		PDM
TP31	MDAC Thermopile	588-1/2 R	Interface T		PDM
TP32	MDAC Thermopile	587-1/2 R	Interface T		PDM
TP33	MDAC Thermopile	586-1/2 R	Interface T		PDM
TP34	MDAC Thermopile	585-1/2 R	Interface T		PDM
TP35	MDAC Thermopile	584-1/2 R	Interface T		PDM
TP36	MDAC Thermopile	583-1/2 R	Interface T		PDM

Table 1

INSTRUMENTATION DATA (Page 4 of 4)

No.	P/N	Station Location	Function (T = Temp)	Range °K(°R)	Data
TP37	MDAC Thermopile	582-1/2 R	Interface T		PDM
LL1	Ohmite Res	383-1/2 R	Liquid Level		S/C
LL2	Ohmite Res	384-1/2 R	Liquid Level		S/C
LL3	Ohmite Res	420-1/2 R	Liquid Level		S/C
LL4	Ohmite Res	456-1/2 R	Liquid Level		S/C
LL5	Ohmite Res	491-1/2 R	Liquid Level		S/C
LL6	Ohmite Res	492-1/2 R	Liquid Level		S/C
LL7	Ohmite Res	528-1/2 R	Liquid Level		S/C
LL8	Ohmite Res	564-1/2 R	Liquid Level		S/C
LL9	Ohmite Res	587-1/2 R	Liquid Level		S/C
LL10	Ohmite Res	588-1/2 R	Liquid Level		S/C
TF1	TS1 1080-1	F_2 Line	GF_2 T	222-305 (400-550)	S/C
TI1	CR-AL T/C	Injector 1st Stage	Injector T	20-1,645 (36-2,960)	S/C
TI2	CR-AL T/C	Injector 2nd Stage		20-1,645 (36-2,960)	S/C
TI3	CR-AL T/C	Injector 2nd Stage		20-1,645 (36-2,960)	S/C

$(0-345 \times 10^3 \text{ N/m}^2 [0-50 \text{ psia}])$ transducer. All pressures were recorded on Leeds and Northrup Speedomax H (Model 1022) strip charts for continuous data evaluation during testing.

MTI SYSTEM MODIFICATIONS

The general MTI system design requirements for this program were the same as for the previous test program under Contract NAS3-13306:

A. Self-regulating.

B. Capable of controlled pressurization, pressure hold, and expulsion at varied LH_2 outflow rates up to a maximum of 6.8 kg/sec (15 lb/sec).

C. Operable at any ullage volume.

D. Capable of a wide range of flow rates and operating pressures.

E. Able to pressurize the tank to within $6,895 \text{ N/m}^2$ (1 psia) of the desired pressure.

F. Capable of safe operation without damaging the injector or tank, or freezing of fluorine in the injector, and causing minimum heat leakage into the tank when not in operation.

The basic MTI control and injection system used for the previous program was used for this one; however, due to the unique nature of the NAR injector, some system modifications were necessary. The new MTI control and injection system is shown schematically in Figure 16 and the reasons for the component selection are discussed below.

For steady LH_2 outflow at constant tank pressure, the maximum MTI pressurization energy requirements occur at the end of the test when the tank is nearly empty because the heat transfer losses to the wall are highest. If the GF_2 injection rate is sized to the maximum energy requirements, excessive GF_2 inflow will occur at the beginning of LH_2 outflow. To control the GF_2 inflow, the flow rate must either

PRESSURE SWITCHES

PRESSURE
TRANSDUCERS

FROM
GF$_2$ SUPPLY

REGULATOR

INJECTOR
VALVE

INJECTOR

VACUUM-JACKETED
LH$_2$ SUPPLY LINE

LH$_2$

TO LOADING AND UNLOADING
FLOW CONTROL VALVES
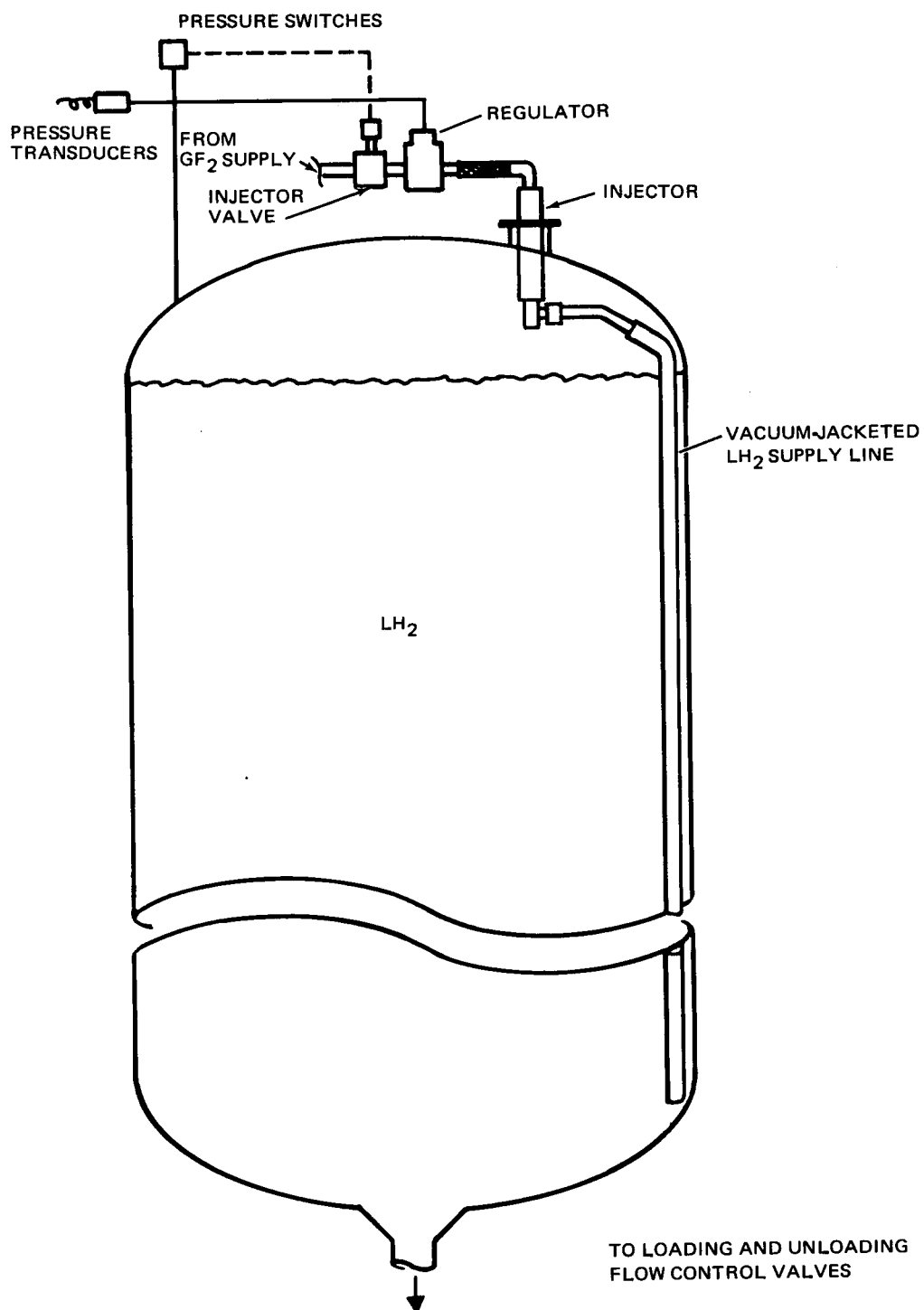
Figure 16. Test Tank Injector Installation

be continuously varied, or the GF_2 flow held constant and cycled on and off to provide the proper energy input. The latter solution, called a "bang bang" system, was used on the previous program and is suitable for this program as well, since the NAR injector is a constant-flow device. The control system is implemented by using pressure switches to sense tank pressure and open and close the injector valve to keep the tank pressure within a narrow band. The pressure switches used were completely redundant individually plumbed mercury-type pressure switches, Mercoid type APH-41-153. The switches have a range of 10.3 to 31 x 10^4 N/m^2 (15 to 45 psia) and could be individually set to any pressure within this range with a maximum actuation band (relay energize-to-denergize) of ±2.58 x 10^3 N/m^2 (±0.375 psia). This switch had a maximum time delay of 15 milliseconds and was safe for operation in an H_2 atmosphere because the contacts were sealed. The switch would not be suitable for flight vehicle use, however, because the mercury element must be level and is thus g-vector sensitive. Bellows-type switches suitable for flight use with the same fast response and narrow actuation band are available, but must be custom-made (especially for H_2 service) and are very expensive. Their use was deemed to be not cost-effective for this program. The chosen switch was available off-the-shelf, inexpensive, and suitable for ground service within an H_2 atmosphere without sacrifice of accuracy, response, or safety.

When the preset actuation pressure (tank pressure) is reached, the pressure switch relay terminates GF_2 inflow by closing the injector valve. When LH_2 outflow or heat transfer causes the tank pressure to drop to the lower limit of the actuation band, the pressure switch relay reopens the injector valve.

The GF_2 supply system used for the previous MTI tests utilized a simple GF_2 storage cylinder blowdown mode, with GF_2 flow principally controlled across the injector valve. However, for the NAR injector tests, two critical flow-control devices exist downstream of the injector valve: The injector proper and the regulator, both of which operate at a near-critical pressure ratio. Because of this, the Fox injector valve, Part No. 610851, as configured and used on the NAS3-13306 tests, would not have been capable of flowing sufficient GF_2 without a prohibitively large pressure drop. Therefore, the Fox valve flow orifice was increased to the maximum diameter possible (approximately 6.35×10^{-3} m [0.25 in.]) without redesign of the actuator assembly. This minimized pressure drop across the injector valve. This modification allowed use of the same reliable injector valve successfully used on the two previous MTI programs under Contracts NAS3-13306 and NAS3-7963.

The Fox injector valve is liquid- and gaseous-fluorine compatible and has a copper-on-stainless-steel seat. The valve was actuated by $3,447 \times 10^3$ N/m^2 (500 psia) helium through two integral solenoids, one to actuate open and the other to actuate closed. The high-pressure helium actuation enabled extremely fast valve response (closed to full-open or vice versa in less than 10 milliseconds. Use of helium (rather than spring-loading) to actuate closed was required to provide the high seat loadings necessary to affect a leak-tight metal-to-metal seal. In the event of power failure, the valve would remain in its last position, which could be open. The valve, therefore, incorporated a pressurized override which was utilized by attaching a normally open valve (energized closed by the main power) to the override. In the event of power failure, the normally open valve would open, thus pressurizing the injector valve closed.

The requirement for pressure regulation of the GF_2 supplied to the NAR injector was necessary to provide sufficient pressure differential in the injector second stage annulus to properly pump LH_2. Nominally, the NAR injector GF_2 inlet pressure should be about 2.25 times the LH_2 inlet (tank) pressure. However, this GF_2 pressure cannot be a fixed value (relative to the preset tank pressure), as shown by the following example: For a tank pressure of 30×10^4 N/m^2 (43 psia), the GF_2 inlet pressure would be 67×10^4 N/m^2 (97 psia), and the second stage ejector static pressure would be 0.16 times that or 10.7×10^4 N/m^2 (15.5 psia). Assuming a 90-percent ullage in the Thor test tank, the LH_2 inlet pressure could start as low as 10.3 $\times 10^4$ N/m^2 (15.0 psia) (initial tank pressure at the start of prepressurization minus the hydrogen head). Thus, during prepressurization, the injector would pump no LH_2 until the LH_2 inlet pressure increased above 10.7×10^4 N/m^2 (15.5 psia) due to the tank pressure rise; even then, the injector would operate at high O/F ratios and temperatures until the tank pressure approached the design tank pressure. For a 90-percent ullage, the prepressurization time could be as long as 60 seconds (Reference 2) and the injector, operating at high O/F ratios, could be hot for several seconds during the prepressurization cycle. This situation would also be true for the injector demonstration test where the LH_2 inlet pressure stays at about 10.1×10^4 N/m^2 (14.7 psia), and there would be no LH_2 flow. It is clear, therefore, that the GF_2 regulator must be designed to provide a constant ratio of 2.25 times LH_2 inlet (tank) pressures from 10.1 to 30×10^4 N/m^2 (14.7 to 43 psia). Further, the regulator must be capable of flowing 0.0317 kg/sec (0.07 lb/sec) of 294°K (530°R) GF_2 at 62×10^4 N/m^2 (90 psia) downstream and approximately 138×10^4 N/m^2 (200 psia) upstream (GF_2 pressure downstream of the injector valve). An off-the-shelf regulator to meet these requirements did not exist; therefore, a special regulator was designed jointly by MDAC and Wintec Corp. A cutaway of this regulator (MDAC P/N 1T42072; Wintec

P/N 1346-5700) is shown in Figure 17. The regulator has many unique features. A differential-area piston in the ratio of 2.25:1 is used to regulate the GF_2 pressure to a value of 2.25 times the tank pressure. The dome of the regulator is pressurized with hydrogen from the tank ullage (see Figure 16). To positively separate the GH_2 in the dome from the GF_2 in the regulator, a double-sealed GN_2-"purged" (actually dead-headed) port is provided. GN_2 was supplied to the port at 138×10^4 N/m^2 (200 psia) so that the pressure in the sealed cavity was always higher than both the dome GH_2 pressure and the regulated GF_2 pressure (even during the starting surge). In addition, an overboard vent was provided under the piston step to relieve any leakage that could occur. Because the regulator had to deliver an absolute pressure ratio of 2:25:1, the atmospheric pressure force under the piston was counteracted with a trim spring. This spring also compensated for the small residual force from the balanced poppet (which was used to minimize the effects of varying upstream pressure). The moving seals in the regulator were of the omni-seal type. In order to minimize the frictional force of the seals, which contribute to hysteresis in the regulation, special close-tolerance seals were procured, and the piston was split to allow seal installation without stretching the seals. The frictional force of the seals contributes to more regulation error at low dome pressures (and low forces) than at high pressures. The trim spring was used to set the regulator to give the best regulated pressure ratio at each basic steady-state dome pressure. The regulator had a 316 stainless steel poppet and a brass seat. The internal leakage was less than 3.17×10^{-7} m^3/sec (19 sccm) but the regulator was situated downstream from the injector valve (see Figure 16) so that with the valve off, the regulator will be wide open, thus allowing greater tolerances on internal leakage across the metal-to-metal regulator seat. The performance of the regulator, reported on in the Experimental Results section, was excellent.

SIGNAL PORT
MS 33649-4
ROTATED 90°CW

PURGE PORT
MS 33649-4
ROTATED 90°
COUNTER CLOCK-
WISE

INLET
MS 33649-16

8.75
MAX

7.500
±.060

3.500
±.060

2.380±.030

3.50

3.875 DIA
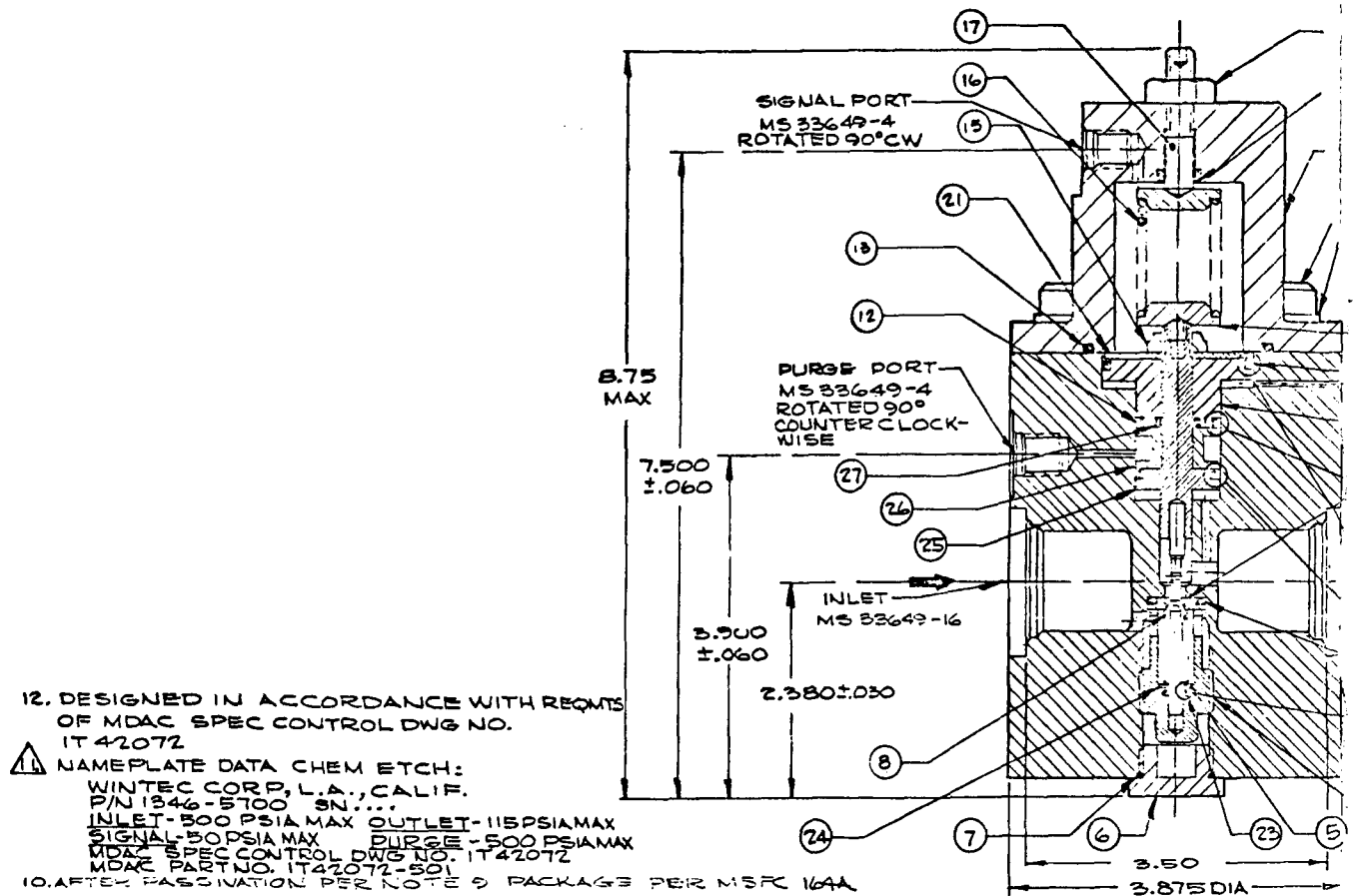
12. DESIGNED IN ACCORDANCE WITH REQMTS
OF MDAC SPEC CONTROL DWG NO.
IT42072

11. NAMEPLATE DATA CHEM ETCH:
WINTEC CORP, L.A., CALIF.
P/N 1546-5700 SN:...
INLET-500 PSIA MAX OUTLET-115 PSIA MAX
SIGNAL-50 PSIA MAX PURGE - 500 PSIA MAX
MDAC SPEC CONTROL DWG NO. IT42072
MDAC PART NO. IT42072-501

10. AFTER PASSIVATION PER NOTE 9 PACKAGE PER MSFC 164A

9. AFTER CLEANING PER NOTE 8 PASSIVATE INLET & OUTLET PER AFRPL-TR-67-309

8. CLEAN PER MSFC 164A

7. TEST PER ATP 1546-5700

6. LEAKAGE: INTERNAL -19 SCCM MAX EXTERNAL-SIGNAL WETTED AREA - BUBBLE TIGHT INLET

5. $C_V = .6$

4. PROOF PRESSURE 1000 PSIA BURST PRESSURE 2000 PSIA

3. OPERATING TEMPERATURE: 85°F TO 125°F

2. PRESSURE RATINGS: PURGE 500 PSIA MAX SIGNAL 15 PSIA TO 50 PSIA INLET 200 PSIA TO 500

1. FLUID MEDIA-INLET & OUTLET - GF$_2$ - PURGE: GN$_2$ OR GH$_E$ - SIGNAL - GH$_E$

NOTES

Figure 17. Pressure Regulator Drawing
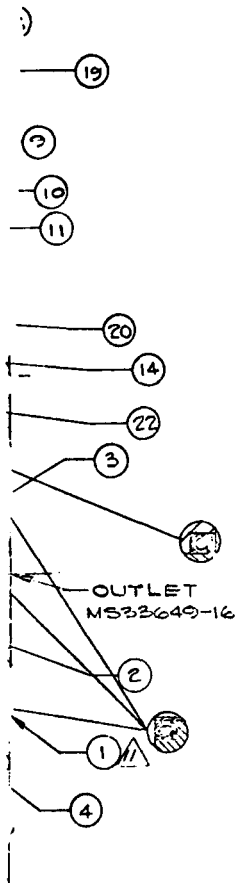
ITEM NO.	QTY.	NAME	PART NO.	MATERIAL	
27	1	O-RING	0208-2012	TEFLON	
26	1	SPACER	1346-5715	CRES	
25	1	GUIDE	1346-5714	CRES	
24	1	WASHER	1346-5713	CRES	
23	1	SEAL	1346-5716-1	TEFLON&CRES	
22	1	PISTON	1346-5712	CRES	
21	1	WASHER, RET.	1346-5711	CRES	
20	2	BUTTON, SPRING	1346-5710	CRES	
19	1	O-RING	0208-2111	TEFLON	
18	1	NUT	AN316-5R		
17	1	SCREW, ADJ	1346-5709	CRES	
16	1	SPRING	122913	CRES 17-7PH	
15	1	NUT	NAS1022C6	CRES	
14	1	SEAL	1346-5716-3	TEFLON&CRES	
13	1	O-RING	0208-2137	TEFLON	
12	2	SEAL	1346-5716-2	TEFLON&CRES	
11	6	WASHER	999020	STL CAD PL	
10	6	SCREW, CAP SOC HD	6-24UNF-3Ax.75LG	STL CAD PL	
9	1	DOME	1346-5707	CRES 316	
8	1	POPPET	1346-5705	CRES 316	
7	1	O-RING	0208-3010	TEFLON	
6	1	PLUG	115150-2	CRES 316	
5	1	SPRING	112727	CRES 17-7PH	
4	1	RETAINER, SEAT	1346-5703	CRES 316	
3	1	SEAT	1346-5702	BRASS	
2	1	O-RING	0208-2015	TEFLON	
1	1	BODY	1346-5701	CRES 316	

LIST OF MATERIAL

1346-5700

(19)

(3)

(10)

(11)

(20)

(14)

(22)

(3)

——OUTLET
MS33649-16

(2)

(1)

(4)

OUTLET WETTED AREA-1x10⁻⁶CC/SEC H$_e$ MAX

PSIA OUTLET 2.25 x SIGNAL ± 10%

During the NAS3-13328 injector acceptance tests (see Reference 3), NAR apparently had considerable difficulty in providing LH$_2$ to the injector, as indicated by Figure 7. Points 001, 003, and 004 lie close to the theoretical line, but point 002 is at a much higher O/F ratio (and much hotter) because of vaporization of LH$_2$ in the feed line to the injector and subsequent restriction of hydrogen flow. It was feared the same problem might occur in the tank tests with large ullages. For some tests, the LH$_2$ feed line from the tank bottom sump to the injector (Figure 16) will pass through a relatively warm ullage, possibly as warm as 333°K (600°R) for a 90-percent ullage prepressurization. The heat flux from the ullage to the LH$_2$ feed line was calculated to vaporize sufficient LH$_2$ to reduce the hydrogen flow rate by a factor of four. The injector feed line must therefore be insulated from the ullage to ensure that LH$_2$ reaches the injector. The insulation must be compatible with LH$_2$, hydrogen fluoride (HF), and high temperatures. The least complex insulation technique was to use a vacuum-jacketed line. Thus a 1.27 x 10^{-2}-m (1/2-in.) diameter vacuum-jacketed line (vendor-pumped and permanently sealed) was installed in the test tank (Figure 16). The line weighed about 6.8 kg (15 lb) but restricted the LH$_2$ flow degradation to a few percent.

The MTI control system used to actuate all valves, etc., was essentially the same as used during the NAS3-13306 tests, and is described in detail in Reference 2. The only major modification to the control system was the elimination of the infrared (IR) ignition detector. This was done for two reasons: (1) It was deemed no longer necessary for system safety. In 11 previous ullage injection tests under Contract NAS3-7963, and 17 previous ullage injection tests under Contract NAS3-13306, there was never a case of nonignition. Further, with the NAR injector and its "preburner" first stage, there is even less chance of nonignition (NAR obtained reliable ignition in all 12 firing

tests under NAS3-13328), (2) The installation of the NAR injector in
the available Thor tank ports precluded being able to look directly
at the injector with the IR detector. In previous "offset injector"
tests under Contract NAS3-13306, the IR detector was unable to look
directly at the injector with the result that there were three test shut-
downs due to spurious IR detector nonignition signals (in fact, two
tests were run without the IR detector in the circuit). To avoid this
problem in this program, the IR detector was eliminated, and ignition
was reliably sensed by the rapid tank pressure rise during firing.

The complete assembled GF_2 injection loop, shown schematically in
Figure 16, is a compact installation on top of the Thor test tank, as
shown in Figure 18. The flex line between the regulator and
injector allowed movement of the injector due to thermal expansion

Figure 18. Injection Assembly Installation on Test Tank

when operating and allowed installation flexibility. The entire assembly was passivated with GF_2 prior to testing and was also used in essentially the same configuration for the injector demonstration tests discussed below.

EXPERIMENTAL RESULTS

INJECTOR DEMONSTRATION TEST

Prior to installation of the NAR injector in the Thor test tank, the injector was hot-fired in a cold GH_2 atmosphere with GF_2 flow on-off cycle rates simulating the injector cycling anticipated in the Thor tank tests.

The purpose of this test was twofold:
1. To verify the structural adequacy of the injector, and reveal any injector burning problems which could occur.
2. To verify the proper operation of the MTI control system and GF_2 supply system.

The apparatus used for this test was essentially the same used for the previous injector demonstration tests under Contract NAS3-13306. The apparatus, shown in Figure 19, consists of a horizontally mounted stainless steel pipe 0.3 m (12 in.) in diameter by 3 m (10 ft) long. Some modifications to the test apparatus were made to adapt it to the NAR injector, which was configured with the first stage outside the pipe at ambient temperature, and the second stage inside the pipe. The injector was mounted axially along the pipe centerline through a blind flange at one end of the pipe. The liquid hydrogen flow was introduced along the bottom of the pipe, where it partially boiled, providing a cold GH_2 atmosphere in the pipe. The pipe apparatus was modified by the addition of a series of baffles and a foam-insulated LH_2 sump, as shown in Figure 19. These decelerated the LH_2 flow and provided a sump from which saturated LH_2 at 10.1×10^4 N/m^2 (14.7 psia) could be drawn to the injector. A 7.6×10^{-2}-m (3-in.)

43

diameter pyrex window was installed near the injector tip, through which high-speed motion pictures were taken at the rate of 250 frames per second with a Mitchell Monitor Model 500 camera. This exposure rate allowed 180 seconds of film time using a 366-m (1,200-ft) magazine, and it had been hoped that direct comparison could be made with the motion pictures taken (also at a 250 frames-per-second rate) of the previous MTI injectors. This was not possible, however, because the view was generally obscured by clouds of H_2 vapor and LH_2 splashing on the camera window.

The test pipe was installed at the Alpha Complex—Site 3, STC (as shown in Figure 20). GF_2 from the MTI control pallet was plumbed to the site, and LH_2 was available from the facility supply. During installation of the injector in the test pipe, the GF_2 flow tube in the injector was accidentally torqued. To verify that no damage had occurred, the injector was flow-proofed with GHe at 10^6 N/m^2 (145 psia), and externally leak-checked with GHe at 7.1 x 10^5 N/m^2 (103 psia). No external leakage was detected, and subsequent measurements indicated that although the injector was twisted slightly, it had not been stretched or otherwise damaged by the incident.

The firing test was conducted according to MDAC Countdown Manual—Site 3 (MDAC Drawing 1T17019) requirements. The plan was to fire the injector continuously for 60 seconds, then cycle the injector for 60 seconds at 0.1 second ON, 0.9 second OFF, and finally cycle the injector for 60 seconds at 0.9 second ON, 0.1 second OFF. During the first 60 seconds of continuous firing, the injector behaved normally, with the first stage temperature stabilizing at 320°K (570°R) and the second stage temperature stabilizing at 935°K (1,680°R). It was noted that the regulated GF_2 pressure to the injector overshot to 3.45 x 10^5 N/m^2 (50 psia) 0.5 second after the injector valve opened, then slowly
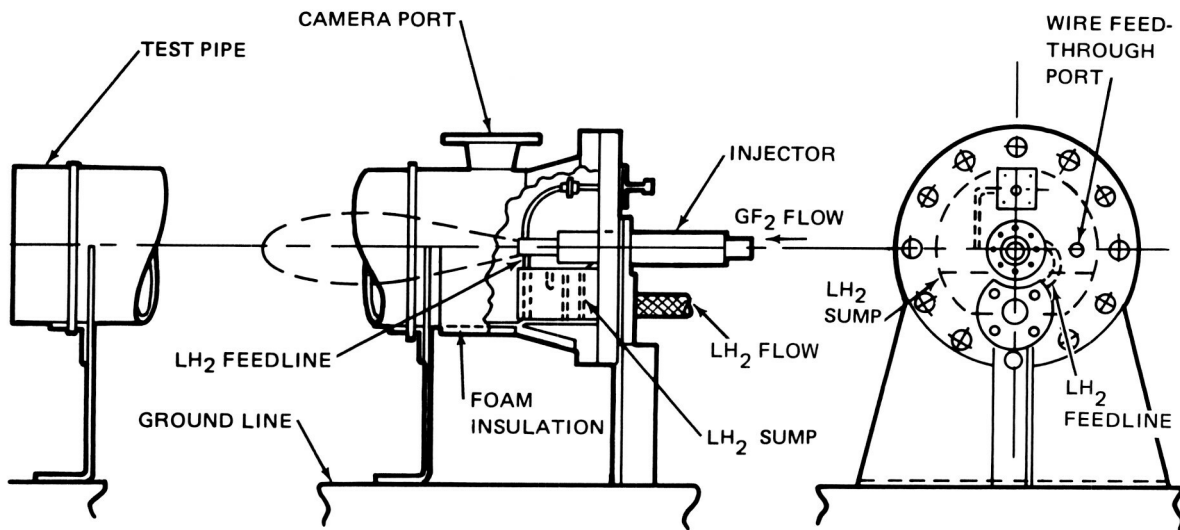
Figure 19. Injector Demonstration Test Apparatus
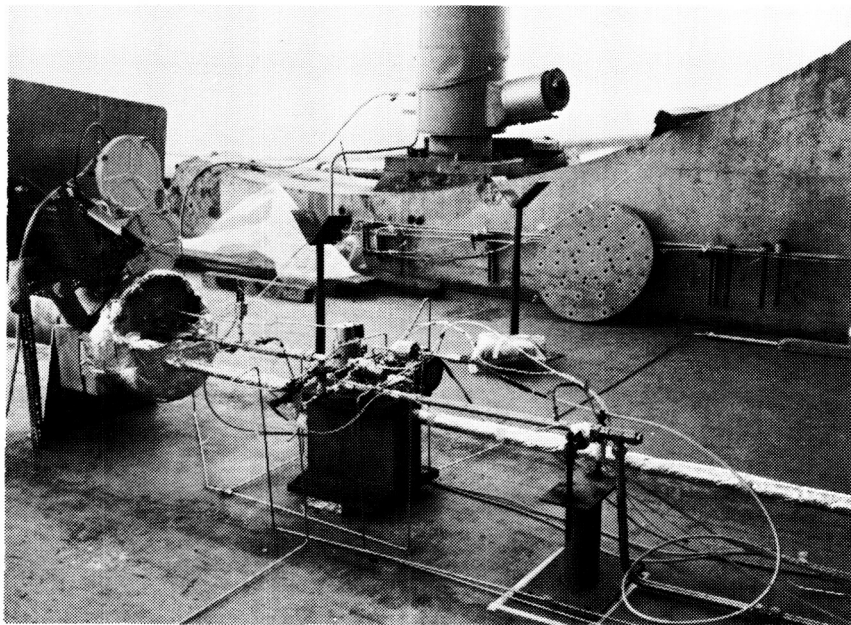
Figure 20. Installation of Injector Test Apparatus

dropped to 2.85×10^5 N/m^2 (41.3 psia) at a time of 64 seconds (the correct regulated pressure should have been 2.35×10^5 N/m^2 [34 psia]).

During the short ON cycle (0.1 second ON, 0.9 second OFF), the first stage temperature increased to 350°K (625°R) and the second stage temperature dropped to 775°K (1,394°R). The regulated GF$_2$ pressure cycled between 2.73×10^5 N/m^2 (30.6 psia) and 1.03×10^5 N/m^2 (15 psia). It appeared that the injector valve was open too short a time (0.1 second) to allow the pressure to reach the 3.45×10^5 N/m^2 (50 psia) overshoot; consequently, the injector temperature decreased to 775°K (1,394°R) because of the relatively long OFF time and the cooling effect of the H$_2$ in the test apparatus. However, during the long ON cycle (0.9 second ON, 0.1 second OFF), the regulator again overshot to 3.52×10^5 N/m^2 (51 psia) and oscillated between 3.52×10^5 N/m^2 (51 psia) and 2.07×10^5 N/m^2 (30 psia). The first stage temperature increased slowly to 514°K (924°R), but the second stage temperature immediately went off scale, indicating temperatures in excess of 1,650°K (2,960°R). This occurred so rapidly that it was thought the thermocouple had failed, and the test was allowed to continue, although it should have been terminated at this time. Following the test, inspection of the injector revealed that the nozzle diffuser, downstream of the second stage throat, had been damaged by overheating. Figure 21 shows the injector following the test. The LH$_2$ sump and feed line are shown. The temperature in the LH$_2$ feed line stayed at 21°K (37°R) throughout the test, although this may have been due to the cold GH$_2$ atmosphere in the test pipe. Apparently the abnormally high regulated GF$_2$ pressure of 3.52×10^5 N/m^2 (51 psia) had reduced the LH$_2$ pumping (aspiration) pressure difference, leading to reduced LH$_2$ flow, higher injector O/F ratio, and excessive temperatures. Injector failure probably did not occur during the initial overshoot to 3.45×10^5 N/m^2 (50 psia) during the

60-second continuous run because the injector was cold, and its thermal capacity allowed the injector to survive until the regulated GF_2 pressure dropped to a lower value.

The injector damage is shown in Figure 22. The view is in the direction of flow and shows the LH_2 pumping annulus (the LH_2 inlet port is top center). Detailed examination of the injector revealed that the damage was fortunately confined to the nozzle diffuser. The delicate expansion region of the second stage throat, although covered with molten metal, was essentially undamaged and was refurbished without replacement. The damaged diffuser was cut off the injector and a new nozzle diffuser was fabricated and welded to the injector, together with an additional thermocouple on the second stage.

It should be noted that the injector pumping ability is very sensitive to second-stage temperature. This is because higher temperatures in the LH_2 pumping region tend to vaporize some of the LH_2 in contact with the pumping annulus, which reduces the LH_2 pumping effectiveness, leading to less LH_2 flow, higher O/F ratios and temperatures, and so forth. This is discussed in detail in the section, Analysis and Comparison of Injectors.

PRESSURIZATION TESTS

The regulator overshoot and subsequent injector failure during the firing test indicated the need for a number of operational changes; these were implemented in the tank pressurization tests. During the injector sequence checks of the pressure switches, the regulator was adjusted under flow to give the correct regulated pressure during overshoot under dynamic (cycling) conditions. In addition, the regulated pressure was viewed as a redline (shutdown) parameter in which, if the regulated pressure were to exceed 120 percent of the correct value (based on tank pressure), the GF_2 flow would be terminated. The firing
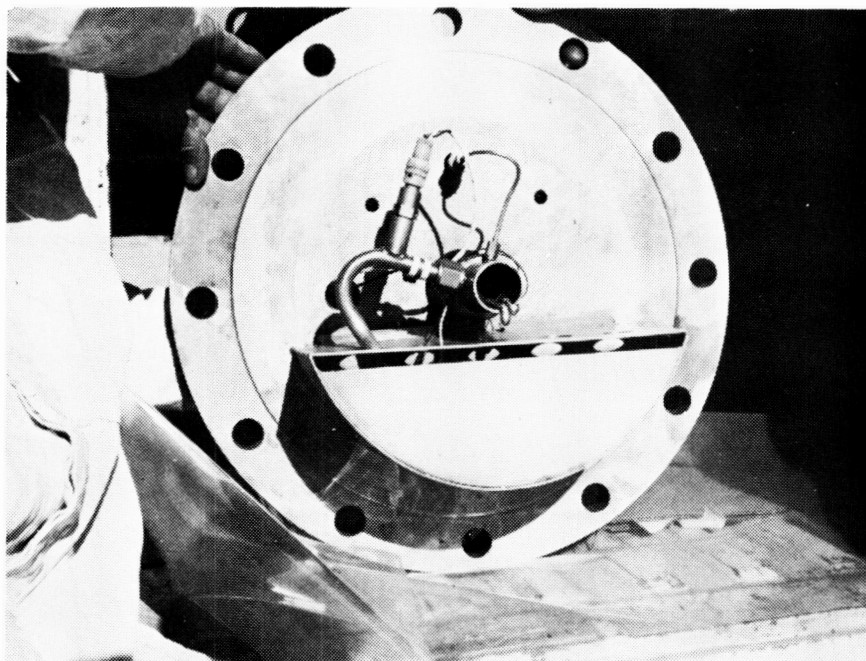
Figure 21. Injector Installation Following Firing Test

Figure 22. Injector Damage From Firing Test

48

test data indicated that the second stage temperature stabilized at a value about 279°K (500°R) less than the theoretical combustion temperature at the presumed O/F ratios which occurred; therefore, for the nominal O/F ratio of 1.8:1 (maximum at a GF_2 pressure of 6.9×10^5 N/m^2 [100 psia]), the second stage temperature was redlined at 1,300°K (2,350°R). It was for redline reasons that a redundant thermocouple was added to the second stage. Further, as was done during the NAS3-13306 tests, the tank ullage pressure was redlined at 3.45×10^5 N/m^2 (50 psia), the ullage gas temperature at 555°K (1,000°R), and the tank wall temperature at 500°K (900°R).

The pressurization test sequence was also altered, so that the 5-percent ullage tests were scheduled first and the 90-percent tests, potentially more prone to injector failure from LH$_2$ starvation, were scheduled last. The revised test sequence is presented in Table 2. The

Table 2

PRESSURIZATION TEST SEQUENCE

Test	Similar NAS3-13306 Test	Tank Pressure (10^4 N/m^2)	(psia)	LH$_2$ Out-flow Rate (kg/ sec)	(lb/ sec)	Ullage (%)	Hold
1	5	30	43	6.8	15	5 to 50	None
2	6	30	43	6.8	15	50 (warm) to empty	None
3	2	30	43	6.8	15	50 to empty	60 sec
4	4	30	43	6.8	15	5 to empty	None
5	7	17	25	2.3	5	5 to empty	60 sec
6	14	17	25	2.3	5	50 to empty	None
7	11	17	25	2.3	5	90 to empty	60 sec

straight-pipe tests of Contract NAS3-13306, which were conducted under similar operating conditions, are shown (also see Reference 2). The test conditions were made as similar as possible in order to more directly compare the performance of the straight-pipe and NAR injectors.

All tests were conducted according to MDAC Countdown Manual—Site 4 (MDAC Drawing 1T17020) requirements. Prior to the tank pressurization tests, the GF_2 system was passivated with GF_2 at 69×10^4 N/m^2 (100 psia) and all GF_2 control components were exercised. Injection sequence checks were made to verify proper operation of the injection loop and pressure switches, and to verify that the GF_2 regulator delivered the correct pressure (approximately 67×10^4 N/m^2 [97 psia] at 30×10^4 N/m^2 [43 psia] in the dome or tank). The tank was loaded with LH_2 and checked for leakage. All LH_2 flow control valves were exercised and all instrumentation was checked for proper functioning.

In the first test attempt, the prepressurization occurred normally, but when initiation of LH_2 outflow was attempted, the main LH_2 flow control valve failed to open. Pressurization was terminated and the tank was vented. The flow control valve then opened normally and was left open. The LH_2 outflow was henceforth initiated by opening the downstream LH_2 rapid-unloading valve, although the outflow rate was controlled by modulating the main flow control valve.

Unfortunately, on the initial aborted pressurization test, the sensing line from the injector second stage static pressure tap to the transducer was burned off. Examination of the line indicated that the probable cause was that the initial surge of GF_2 through the injector pushed a flame front up the GH_2-filled sensing line. The static pressure

transducer henceforth actually indicated tank pressure, but this was
not detected during the test series because it had been anticipated
that the static pressure would probably be close to tank pressure
(as was the case in the injector firing test).

The overall MTI test results are shown in Table 3. The times shown
are the times following initial tank pressure rise until the pressure
switch actuated, then the time at which outflow began, and then the
time at which a sensor at a particular level indicated the exact ullage
volume. The tank pressures shown in parentheses are not necessarily
the exact pressures at that time, but indicate the low point of the initial
pressure band (the most extreme). The LH_2 outflow rate is the average
between the time given and the previous time (e.g., for Test 1, between
t = 4 seconds and 51 seconds, the average LH_2 outflow rate was 6. 13 kg/
sec [13.5 lb/sec]). The cumulative GF_2 consumption is shown for each
time, as are the maximum ullage and wall temperatures.

The MTI control system performed in a nominal manner, exactly as it
had in the NAS3-13306 tests. This was because the response of the
control system is strongly dependent on the pressure switch response,
which did not change. Figure 23 shows the tank pressure history for
Test 4 (5-percent initial ullage) during prepressurization and outflow,
together with the regulated GF_2 pressure history. Despite the very
rapid prepressurization (~4 seconds), the control system maintains a
tank pressure band of about 2×10^4 N/m^2 (3 psia) which soon narrows
to less than 1.4×10^4 N/m^2 (2 psia). Note the abrupt change in the
slope of the tank pressure decay from hold to outflow. The regulated
GF_2 pressure has a characteristic response caused by initial over-
shoot with the regulator wide open when the injector valve opens. This
is followed by a period of roughly constant pressure until the tank
pressure increases sufficiently to overcome the regulator seal friction

51

Table 3

PRESSURIZATION TEST DATA SUMMARY

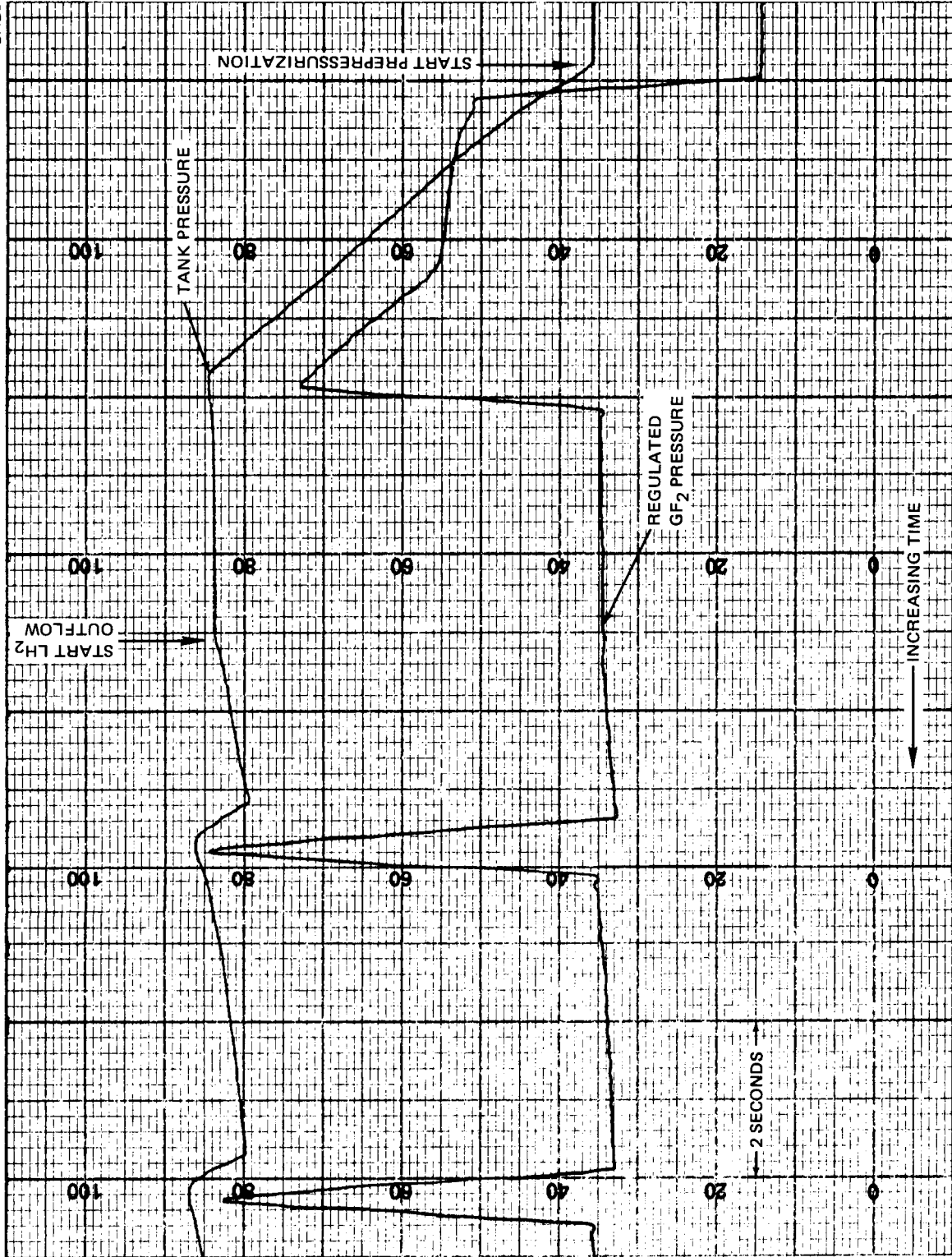| Test	Time (sec)	Tank Pressure (10⁴ N/m²)	Tank Pressure (psia)	Ullage Volume (m³)	Ullage Volume (ft³)	Average LH2 Outflow Rate (kg/sec)	Average LH2 Outflow Rate (lb/sec)	Cumulative GF2 Consumption (kg)	Cumulative GF2 Consumption (lb)	Maximum Ullage Temperature (°K)	Maximum Ullage Temperature (°R)	Maximum Wall Temperature (°K)	Maximum Wall Temperature (°R)	Remarks
1	0	11.7	17.0	3.0	106	Start Prepressurization		-	-	22.8	41	29.5	53	Warm ullage initially
	4	29.0	42.0	3.0	106			0.0975	0.215	38.4	69	29.5	53	
	51	(27.2)	(39.4)	7.2	255	6.13	13.5	0.429	0.942	51.1	92	35.0	63	
	99	29.3	42.5	11.4	404	6.00	13.2	0.714	1.572	71.6	129	40.6	73	
	146	29.3	42.5	15.1	553	6.13	13.5	1.088	2.396	92.8	167	50.0	90	
2	0	25.9	37.6	15.1	553	Start Prepressurization		-	-	96.1	173	62.8	113	
	2	29.1	42.2	15.1	553	Hold		0.0704	0.155	96.1	173	62.8	113	
	8	(27.6)	(40.0)	15.1	553			0.0704	0.155	96.6	174	62.8	113	
	60	29.0	42.0	19.9	702	5.54	12.2	0.511	1.124	111.1	200	66.6	120	
	105	29.0	42.0	24.1	851	6.40	14.1	0.906	1.996	129.5	233	71.6	129	
	146	29.0	42.0	26.9	950	4.68	10.3	1.390	3.061	147.8	266	77.2	139	
3	0	12.4	18.0	15.1	553	Start Prepressurization		-	-	26.5	48	71.6	129	
	10	28.5	41.3	15.1	553	Hold		0.253	0.557	53.9	97	71.6	129	
	101	(28.0)	(40.5)	15.1	553			0.340	0.749	82.8	149	75.5	136	
	151	29.0	42.0	19.9	702	5.76	12.7	0.700	1.542	97.2	175	79.4	143	
	194	29.0	42.0	24.1	851	6.72	14.8	1.038	2.285	116.1	209	86.6	156	
	221	29.0	42.0	26.9	950	7.13	15.7	1.540	3.390	134.5	242	90.0	162	
4	0	11.7	17.0	3.0	106	Start Prepressurization		-	-	21.7	39	36.7	66	Stopped GF2 injection at t ~ 187 seconds because of spurious redline. Attempted restart for 10 seconds, then again stopped injection.
	4	28.6	41.4	3.0	106	Hold		0.098	0.216	36.7	66	36.7	66	
	7	(26.8)	(38.8)	3.0	106			0.098	0.216	36.7	66	36.7	66	
	67	29.0	42.0	7.2	255	4.81	10.6	0.651	1.436	55.5	100	44.5	80	
	112	28.3	41.0	11.4	404	6.40	14.1	0.940	2.071	75.5	136	51.7	93	
	160	28.3	41.0	15.1	553	6.04	13.3	1.273	2.803	93.4	168	58.9	106	
	209	22.9	33.2	19.9	702	5.90	13.0	1.518	3.340	105.0	189	62.8	113	
	265	22.8	33.0	24.1	851	5.18	11.4	1.805	3.975	107.2	211	71.6	129	
	317	19.0	27.5	26.9	950	3.72	8.2	1.805	3.975	124.0	223	79.4	143	
5	0	12.1	17.6	3.0	106	Start Prepressurization		-	-	23.3	42	29.5	53	
	3	20.0	29.0	3.0	106	Hold		0.0432	0.095	36.7	66	29.5	53	
	73	(18.4)	(26.6)	3.0	106			0.0432	0.095	45.6	82	40.0	72	
	192	20.1	29.2	7.2	255	2.41	5.3	0.174	0.383	67.8	122	51.7	93	
	321	20.0	29.0	11.4	404	2.22	4.9	0.348	0.767	91.1	164	61.1	110	
	449	19.3	28.0	15.1	553	2.27	5.0	0.632	1.392	105.6	190	68.4	123	
	585	19.3	28.0	19.9	702	2.27	5.0	0.959	2.112	120.6	217	79.5	143	
	709	19.3	28.0	24.1	851	2.32	5.1	1.286	2.832	138.4	249	88.4	159	
	797	19.3	28.0	26.9	950	2.18	4.8	1.612	3.552	156.8	282	95.5	172	
6	0	11.25	16.3	15.1	553	Start Prepressurization		-	-	28.9	52	53.3	96	
	9	19.7	28.5	15.1	553	Hold		0.137	0.301	58.9	106	53.3	96	
	34	(18.8)	(27.3)	15.1	553			0.159	0.350	82.2	148	57.2	103	
	170	19.5	28.3	19.9	702	2.14	4.7	0.361	0.795	95.0	171	70.0	126	
	287	19.3	28.0	24.1	851	2.45	5.4	0.653	1.438	110.6	199	79.5	143	
	393	19.3	28.0	26.9	950	1.82	4.0	0.980	2.179	130.0	234	88.3	159	
7	0	11.4	16.5	26.9	950	Start Prepressurization		-	-	50.6	91	86.6	156	
	18	19.4	28.1	26.9	950	Hold		0.276	0.607	82.8	149	86.6	156	
	113	(18.9)	(27.4)	26.9	950			0.298	0.657	107.3	193	93.9	169	

52

Figure 23. MTI Control System Response—5% Ullage

53

and provide regulation. The regulated pressure then follows (with some lag) the increasing tank pressure. The ON time fraction is quite low (<10 percent during outflow and <2 percent during hold). Figure 24 shows the control system response for prepressurization of 50-percent ullage. Again, the tank pressure decay during hold is very slow, and the regulated pressure follows the same characteristic response curve. Figure 25 shows the dramatic change in injector valve cycle rate and ON time fraction when outflow starts. It was noted in all tests that tank pressure was controlled to within 0.69×10^4 N/m^2 (1.0 psia) under essentially all conditions.

During the testing, it was observed that the GF_2 usage and the ullage temperatures were very low (about half) compared to those of the straight-pipe tests under Contract NAS3-13306. Detailed analysis and correlation of the GF_2 usage and ullage temperature history is described in the next section, Analysis and Comparison of Injectors. While testing was in progress, it was thought that the injector was aspirating as designed, with GH_2 mass addition to the ullage responsible for keeping the ullage temperatures low, thus reducing GF_2 usage. However, following the test series, which demonstrated excellent pressurization characteristics in every respect, the injector was removed from the tank and it was found that the nozzle diffuser downstream of the second stage throat was again damaged by overheating (see Figure 26). The LH_2 pumping annulus was melted, and the damage was virtually identical to that sustained during the injector firing test. The melting was again apparently caused by insufficient pumping of LH_2 in the second stage.

Analysis of the data indicated the regulator (which was suspected of causing the damage in the injector firing test) had performed in a nominal fashion. The injector thermocouples indicated steadily increasing
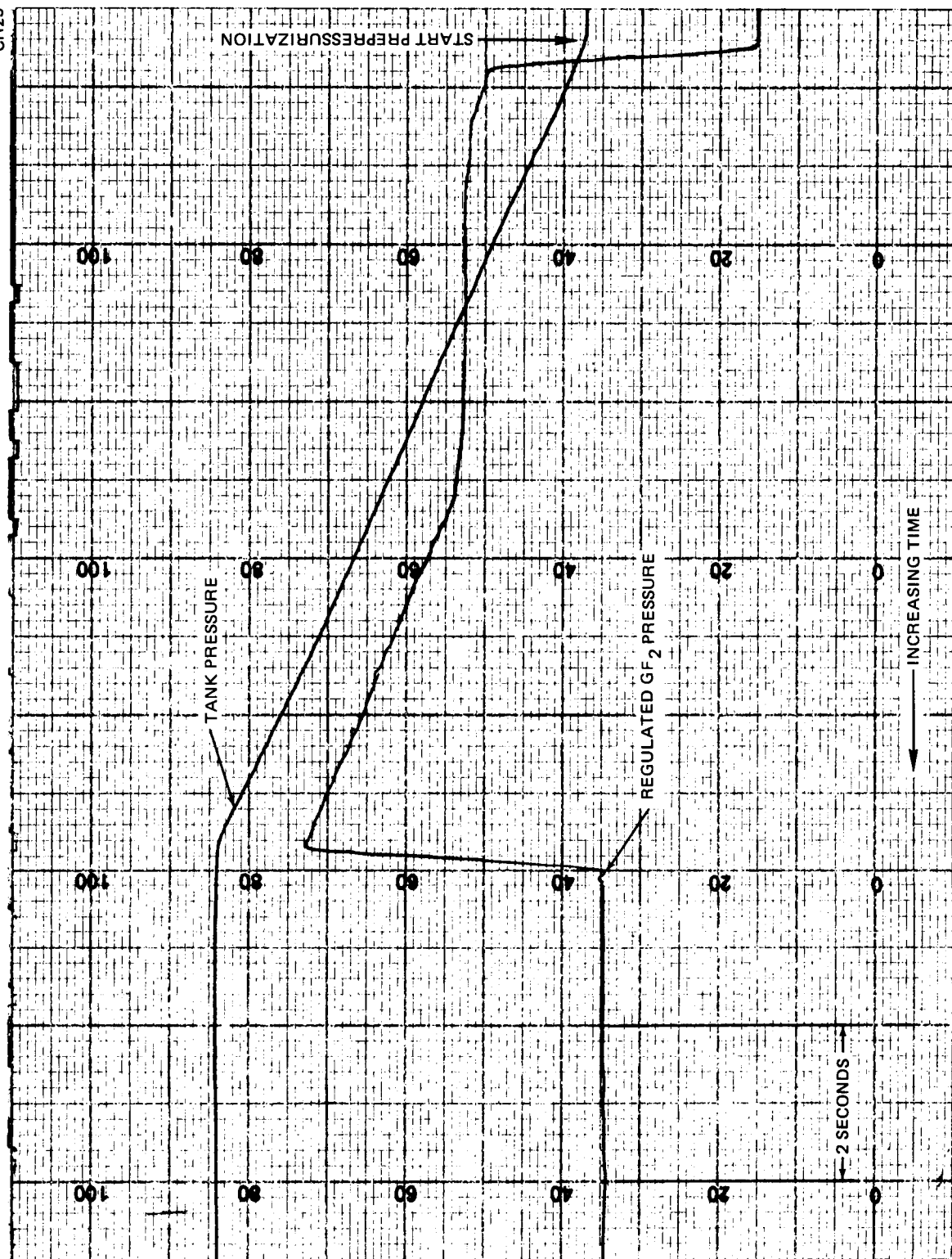
Figure 24. MTI Control System Response—50% Ullage Prepressurization
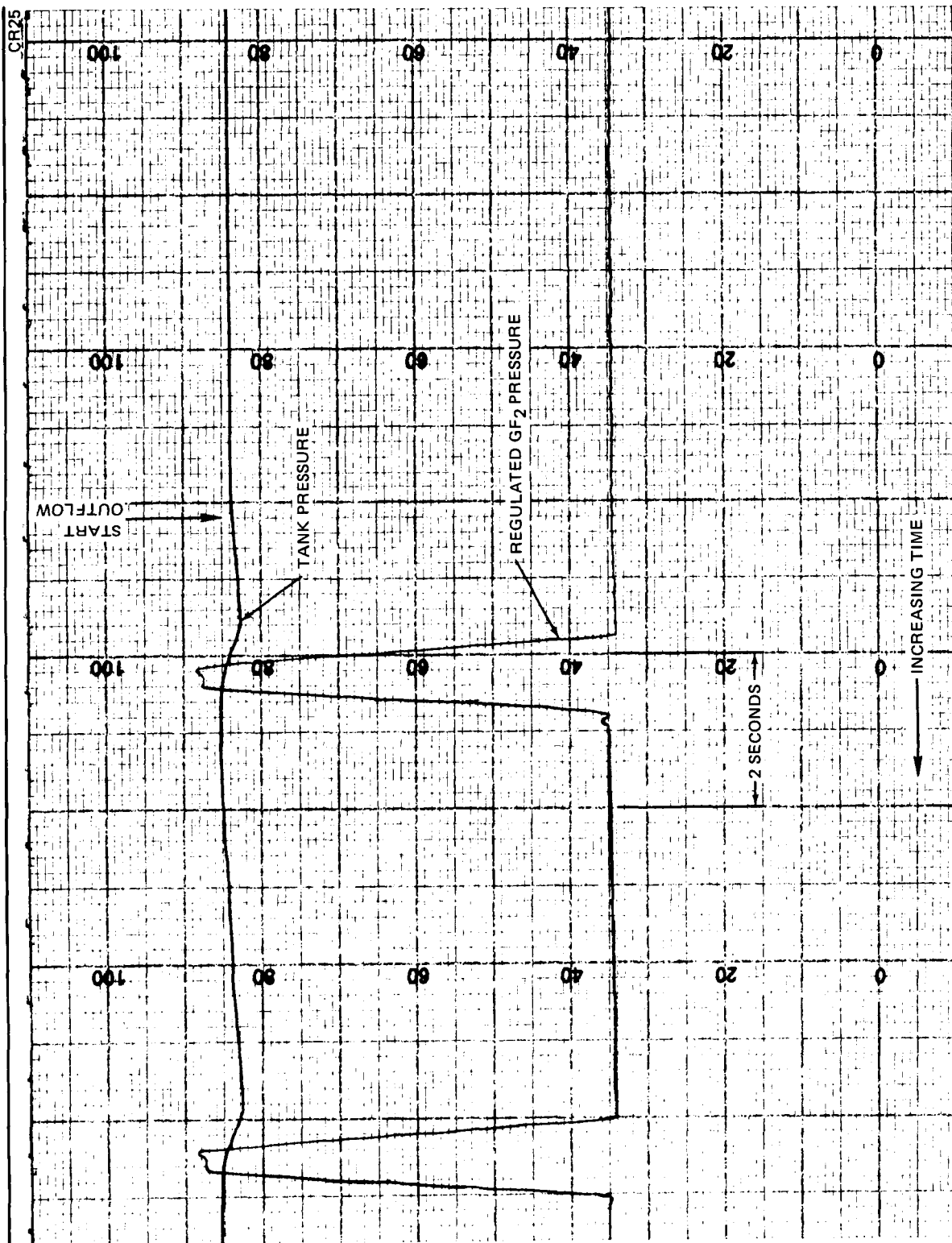
55

Figure 25. MTI Control System Response—50% Ullage—Outflow

56

Figure 26. Injector Damage from Pressurization Tests

temperatures (as soon as GF_2 injection began) but stayed below the redline values. The most informative data were obtained from the temperature transducer (TL9) in the LH_2 feed line to the injector. The data from two tests are shown in Figure 27 on a vertical scale of 19.5°K (35°R) to 89°K (160°R). Figure 27(a), for 5-percent initial ullage (test 5) with the tank nearly full, shows the initial temperature in the LH_2 line to be 20°K (36°R). Immediately following injection, the temperature jumped upward. This jump is attributed to backflow in the LH_2 line caused by the initial surge of GF_2. Following this initial transient, the injector did pump LH_2, as evidenced by a temperature drop to 21°K (38°R). However, as soon as GF_2 flow was terminated following prepressurization, the LH_2 line temperature jumped to a value of 69.5°K (125°R) which was an approximate equilibrium temperature determined by the injector temperature (~108°K [194°R]) and the ullage gas temperature (~36.7°K [66°R]) following prepressurization. The LH_2 line temperature stayed at about 55°K (100°R) throughout the hold period because the injector valve did not cycle. However, as soon as LH_2 outflow started and the injector valve cycled, the injector tried to aspirate (note the temperature dip) but the LH_2 line temperature immediately went off scale when injection ceased for that cycle. This indicates that the injector can pump LH_2 during steady-state operation with small ullages, but cannot aspirate LH_2 when the injector becomes warm during cyclic operation.

Figure 27(b) shows the temperature history of the LH_2 line for 90-percent initial ullage (test 7) with the tank nearly empty. The initial temperature in the LH_2 inlet line was 30°K (54°R). During the 18-second prepressurization, the injector pumped GH_2, as evidenced by the drop in temperature to 27.5°K (49.5°R) which is more than 5.5°K (10°R) above the saturation temperature at 19.3×10^4 N/m^2 (28 psia). Again, following injection termination at the end of prepressurization, the temperature jumped to the vicinity of 50°K (90°R) where it pulsed
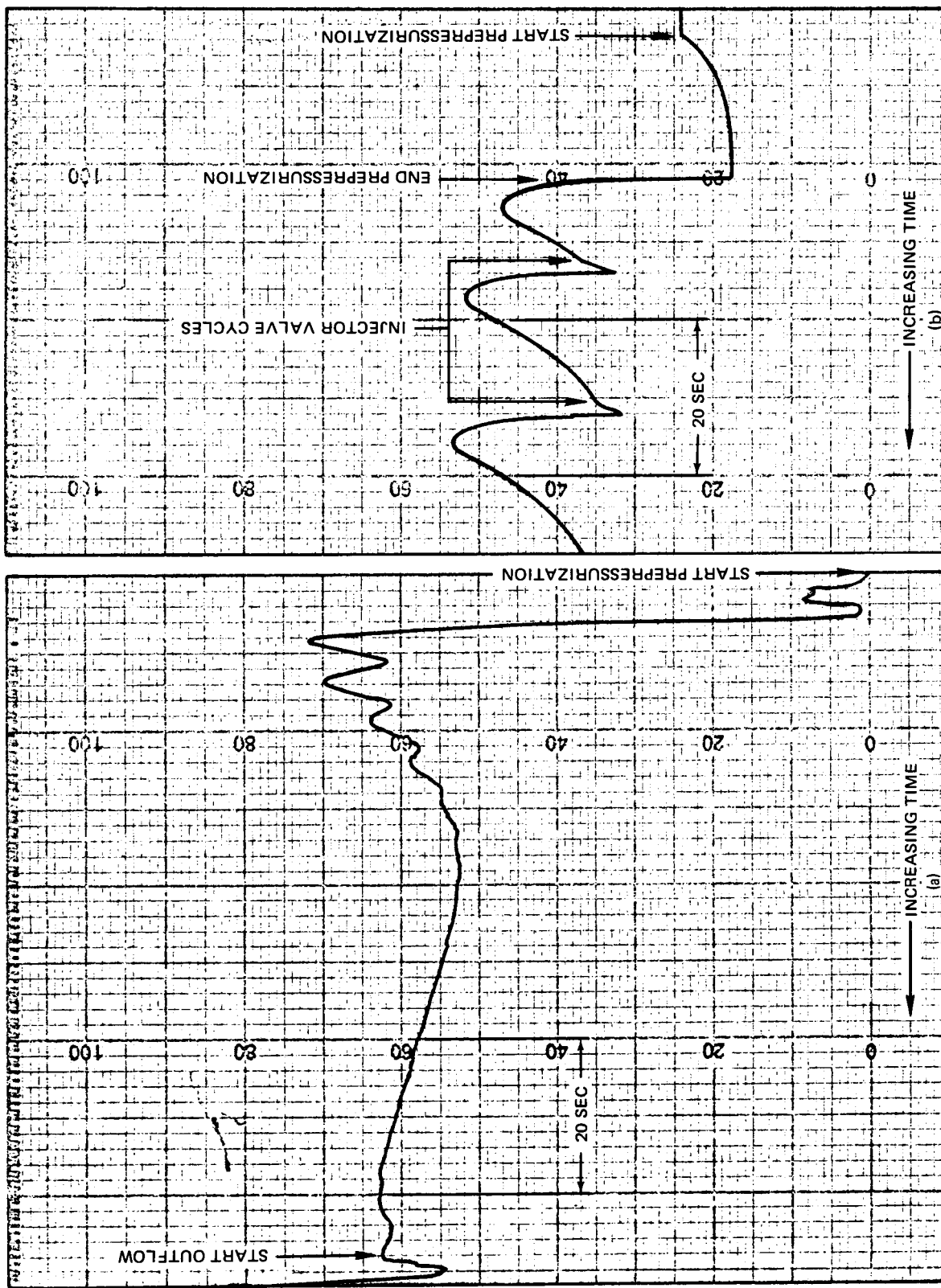
Figure 27. Injector LH$_2$ Line Temperature History

59

sharply downward with each injection cycle. This indicates that the injector was unable to pump LH_2 up 5.8 m (19 ft) through the relatively warm ullage during the rather brief prepressurization.

It was probable that the injector damage occurred progressively throughout the test series, although a significant percentage of the damage may have occurred during the last test. The reason for this (and the basic reason for injector damage) was that the injector was designed to operate fuel-rich, at an O/F weight ratio of about 1.8:1, when pumping LH_2. The equilibrium combustion temperature at an O/F ratio of 1.8:1 is 1,580°K (2,840°R), below the nickel 200 melting temperature of 1,715°K (3,090°R). If the injector pumped saturated H_2 vapor (rather than LH_2) through the same pumping area, the O/F ratio would be 36:1 at a tank pressure of 30×10^4 N/m^2 (43 psia) with an equilibrium combustion temperature of 3,060°K (5,500°R). In addition, in the transition from LH_2 to GH_2 pumping, the injector O/F ratio could pass through stoichiometric (O/F = 19) with an equivalent combustion temperature of 4,160°K (7,500°R).

In test 7, when the injector was pumping H_2 vapor at 27°K (49°R), assuming the design pumping area, the injector was operating at an O/F ratio of about 70 (with an equivalent combustion temperature of 1,720°K [3,100°R] for up to 18 seconds. If the pumping area was larger (from annulus melting), more GH_2 would have been pumped, with a lower O/F ratio and higher combustion temperatures. Interestingly, the minimum LH_2 flow area was the same after the testing damage as it was before. Although the annulus area was increased by melting from 0.449×10^{-4} m^2 (0.0696 in.^{2}) to 9.76×10^{-4} m^2 (1.512 in.^{2}), the LH_2 inlet fitting was partially plugged by molten metal, reducing the original area of 0.895×10^{-4} m^2 (0.1386 in.^{2}) to 0.448×10^{-4} m^2 (0.0693 in.^{2}). However, the flow area was probably

generally larger than the minimum during the testing so that the temperatures downstream of the second stage were probably in excess of 1, 720°K (3, 100°R), hence the melting of the nozzle diffuser.

The data indicate that the injector only pumps LH_2 during prepressurization at 5-percent initial ullage. The consequences of this for pressurization are shown by the examples in Table 4.

It can be seen that the quantity of H_2 pumped into the ullage by the injector is insignificant (and immeasurable) compared to the evaporated mass or the total ullage mass in all cases. Therefore, it appears that the injector did not perform its function of jet-pumping significant quantities of H_2 into the ullage. However, the NAR injector did display superior pressurization performance, compared to the straight-pipe injector, with lower ullage temperatures and reduced GF_2 usage. The reasons for this superior performance are that design features of the injector result in greater injection jet penetration, ullage mixing, and increased LH_2 interface mass addition. These factors alone are the reasons for the superior performance, as will be described and analyzed in detail in the following section, Analysis and Comparison of Injectors.

Table 4

INJECTOR H_2 PUMPING PERFORMANCE

	GF_2 Usage*		Minimum O/F	H_2 Pumped into Ullage	
	(kg)	(lb)	Ratio	(kg)	(lb)
5-Percent Ullage					
Prepressurization	0.098	0.216	1.8:1	0.0545	0.120
Outflow	2.31	5.1	36:1	0.0645	0.142
				0.119	0.262
H_2 added to ullage by interface evaporation**				9.5	21
Total ullage mass**				12.7	28
50-Percent Ullage					
Prepressurization and Outflow	1.75	3.85	36:1	0.0486	0.107
H_2 added to ullage by interface evaporation**				0	0
Total ullage mass**				19.5	43
90-Percent Ullage					
Prepressurization (low pressure)	0.276	0.607	70:1	0.004	0.0087
H_2 added to ullage by interface evaporation**				0	0
Total ullage mass**				26.3	58

*See Table 3
**See discussion on mass balance in Analysis and Comparison of Injectors section.

ANALYSIS AND COMPARISON OF INJECTORS

The basic MTI pressurization analysis (MDAC computer code H819)
developed under contract NAS3-13306 is reviewed in this section,
followed by a comparison of experimental data from the straight-pipe
tests (NAS3-13306) with data from the NAR injector tests. The analytic
techniques required for correlation of the experimental data from the
NAR injector pressurization tests are then discussed, followed by a
description of the modifications of the H819 computer code required to
allow performance prediction for straight-pipe, diffuser, and jet-pump
injector types over the full range of hydrogen-fueled space vehicles.

BASIC ANALYSIS

The complete derivation of the MTI pressurization analysis is presented
in Reference 2. Only the basic equations are summarized in this
subsection.

The tank, propellant, and ullage are represented by a one-dimensional
model. Variations in temperature and temperature-dependent proper-
ties occur only along the vertical tank axis with no radial or circumfer-
ential variations. This model is the basis for several analyses of
conventional heated-gas tank pressurization (References 4, 5, 6) and
its validity is well established. Buoyant forces caused by gravity or
vehicle acceleration tend to produce a stable thermal stratification in
the gas and liquid, resulting in a temperature distribution that is
essentially one-dimensional.

The computations are based on a finite difference representation of the physical system. The tank wall, internal hardware, propellant, and ullage are each divided by horizontal planes into a number of nodes, as shown schematically in Figure 28, with the properties within each node being uniform. The axial thickness and location of the gas and liquid nodes can vary during the solution, while the wall and hardware nodes are of equal thickness and fixed.

Ullage mixing is a key feature of the MTI analysis. The injectant inflow causes gas mixing in the region near the injector, resulting in a nearly uniform temperature in the top part of the ullage. This mixed zone is represented by the large, single, upper gas node shown in Figure 28. Nonuniformities exist directly in the injectant flow path, particularly with the MTI flame; however, in the vicinity of the wall heat transfer surface, a nearly uniform temperature is maintained in the mixing zone.

The extent of the mixed ullage region is directly related to the depth of penetration into the ullage of the downward-flowing injectant jet. The velocity of this jet decreases with distance from its origin due to buoyancy because it is at higher temperature and lower density than the ullage and because of viscous mixing with the surroundings. These processes slow the jet to a zero axial velocity at some point, which is the jet penetration limit. An analysis for predicting this jet penetration depth was developed initially for nonreacting jets (Reference 7) and was extended to the reacting MTI case.

The basic equation for the deceleration of the jet centerline velocity due to buoyancy is

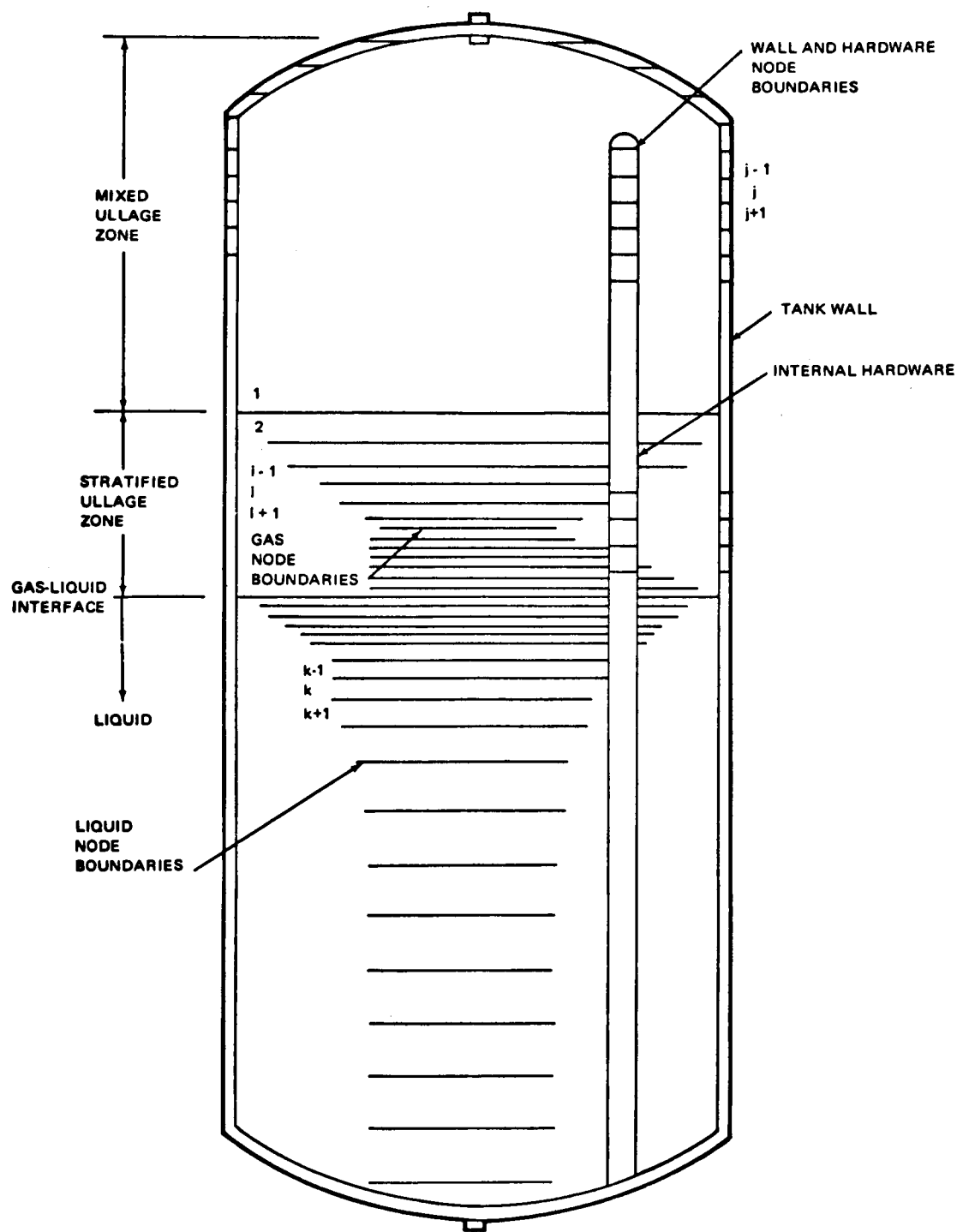$$1/2 \; \rho_j \; d(U_j^2) = a(\rho_j - \rho_u) \; dX \tag{1}$$

Figure 28. Finite Difference Node System

or

$$d(U_j{}^2) = 2a(1 - \frac{\rho_u}{\rho_j}) \, dX.$$ (2)

Because the ullage may be near LH_2 temperatures initially, a compressibility factor is included in the equation for ρ_u, but the warmer jet is assumed to be a perfect gas; Equation (2) becomes

$$d(U_j{}^2) = 2a \left(1 - \frac{T_j}{W_j} \frac{W_u}{Z_u T_u}\right) dX$$ (3)

where T_j is the temperature and W_j is the molecular weight on the centerline of the jet, both of which vary with distance X in the flame structure. The variation in velocity because of turbulent jet mixing must also be specified.

For the nonreacting jet analysis (Reference 7), the equations of Laufer (Reference 8) were used for T_j, W_j, and the velocity decay caused by jet mixing. The same equation form is used for the reacting jet. The centerline velocity variation caused only by viscous mixing is assumed to be unaffected by the MTI reaction:

$$\frac{U_j}{U_{jo}} = \frac{X_c}{X} \qquad\qquad X > X_c$$ (4)

where X_c is the velocity core length. The temperature equation is modified by using the flame length X_F as the effective temperature core length:

$$\frac{T_j - T_o}{T_{jm} - T_o} = \frac{X_F}{X} \qquad X > X_F . \qquad (5)$$

In the flame region, a linear increase in centerline temperature is assumed:

$$\frac{T_j - T_{jo}}{T_{jm} - T_{jo}} = \frac{X - X_c}{X_F - X_c} \qquad X_c < X \leq X_F \qquad (6)$$

and T_j remains equal to T_{jo} in the velocity core region $(X < X_c)$. The centerline gas composition is also given by Equations (5) and (6), replacing the left side of both by Y_j, the mass fraction of HF which is equal to one at the maximum temperature point and zero in the surrounding medium, and at the jet exit. The jet centerline molecular weight is then given by

$$W_j = \frac{W_o W_{HF}}{Y_j \left(W_o - W_{HF} \right) + W_{HF}} . \qquad (7)$$

where $W_o = W_{H_2}$ for $X > X_F$ and $W_o = W_{F_2}$ for $X_c < X \leq X_F$.

The values of X_c and X_F were determined empirically. The velocity core length was evaluated from nonreacting jet test data (Reference 9).

$$X_c = 23.0 \left[\rho_{jo} d^2 / 8 \rho_u \right]^{1/2} . \qquad (8)$$

67

The flame length was measured from photographic data taken during the NAS3-7963 tests (Reference 1) and defined as

$$X_F = X_c + 67 d \tag{9}$$

where both X_c and X_F are measured from the jet exit.

The centerline velocity-squared decrement caused by buoyancy forces on the hot, downward flowing jet is found by combining and integrating the above equations, giving three different equations for the three regions of the jet structure: the velocity core, the flame zone, and beyond the flame zone.

Velocity core zone $(X \leq X_C)$:

$$\Delta(U_j^2)_b \Big|_{X_1}^{X_2} = 2a \left(1 - \frac{T_{jo} W_{H_2}}{W_{F_2} Z_u T_u} \right) (X_2 - X_1) \tag{10}$$

Flame zone $(X_c < X \leq X_F)$:

$$\Delta(U_j^2)_b \Big|_{X_1}^{X_2} = 2a \left\{ A(X_2 - X_1) \right.$$

$$+ \frac{B}{2} \left[(X_2 - X_c)^2 - (X_1 - X_c)^2 \right] \tag{11}$$

$$\left. + \frac{C}{3} \left[(X_2 - X_c)^3 - (X_1 - X_c)^3 \right] \right\}$$

68

where

$$A = 1 - \frac{T_{jo} \, W_{H_2}}{W_{F_2} \, Z_u \, T_u}$$

$$B = - \frac{W_{H_2} \left[T_{jo} \left(W_{F_2} - W_{HF} \right) + W_{HF} \left(T_{jm} - T_{jo} \right) \right]}{W_{F_2} \, W_{HF} \, Z_u \, T_u \left(X_F - X_c \right)}$$

$$C = - \frac{W_{H_2} \left(W_{F_2} - W_{HF} \right) \left(T_{jm} - T_{jo} \right)}{W_{F_2} \, W_{HF} \, Z_u \, T_u \left(X_F - X_c \right)^2}$$

Beyond the flame zone $(X > X_F)$:

$$\Delta (U_j^{\,2})_b \, \Big|_{X_1}^{X_2} = 2a \left[D \left(X_2 - X_1 \right) + E \ln \left(\frac{X_2}{X_1} \right) - F \left(\frac{1}{X_2} - \frac{1}{X_1} \right) \right]$$

where

$$D = 1 - \frac{T_o}{Z_u \, T_u} \qquad\qquad (12)$$

$$E = -\frac{X_F\left[T_o\left(W_{H_2} - W_{HF}\right) + W_{HF}\left(T_{jm} - T_o\right)\right]}{W_{HF}\, Z_u\, T_u}$$

$$F = -\frac{X_F^2\left(W_{H_2} - W_{HF}\right)\left(T_{jm} - T_o\right)}{W_{HF}\, Z_u\, T_u}$$

In all regions of the jet flow, the centerline velocity-squared decrement from locations X_1 to X_2 caused by turbulent mixing with the surrounding ullage is given by

$$\Delta(U_j^2)_M\Big|_{X_1}^{X_2} = U_{jo}^2\, X_c^2\left(\frac{1}{X_2^2} - \frac{1}{X_1^2}\right) \tag{13}$$

from Equation (4). The total centerline velocity-squared decrement is the sum of the mixing and buoyancy contributions

$$\Delta(U_j^2)\Big|_{X_1}^{X_2} = \Delta(U_j^2)_M\Big|_{X_1}^{X_2} + \Delta(U_j^2)_b\Big|_{X_1}^{X_2} \tag{14}$$

where the mixing contribution is zero when $X < X_c$.

Equation (14) determines the jet penetration depth X_p at which the centerline velocity has decreased to zero. The depth of the mixed ullage zone X_{mix} may be less than X_p; therefore,

$$X_{mix} = f_m X_p \qquad (15)$$

defines a mixing fraction factor f_m, which is a measure of the effectiveness of the ullage mixing.

The jet penetration and ullage partial-mixing models are of primary importance to the overall MTI pressurization analysis. All heat released by the flame goes into the mixed zone because this is the region directly affected by the injectant flow. Forced convection heat transfer to the tank wall occurs in this region due to the agitation caused by the gas mixing. The heat and mass transfer at the gas-liquid interface are determined by the injectant jet penetration because the dominant mode of interface heat transfer results from direct impingement of the injectant flow upon the liquid surface. Other aspects of the analysis are similar to that of a conventional heated-gas pressurization system.

The MTI pressurization computer program (H819) incorporating the above features includes essentially all capabilities of existing pressurization programs: variable properties for the gas, liquid, wall, and internal hardware; unrestricted tank configuration; injectant supply system computations; operating parameters specified by either time-variable tabular inputs or internal calculations, and a number of different operating modes. In normal usage, the fluorine supply system and propellant outflow rates are specified and the computer program calculates the temperature distributions in the wall, hardware, liquid, and gas, as well as the liquid vaporization rate and tank pressure, all

of which vary with time during the solution. These data may be output from the program as frequently as desired.

COMPARISON OF INJECTORS

During pressurization testing, it was obvious that the NAR injector was maintaining a much colder ullage and was using much less GF_2 than was the case during the straight-pipe injector tests conducted under contract NAS3-13306. Fortunately, the test conditions often were practically identical for both the NAR injector and straight-pipe injector tests (see Table 2). For example, Test 2 from the NAS3-13306 tests is comparable to Test 3 from this program. Both tests had 50-percent initial ullage, operated at a tank pressure of 30×10^4 N/m^2 (43 psia), and had essentially identical LH_2 outflow rates and test times. The ullage gas temperature history for both tests is shown in Figures 29a, b, and c. It is obvious from Figures 29b and 29c that the NAR injector has greater jet penetration and ullage mixing than the straight-pipe. Figures 29b and 29c also illustrate the acceleration of temperature rise when the ullage gets warm. This leads to increased heat transfer, GF_2 demand, higher temperatures, etc., until the GF_2 flow is on all the time, which leads to in-tank circulation and stratification, as shown by Test 2 results shown in Figure 29c (Reference 2). A comparison of GF_2 usage for the tests is shown in Table 5.

Table 5
GF_2 USAGE COMPARISON

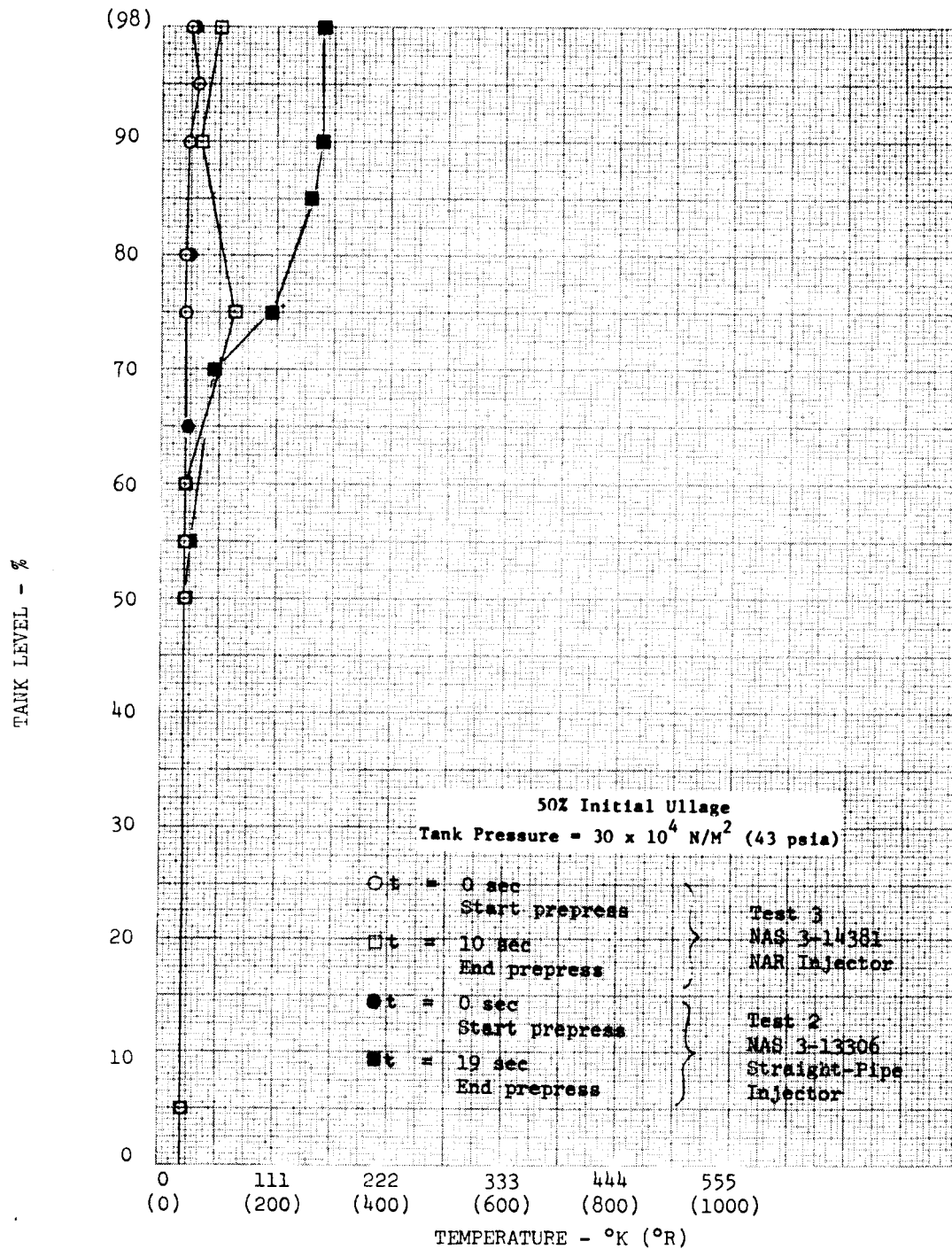| Ullage Level	Test 3, NAS3-14381 (NAR Injector)		Test 2, NAS3-13306 (Straight-Pipe)	
	kg	lb	kg	lb
End prepres-surization	0.253	0.557	0.585	1.290
50%	0.365	0.803	0.785	1.730
35%	0.765	1.687	1.650	3.630
20%	1.145	2.522	2.550	5.630
10%	1.750	3.850	3.030	6.680

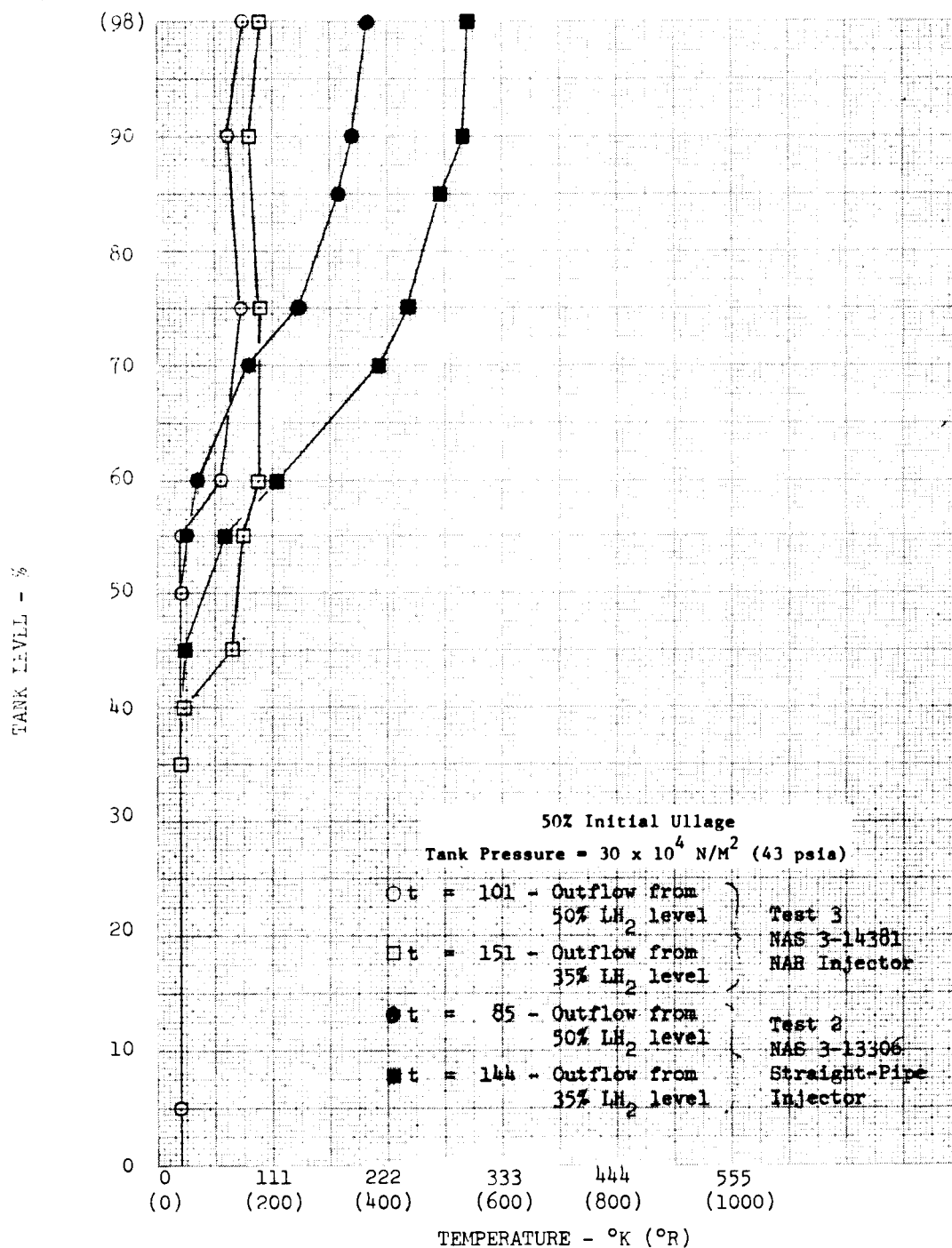Figure 29a. Ullage Gas Temperature Comparison, 50-Percent Ullage

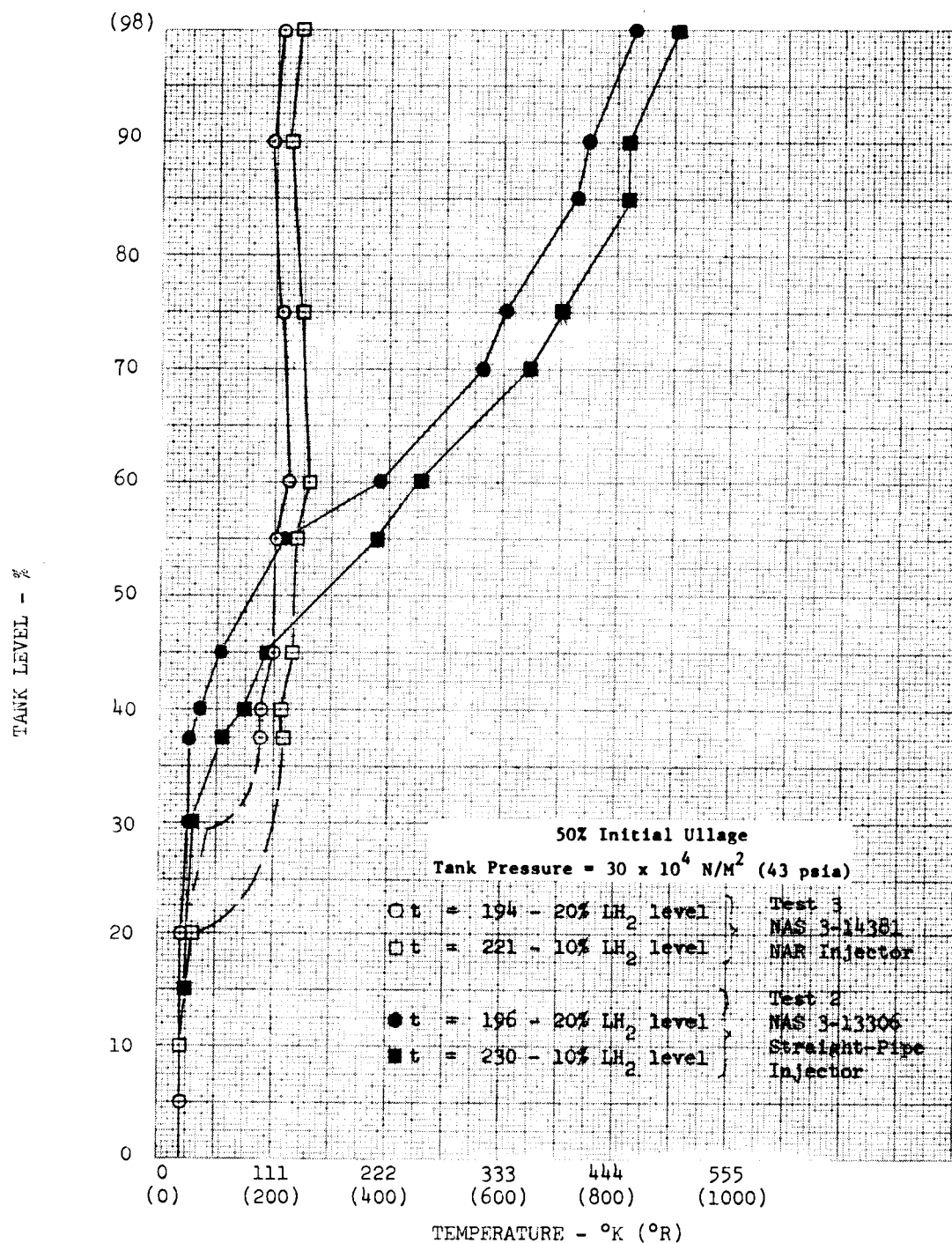Figure 29b. Ullage Gas Temperature Comparison, 50-Percent Ullage

Figure 29c. Ullage Gas Temperature Comparison, 50-Percent Ullage

75

The NAR injector consistently used about half as much GF_2 as the straight-pipe injector, which is a direct indication of the NAR injector's superior jet penetration and mixing, and demonstrates the importance of these parameters.

Test 7 from the NAS3-13306 tests and Test 5 from this program also were compared. Both tests had 5-percent initial ullage, operated at a tank pressure of 18.6×10^4 N/m^2 (27 psia), and has essentially identical LH_2 flow rates and test times. The ullage gas temperature history for these tests is shown in Figures 30a, b, c, and d. It can be seen from Figures 30a and 30b that the temperatures and penetration for the two injectors are essentially the same down to the 65-percent level. At that point, the straight-pipe temperatures rise rapidly and diverge from the NAR injector data (see Figures 30c and 30d). This, basically, is because the NAR injector has greater evaporation of LH_2 at the interface, and therefore lower ullage temperatures. The GF_2 usage and LH_2 evaporation are compared in Table 6. The table data show that the GF_2 usage is also close, down to the 65-percent level, before the straight-pipe GF_2 usage increases rapidly. In fact, the NAR injector uses 0.036 kg (0.08 lb) more GF_2 than the straight-pipe at the 80- and 65-percent levels. This extra GF_2 goes directly into the increased LH_2 evaporation of 1.36 kg (3.0 lb) that the NAR injector shows at the 80- and 65-percent levels. (The combustion energy from 0.036 kg [0.08 lb] of GF_2 can evaporate 1.18 kg [2.6 lb] of LH_2.) For the straight pipe, the LH_2 evaporation stops at the 65-percent level (when the liquid penetration by the jet ceases), but the NAR injector, with its superior jet penetration, continues to penetrate the liquid and evaporate LH_2 down to nearly the 35-percent level. The large evaporation numbers shown in parentheses in Table 6 are in error, and are caused by the linear extrapolation from the 40-percent level down, due to inoperable temperature sensors at these levels. In actuality, the NAR
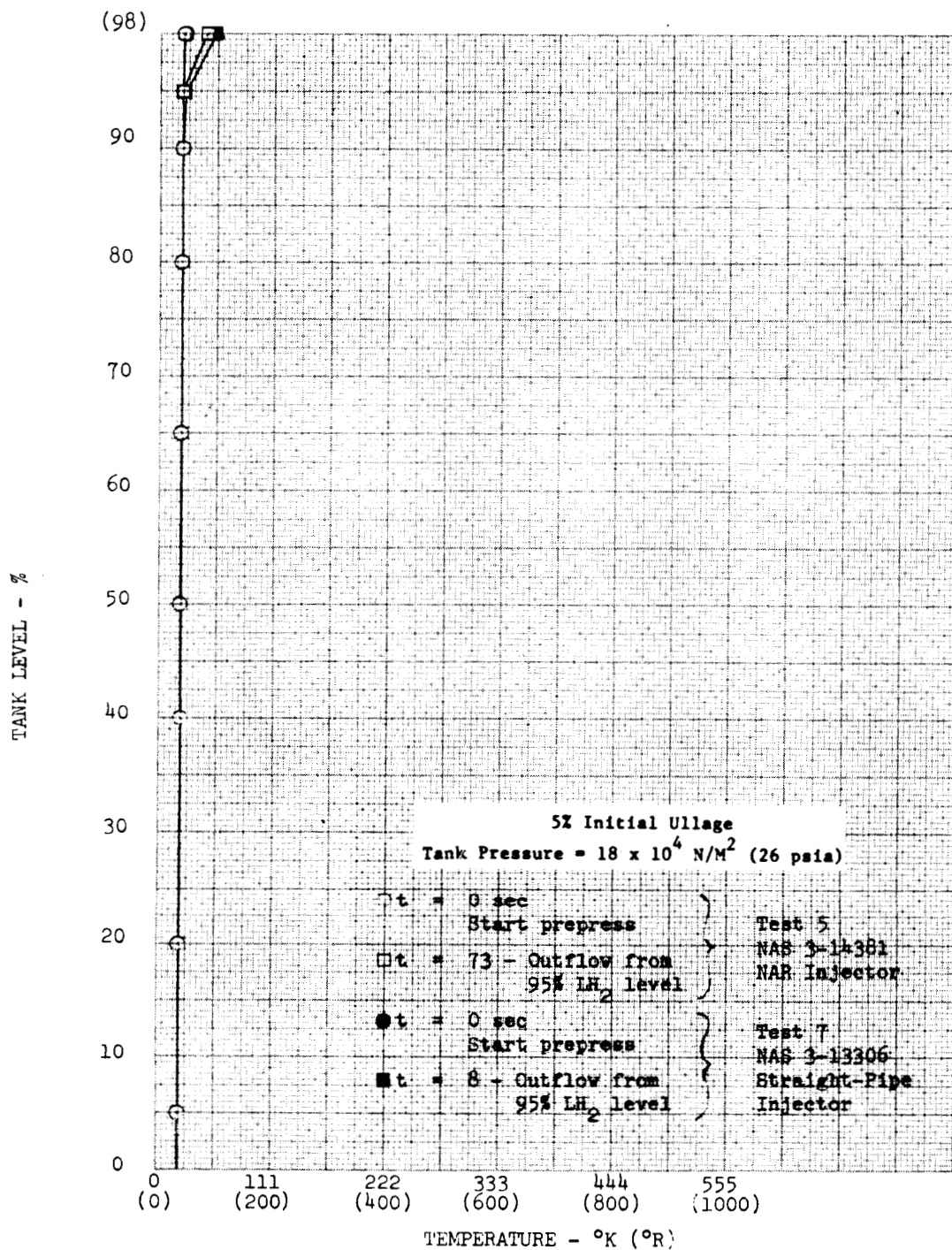
76

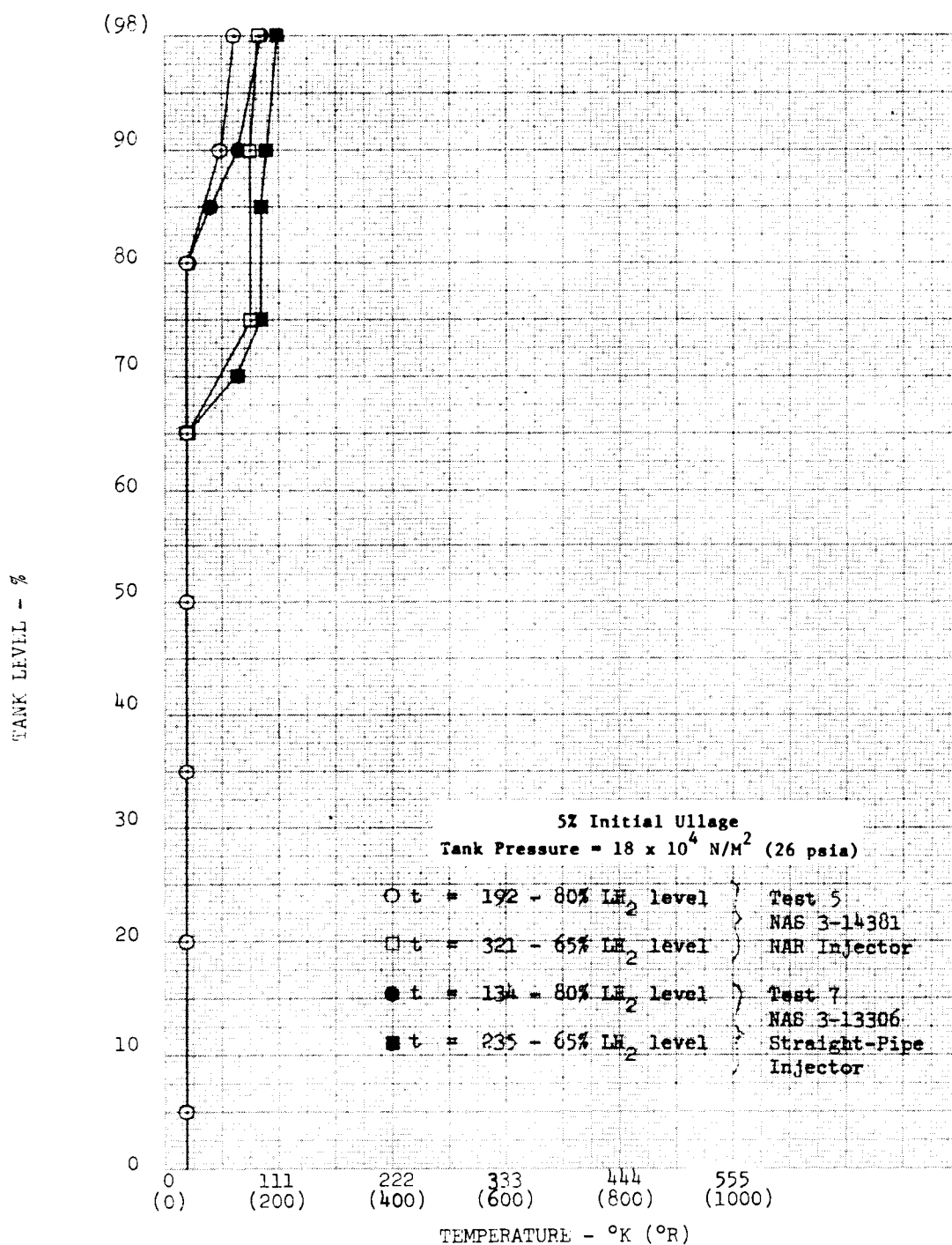Figure 30a. Ullage Gas Temperature Comparison, 5-Percent Ullage

Figure 30b. Ullage Gas Temperature Comparison, 5-Percent Ullage
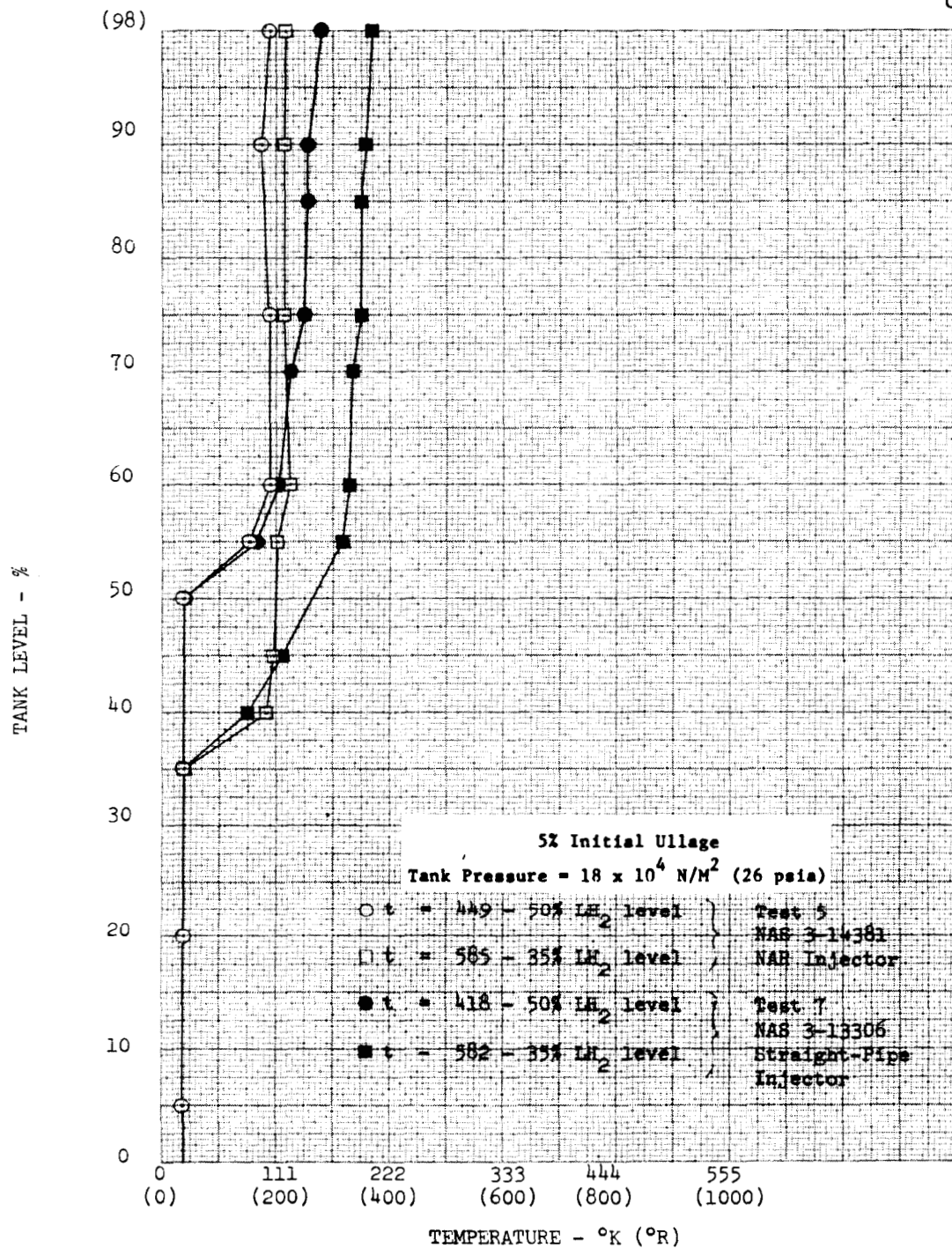
Figure 30c. Ullage Gas Temperature Comparison, 5-Percent Ullage
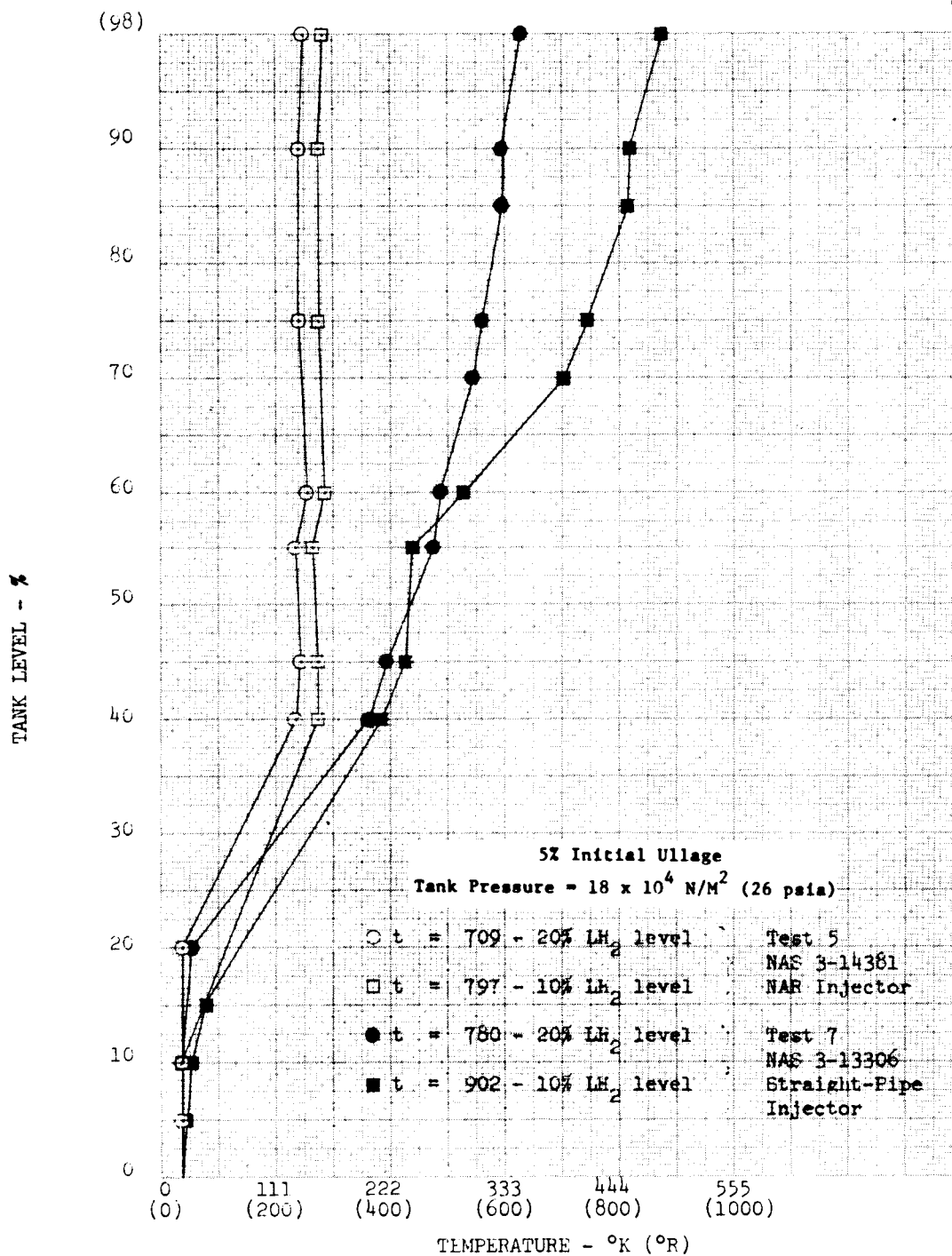
Figure 30d. Ullage Gas Temperature Comparison, 5-Percent Ullage

Table 6

COMPARISON OF GF$_2$ USAGE AND LH$_2$ EVAPORATION

Ullage Level	GF$_2$ Usage				LH$_2$ Evaporation			
	Test 5, NAS3-14381 (NAR Injector)		Test 7, NAS3-13306 (Straight-Pipe)		Test 5, NAS3-14381 (NAR Injector)		Test 7, NAS3-13306 (Straight-Pipe)	
	kg	lb	kg	lb	kg	lb	kg	lb
End prepres-surization	0.043	0.095	0.0354	0.078	—	—	—	—
95%	0.043	0.095	0.0354	0.078	0.183	0.402	0.065	0.143
80%	0.174	0.383	0.136	0.300	3.485	7.686	1.980	4.362
65%	0.348	0.767	0.312	0.687	4.140	9.118	2.735	6.024
50%	0.632	1.392	0.819	1.805	4.490	9.885	2.780	6.129
35%	0.958	2.112	1.520	3.350	5.200	11.447	2.895	6.382
20%	1.285	2.832	3.200	7.050	(7.240)	(15.956)	2.783	6.136
10%	1.612	3.552	4.450	9.800	(8.090)	(17.811)	(4.070)	(8.971)

Parenthetical values based on linear interpolation due to missing temperature sensors.

injector doubtless penetrates several feet further than shown, which would give evaporation values in line with the 5.2 kg (11.45 lb) shown. Development of jet penetration, interface heat transfer, and tank wall heat transfer models to allow prediction of ullage temperatures, GF_2 usage, and LH_2 evaporation for the NAR injector are described in the following section.

ANALYTIC CORRELATION WITH EXPERIMENTAL DATA

Ullage Gas Temperature and GF_2 Usage

Two of the most important parameters in the prediction of MTI injector performance are GF_2 usage and the temperature of the ullage gas (which directly affects both tank wall heating and GF_2 usage). These parameters are directly related to the degree of ullage mixing. With good ullage mixing, the ullage gas temperature is lower, heat transfer to the wall is lower, and GF_2 requirements therefore are minimized. The reverse is also true: Poor mixing results in higher ullage temperature, higher heat transfer, and greater GF_2 usage. If the ullage is completely mixed to the depth of the predicted injectant penetration, the mixing fraction factor, f_m, equals 1.0 (see Equation 15). If $f_m < 1.0$, the injectant jet penetration itself is not directly affected, but the mixed depth is less, and thus the temperature in the mixed region is higher.

In the previous investigation under NAS3-13306 (Reference 2), for those tests with large initial ullages (no interface mass transfer) and high tank pressures, where the GF_2 requirements demanded large injector on-time fractions, the ullage gas temperatures were correlated by assuming $f_m = 0.8$. But the low-pressure cases, where smaller GF_2 requirements were satisfied by small on-time fractions, temperatures were correlated by assuming $f_m = 0.9$. The difference was possibly due to an ullage circulation flow field which occurred with long on-time fractions, and led to temperature stratification in the tank and reduced ullage mixing. The tests with the NAR injector were all characterized by very short injector on-time fractions, and deep, uniform temperature profiles, so that the correlation was done with an assumed $f_m = 0.9$.

The processes occurring in the NAR injector are much more complex than in the simple straight pipe previously tested. The injectant gas flow at the injector exit is likely to have nonuniform distribution of temperature, composition, and velocity, and it is not obvious how the jet penetration process should be modeled. It was first assumed that the mixing between the GF_2 stream and the aspirated GH_2 in the second stage diffuser was no different than that occurring for a GF_2 flow into an unconfined ullage. The jet-exit parameters were set for the conditions at the second stage venturi exit. This high-velocity, small-diameter jet did not give adequate ullage penetration for GF_2 inlet temperature of either 333°K (600°R) or 555°K (1,000°R). It was then assumed that the GF_2 flow from the second stage venturi went through a normal shock to become subsonic and then filled the entire 3.3×10^{-2}-m (1.3-in.) diameter injector width, with negligible GH_2 flow. The analysis again predicted insufficient ullage penetration depth and excessive ullage temperature even with $f_m = 1.0$, as shown in Figure 31 for test 3 (50-percent initial ullage). The lines shown indicate the predicted mixed-zone depth and temperature (the stratified ullage below the mixed zone is not shown for clarity) compared to the experimental points. It seems clear that the injector was pumping enough hydrogen to affect the behavior of the jet.

If the injector was assumed to be pumping GH_2 at a large O/F ratio (for example, 36), the weight of pumped H_2 was small, but the molar flow of the low-molecular weight H_2 is nearly half that of the GF_2 and is enough to effectively confine the GF_2 flow, thus giving higher injectant velocity and penetration. The following equations indicate this effect:

$$U = \frac{\dot{m}_J}{\rho_J A} \tag{16}$$
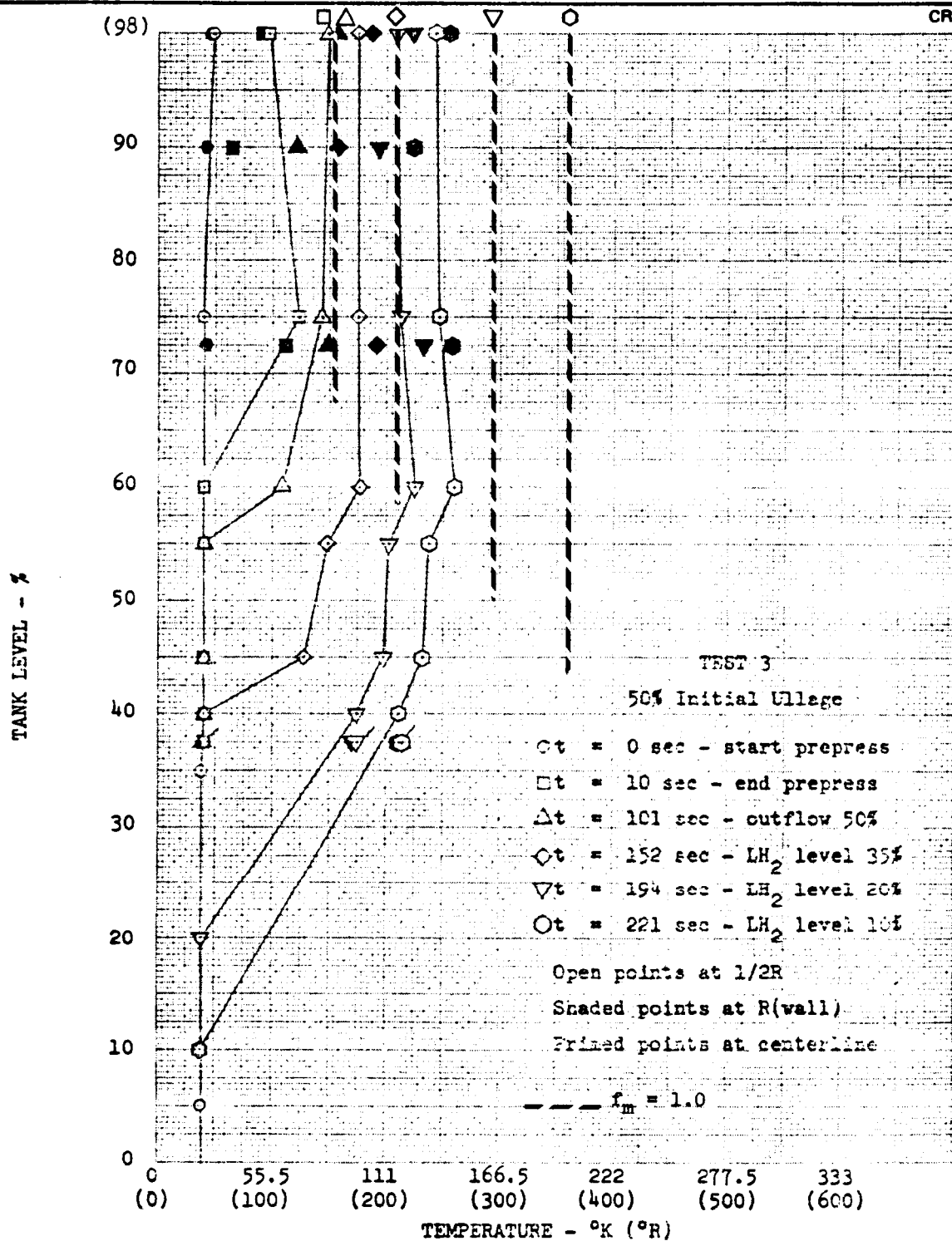
Figure 31. Temperature Correlation for Test 3, NAS3-14381, Zero H_2 Aspiration

assuming perfect gas,

$$\rho_J = \frac{P}{\frac{R}{W_J} T_J} \tag{17}$$

substituting in (16)

$$U = \frac{\dot{m}_J}{W_J} \frac{RT_J}{PA} \tag{18}$$

and

$$\frac{\dot{m}_J}{W_J} = \frac{\dot{m}_{F_2}}{W_{F_2}} + \frac{\dot{m}_{H_2}}{W_{H_2}} = \frac{\dot{m}_{F_2}}{W_{F_2}} + \frac{\dot{m}_{F_2}}{(O/F)W_{H_2}} \tag{19}$$

substituting in (18)

$$U = \left(\frac{1}{W_{F_2}} + \frac{1}{(O/F)W_{H_2}}\right) \frac{\dot{m}_{F_2} RT_J}{PA} \tag{20}$$

In addition, some of the GF_2 combusts inside the injector and thus contributes to increased injectant velocity by raising the mean effective jet temperature (T_J in Equation 20). This does not mean that the flow is mixed and at an average temperature, but rather that the mean velocity of the jet corresponds to the mean effective temperature. For example, if 9 percent of the GF_2 combusts with pumped GH_2 in the injector, then T_J would equal 1, 111°K (2, 000°R), assuming the GF_2 from the first stage is at 333°K (600°R).

The O/F ratio and mean effective temperature determine the jet-exit velocity. The jet-centerline properties for the penetration depth

analysis are determined by the unreacted core of the jet pump flow, that is, pure GF_2 at 333°K (600°R). The jet pump outflow is presumed to be a central core of GF_2 surrounded by an outer sheath of pumped GH_2 which join in a mixing/reaction zone. Extremely high temperatures occur in the reaction zone, resulting in a higher mean temperature for the total flow although most of the GF_2 core will be unaffected. The GF_2 temperature is that resulting from combustion in the first stage of the injector. The design O/F = 800 with a temperature of 555°K (1,000°R) assumes LH_2 enters the heat exchanger in the first stage feed line. Experimental data indicate that GH_2 entered the heat exchanger, which gives a much higher GH_2 inlet temperature to the first stage combustor, higher O/F ratio, and lower combustion product temperature; therefore, the first stage temperature was set at 333°K (600°R).

Based on the above assumptions (O/F = 36; T_J = 1,111°K [2,000°R]), the ullage gas mixed-zone temperature history was predicted for the large ullage volume tests (3, 6, 7, and 2) as shown in Figures 32, 33, 34, and 35. The agreement is excellent, except for Test 2, a warm initial ullage case with small on-time fractions where f_m = 0.9 gave excessive ullage temperatures and GF_2 usage. The same situation was encountered in Test 13 from NAS3-13306, also a warm initial ullage test with small on-time fraction, and the data from test 13 were best correlated with f_m = 1.0. It was postulated at the time that the warm initial ullage resisted establishment of the ullage circulation field, but substantiation of this thesis was not possible. However, Test 2 from this program was also well correlated with f_m = 1.0, so that an ullage temperature effect does in fact seem to act in these cases.

In addition to accurate jet penetration predictions, the heat transfer characteristics from the ullage gas must be known to accurately
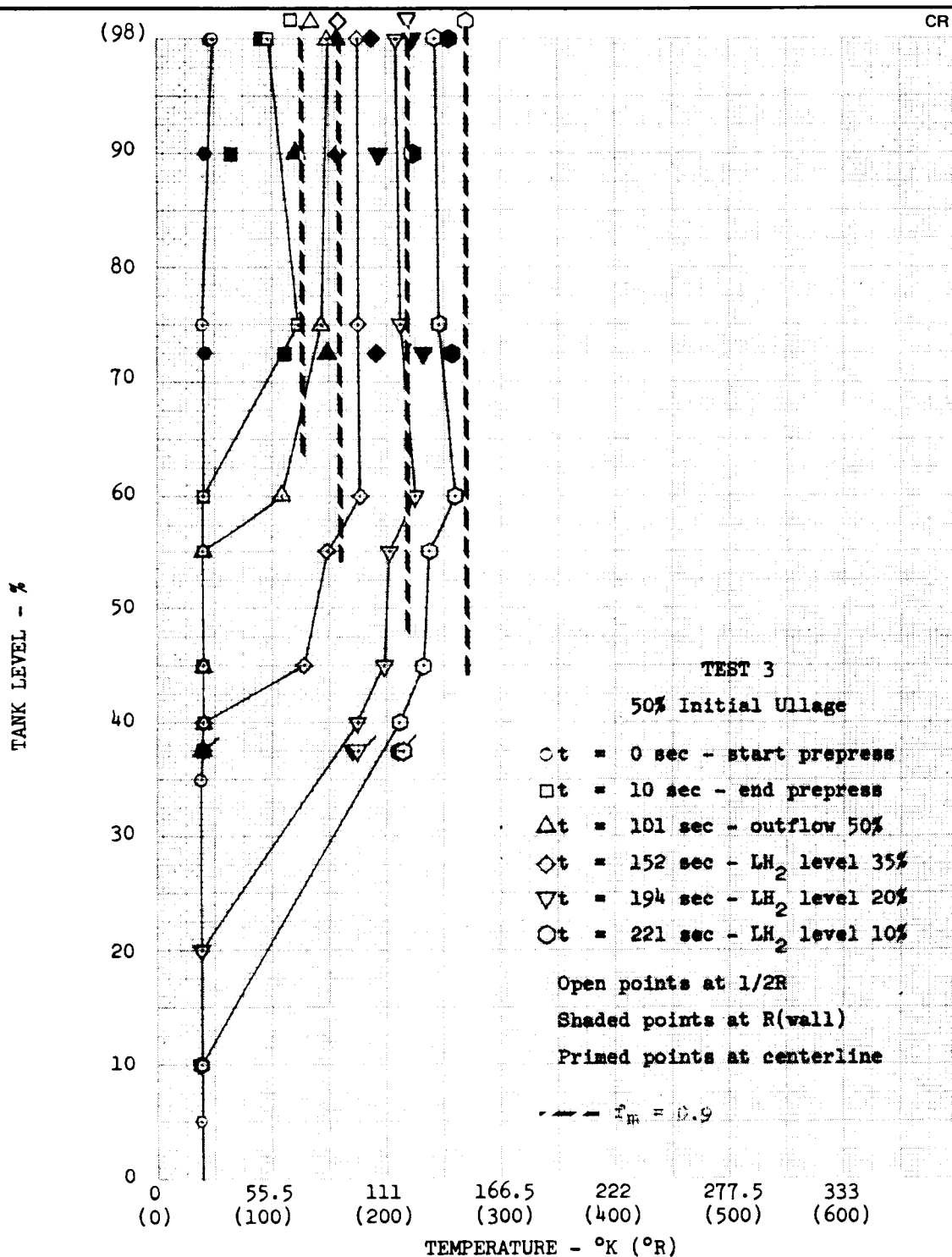
Figure 32. Temperature Correlation for Test 3, NAS3-14381, With H_2 Aspiration
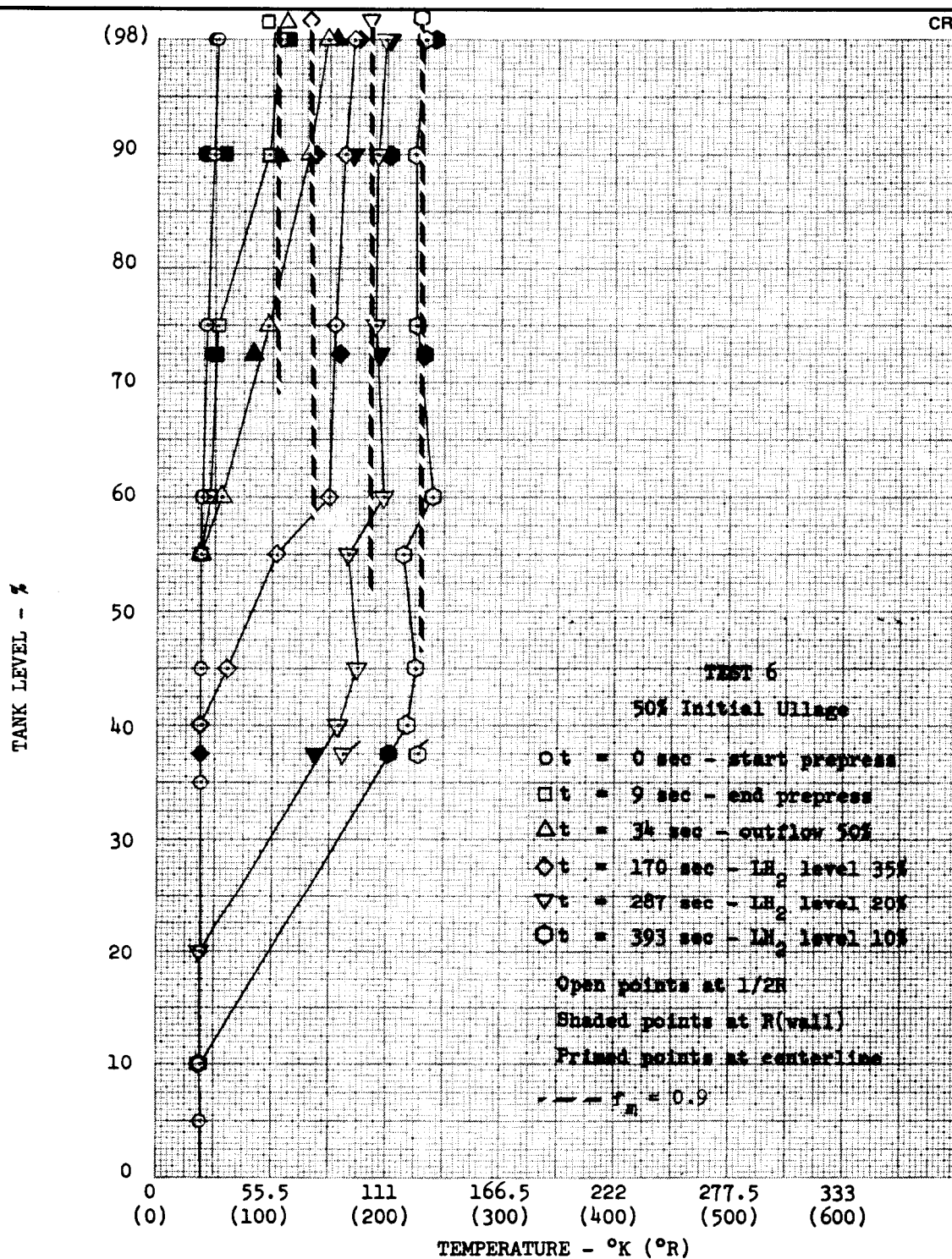
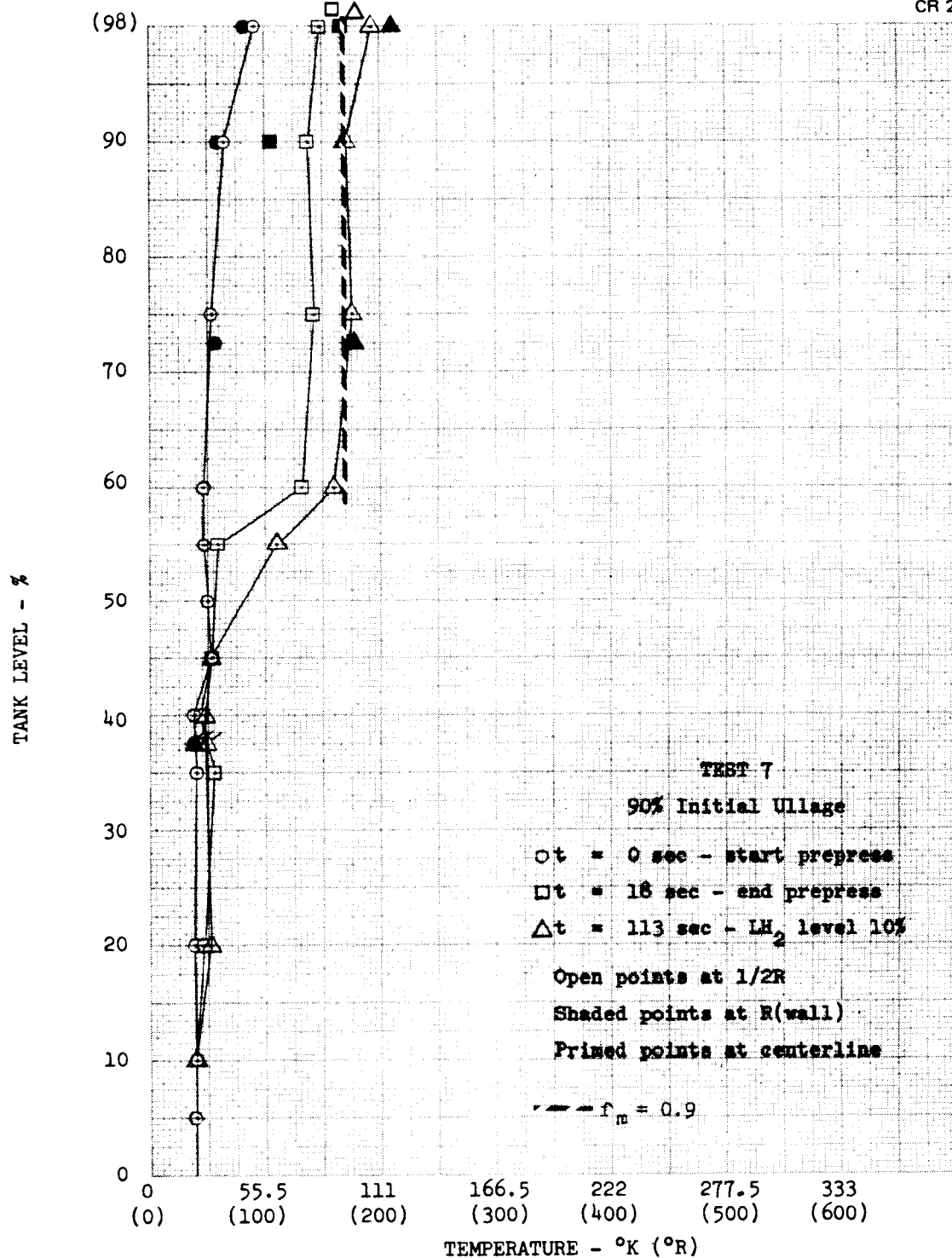Figure 33. Temperature Correlation for Test 6, NAS3-14381

Figure 34. Temperature Correlation for Test 7, NAS3-14381
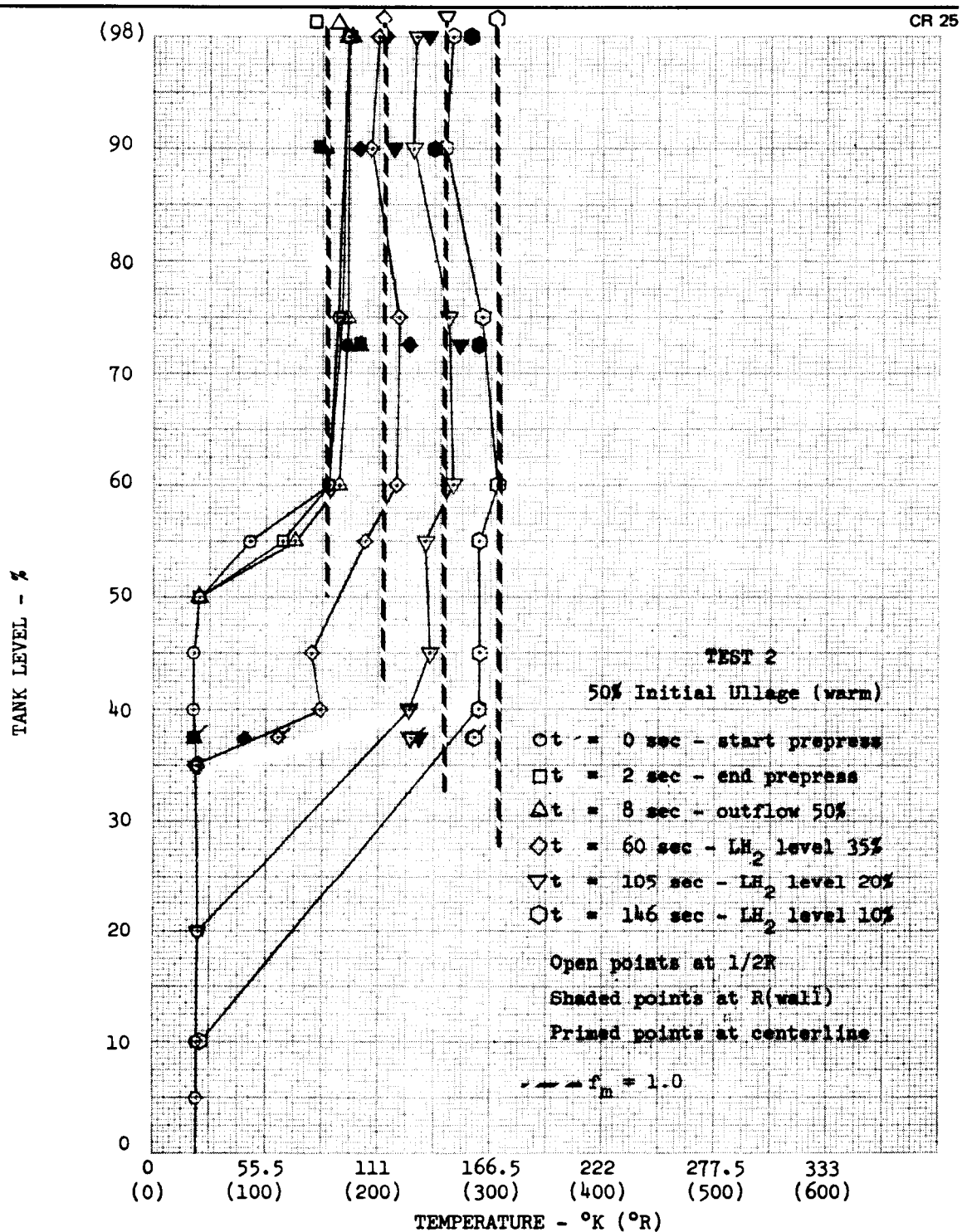
Figure 35. Temperature Correlation for Test 2, NAS3-14381

predict the GF_2 usage. In the previous tests under Contract NAS3-13306, the heat flux data were quite limited since a number of fluxmeters succumbed to the high ullage temperatures. In this program, since the ullage temperatures were much lower, consistent heat flux data were obtained for all tests. The heat flux data from these tests indicate heat transfer substantially in excess of that accounted for by free convection. The difference between the measured heat transfer coefficient and the free convection heat transfer coefficient was assumed to be the forced convection heat transfer coefficient. From Reference 10, the equation for forced convection to a vertical flat plate is:

$$\frac{h_{fo} d}{K} = 0.037 \left(\frac{\rho U d}{\mu}\right)^{4/5} \left(\frac{C_p \mu}{K}\right)^{1/3} \tag{21}$$

The forced convection heat transfer coefficient is weakly dependent on a characteristic dimension $(d^{-1/5})$ which was arbitrarily set at 0.1017 m (4 in.), the width and height of the fluxmeter. The velocity needed to give the correct forced convection coefficient was determined. In the previous tests it was observed that this velocity was related to the GH_2 velocity in the injector and to the injector on-time fraction for the fluxmeters in the mixed zone (top of the ullage), by the correlation.

$$U_{fo} = .12 \, U_{Jo} \cdot f \tag{22}$$

In the previous tests, the injectant velocity, U_{Jo}, generally ranged from 6.1 to 9.1 m/sec (20 to 30 ft/sec) and the on-time fraction was generally quite large (> 0.5), except for the small ullage tests. The correlation was conveniently mechanized in the H819 computer code by setting U_{fo} to equal 12 percent of the injectant velocity, and allowing forced convection to occur only during injection (which accounted

for the f dependence) even though it was apparent that forced convection heat transfer was occurring to some degree when injection was not occurring. For the tests where forced convection heat transfer was significant in predicting GF_2 usage, the on-time fraction was usually near 1.0, so that the computer mechanization of the correlation was in line with physical reality, and gave accurate results.

For the tests in this program, U_{Jo} ranged from 61 to 70 m/sec (200 to 230 ft/sec) and the on-time fractions were always very small (< 0.25). If the previous correlation and mechanization were used, the predicted heat transfer and GF_2 usage were much smaller than observed. The reason, of course, was that forced convection heat transfer actually occurred for periods of time much longer than the on-time (as shown by the fluxmeter data). If the correlation was modified to give the observed heat transfer during injector cycling, the forced-convection velocity was unrealistically large (essentially equal to or greater than injection velocity), which caused problems of excessive heat transfer during relatively long prepressurizations.

It was determined that a different mechanization for the heat transfer process, more in line with physical reality, would be necessary to give the correct correlation of heat transfer data obtained in both the previous and current test programs. The forced convection heat transfer was assumed to occur all of the time (as indicated by the data) with an equivalent forced convection velocity equal to 6 percent of the injectant velocity, as shown in Figure 36. Again, forced convection is assumed to occur only in the mixed zone; in the lower unmixed portion of the ullage, the overall heat transfer coefficient was that for free convection only.

93
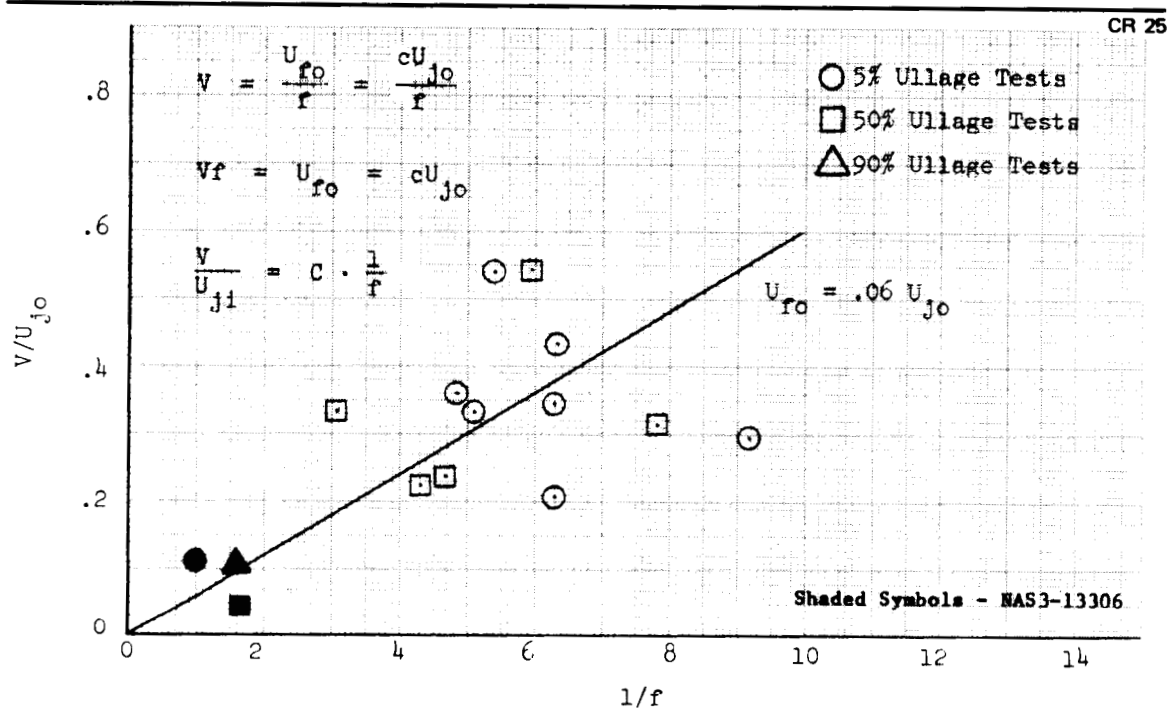
Figure 36. Forced Convection Heat Transfer Velocity Correlation

The jet penetration and heat transfer models gave good agreement between predicted and measured GF_2 usage as shown in Table 7, despite the scatter in the computed velocity data shown in Figure 36.

In order to ensure that the new heat transfer mechanization did not have adverse effects on the correlation of the previous straight-pipe tests from NAS3-13306, representative tests were correlated using the current heat transfer model, as shown in Figure 37 for Test 2 (NAS3-13306), a high-pressure 50-percent ullage case, and in Figure 38 for Test 14 (NAS3-13306), a low-pressure 50 percent ullage case. Again, the agreement between prediction and experiment is excellent (especially for Test 2). A comparison of the GF_2 usage predictions, both current and previous, with the observed GF_2 usage is shown in Table 8.

Table 7

COMPARISON OF OBSERVED AND PREDICTED
CUMULATIVE GF_2 USAGE

Test	Time	Observed GF_2 Usage (kg)	(lb)	Predicted GF_2 Usage (kg)	(lb)	Error (%)
1	4	0.097	0.215	0.108	0.239	+11.2
	51	0.429	0.942	0.488	1.075	+14.1
	99	0.714	1.572	0.762	1.680	+ 6.9
	146	1.088	2.396	1.109	2.441	+ 1.9
2	2	0.070	0.155	0.063	0.140	- 9.7
	8	0.070	0.155	0.087	0.192	+23.9
	60	0.511	1.124	0.557	1.228	+ 9.3
	105	0.906	1.996	1.182	2.606	+30.6
	146	1.390	3.061	1.804	3.980	+30.3
3	10	0.253	0.557	0.255	0.562	+ 0.9
	101	0.340	0.749	0.255	0.562	+25.0
	151	0.700	1.542	0.548	1.208	-21.6
	194	1.038	2.285	1.033	2.280	- 0.2
	221	1.540	3.390	1.470	3.243	- 4.3
4	4	0.098	0.216	0.114	0.251	+16.2
	7	0.098	0.216	0.132	0.291	+34.7
	67	0.651	1.436	0.468	1.031	-28.2
	112	0.940	2.071	0.746	1.645	-20.6
	160	1.273	2.803	1.110	2.444	-12.8

Table 7 (Continued)

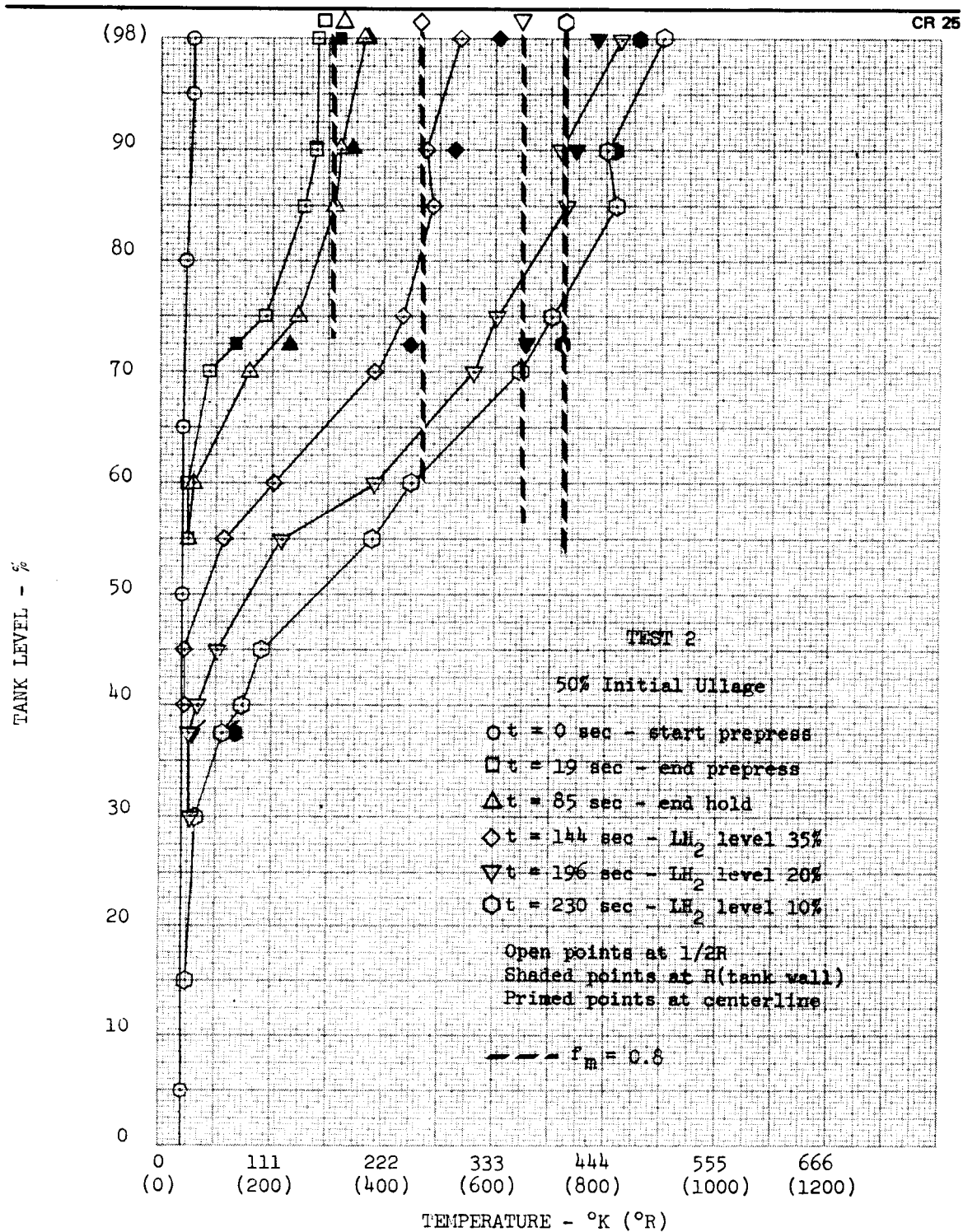| Test	Time	Observed GF$_2$ Usage		Predicted GF$_2$ Usage		Error
		(kg)	(lb)	(kg)	(lb)	(%)
	209	1.518	3.340	(1.332)	(2.941)	-11.9
	265	1.805	3.975	*	*	*
	317	1.805	3.975	*	*	*
5	3	0.043	0.095	0.027	0.059	-37.9
	73	0.043	0.095	0.027	0.059	-37.9
	192	0.174	0.383	0.244	0.495	+29.2
	321	0.348	0.767	0.463	1.020	+33.0
	449	0.632	1.392	0.701	1.544	+10.9
	585	0.959	2.112	0.991	2.182	+ 3.3
	709	1.286	2.832	1.490	3.286	+16.0
	797	1.612	3.552	2.000	4.410	+19.5
6	9	0.137	0.301	0.120	0.265	-12.0
	34	0.159	0.350	0.120	0.265	-24.3
	170	0.361	0.795	0.296	0.654	-17.7
	287	0.653	1.438	0.607	1.337	- 7.0
	393	0.980	2.179	0.929	2.046	- 6.1
7	18	0.276	0.607	0.287	0.633	+ 4.1
	113	0.298	0.657	0.350	0.749	+14.0

*Correlation not completed for interrupted test.

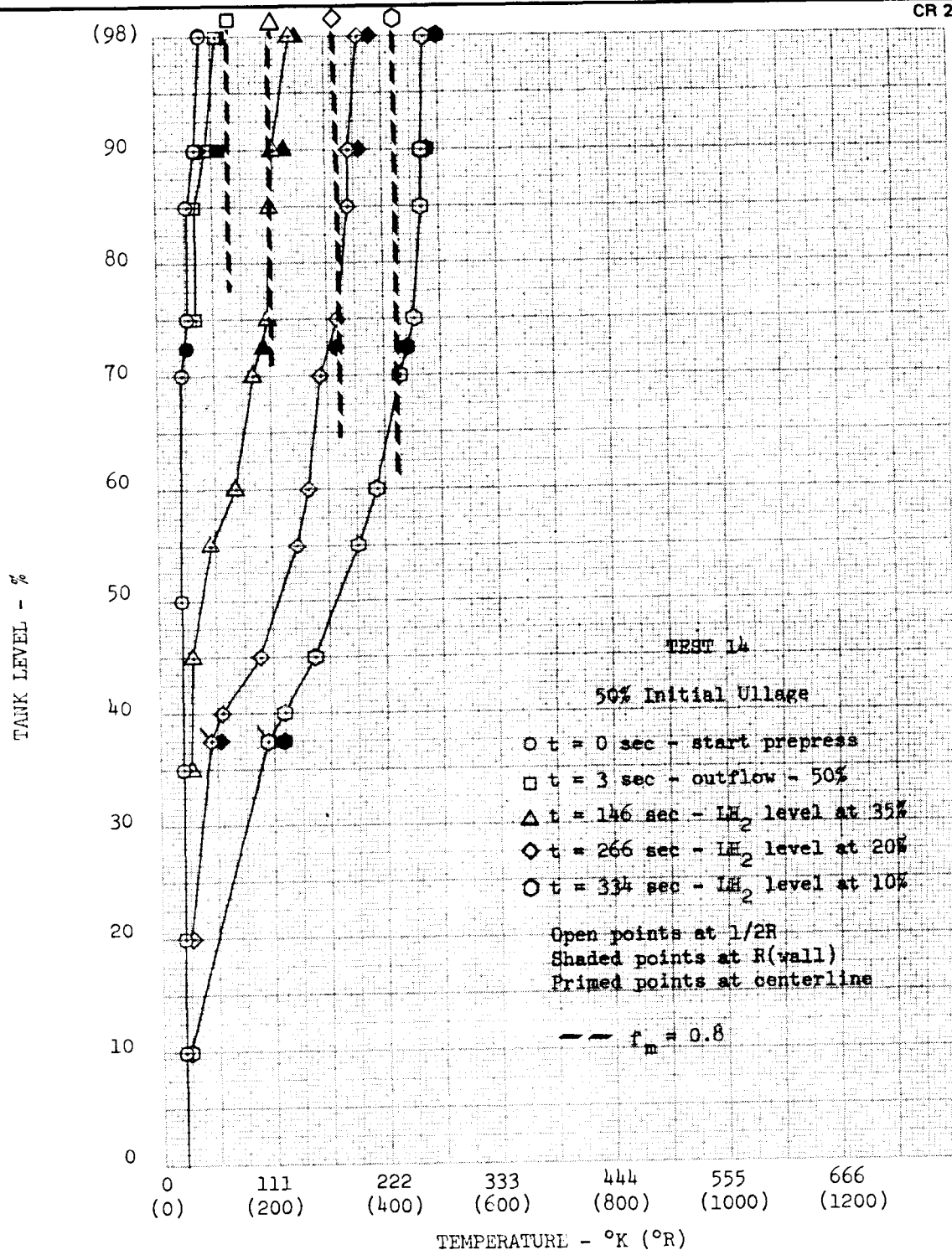Figure 37. Temperature Correlation for Test 2, NAS3-13306, Straight-Pipe

Figure 38. Temperature Correlation for Test 14, NAS3-13306, Straight-Pipe

Table 8

COMPARISON OF OBSERVED AND PREDICTED CUMULATIVE GF$_2$ USAGE FROM NAS3-13306

Test	Time (sec)	Observed GF$_2$ Weight (kg)	(lb)	Previously Predicted GF$_2$ Weight (kg)	(lb)	Error (%)	Currently Predicted GF$_2$ Weight (kg)	(lb)	Error (%)
2	19.2	0.585	1.290	0.500	1.102	-14.6	0.515	1.134	-12.1
	85	0.785	1.730	0.672	1.480	-14.5	0.754	1.661	- 4.0
	144	1.648	3.630	1.420	3.127	-13.9	1.448	3.192	-12.1
	196	2.556	5.630	2.444	5.380	- 4.5	2.488	5.489	- 2.5
	230	3.033	6.680	3.087	6.800	+ 1.8	3.095	6.816	+ 2.0
14	3	0.085	0.188	0.073	0.160	-14.9	0.073	0.162	-13.8
	146	0.249	0.549	0.241	0.530	- 3.5	0.211	0.465	-15.3
	266	0.724	1.595	0.695	1.531	- 4.0	0.665	1.467	- 8.0
	334	1.407	3.100	1.265	2.785	-10.5	1.166	2.571	-17.0
5	3.2	0.107	0.236	0.124	0.273	+15.7	0.079	0.174	-26.3
	75	0.189	0.417	0.124	0.273	-	0.085	0.188	-
	130	0.442	0.974	0.417	0.919	- 5.6	0.449	0.989	+ 1.5
	164	0.836	1.842	0.970	2.138	+15.9	1.031	2.277	+23.6
	215	1.890	4.165	2.037	4.484	+ 7.6	2.057	4.539	+ 9.0
7	1	0.035	0.078	0.020	0.045	-42.0	0.020	0.045	-42.0
	8	0.035	0.078	0.020	0.045	-42.0	0.020	0.045	-42.0
	134	0.136	0.300	0.198	0.437	+45.6	0.181	0.398	+32.7
	235	0.312	0.687	0.399	0.879	+28.0	0.392	0.865	+25.9
	418	0.820	1.805	0.765	1.686	- 6.6	0.754	1.661	- 8.0
	582	1.521	3.350	1.448	3.19	- 4.8	1.413	3.118	- 6.9
	780	3.200	7.050	2.854	6.29	-10.8	2.677	5.892	-16.4
	902	4.450	9.800	4.513	9.954	+ 1.5	3.922	8.648	-13.8

99

Following the successful correlation of the large-ullage tests (which verify the jet penetration and heat transfer models), the small-ullage tests were analyzed. In order to accurately predict ullage temperature history, GF_2 usage, and LH_2 evaporation, the LH_2 interface mass and heat transfer processes must be accurately modeled.

The correlation established in the previous investigation (NAS3-13306, see Reference 2) for interface heat and mass transfer was expressed by

$$\dot{q}_g = 0.6 \ X_L^2$$

$$\dot{q}_L = 0.2 \ q_g \tag{23}$$

for the gas-to-interface and interface-to-liquid heat transfer rates, respectively. The difference $\dot{q}_g - \dot{q}_L$ is the heat input rate to liquid vaporization. These same equations were retained initially in the 5-percent ullage computations for the jet pump injector tests, but gave much less vaporization than indicated by the mass balance. The initial liquid penetration depth, X_L, with the NAR injector was similar to that with the straight-pipe injector, although the injector-to-liquid distance was more than three times as great with the jet pump. It is apparent that the injector-to-liquid distance is an important parameter in determining the heat transfer and evaporation rates. The total heat rate was assumed proportional to the area of the jet impingement (proportional to the square of the injector-to-liquid distance) as well as the intensity of the convective disturbance (proportional

to the square of the penetration depth). The resulting correlation of this form is

$$\dot{q}_g = 0.15 \, (X_{if} - X_{in})^2 \, X_L^2 \qquad (24)$$

where the coefficient value of 0.15 was determined from the NAR injector test data. This correlation is effective for reasonably large injector-to-liquid distances. However, the heat transfer rate approaches zero as the injector exit approaches the interface (as $[X_{if} - X_{in}]$ approaches zero). This is not physically valid; therefore, a minimum value of $(X_{if} - X_{in}) = 0.3048$ m (1.0 ft) is maintained in the computer code for this relationship. Of the total heat transferred from the gas, 20 percent is lost to liquid heating and 80 percent vaporizes liquid as in the previous correlation.

With this interface model, the ullage gas temperatures were predicted accurately for Tests 1 and 4 as shown in Figures 39 and 40. The GF_2 usage for these tests was also accurately predicted, as shown in Table 7. (The correlation was not pursued to the end of Test 4 because the GF_2 injection was shut down at t = 187 seconds, restarted, and again shut down at indeterminate ullage volumes.) When compared to representative 5 percent ullage tests from NAS3-13306 (Tests 4 and 5) the new correlation gave conservative temperature prediction (the least accurate match is shown in Figure 41 for Test 5) at the previously assumed $f_m = 0.8$.

The correlation was not successful for Test 5, which was a low pressure, low LH_2 outflow rate, long duration (800 seconds) test. In the previous program under Contract NAS3-13306, Test 7 was the same kind of test and also was not correlated by Equation (23). The reason advanced at that time was that the long duration of the test allowed external heat leak to cause a layer of saturated LH_2 to build
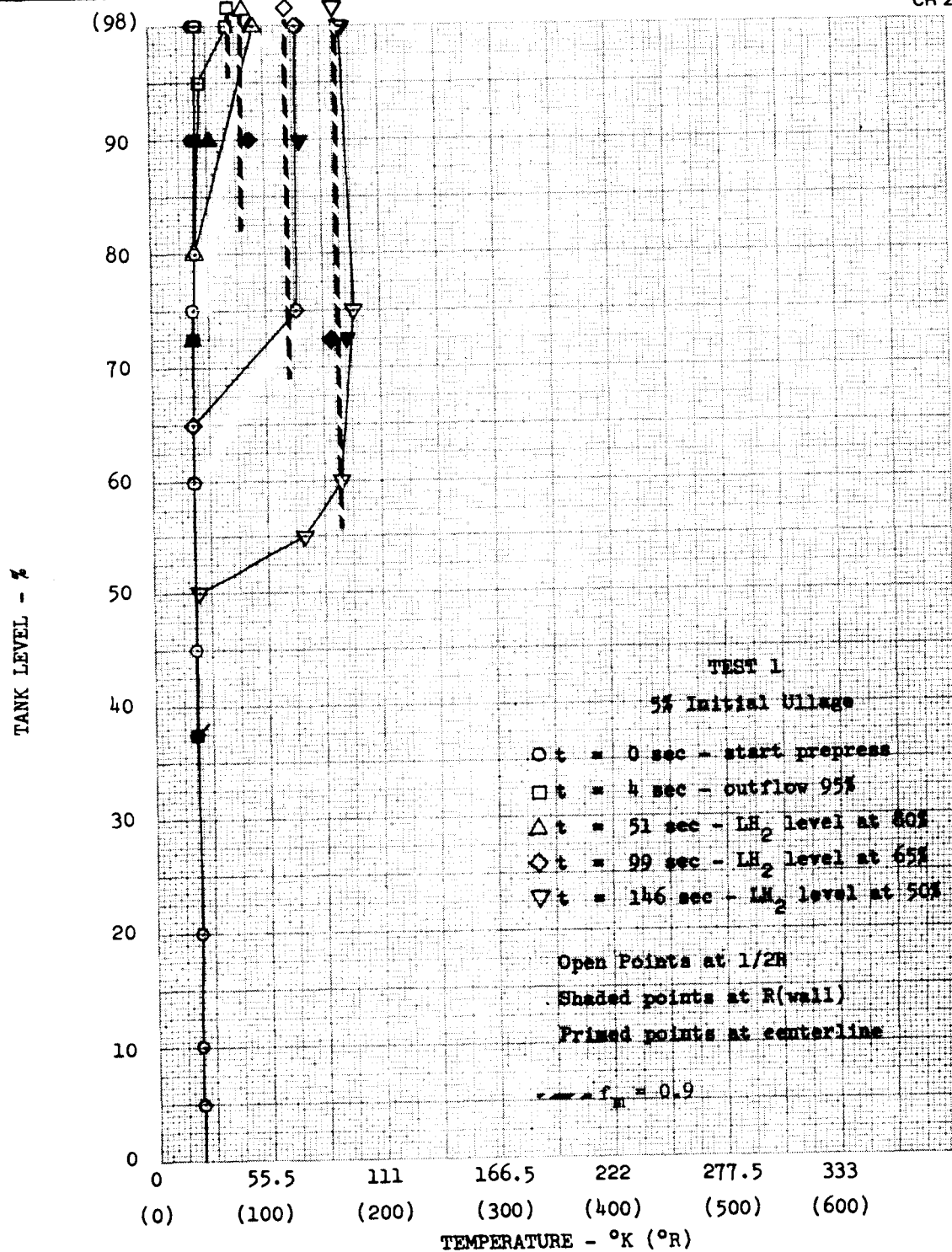
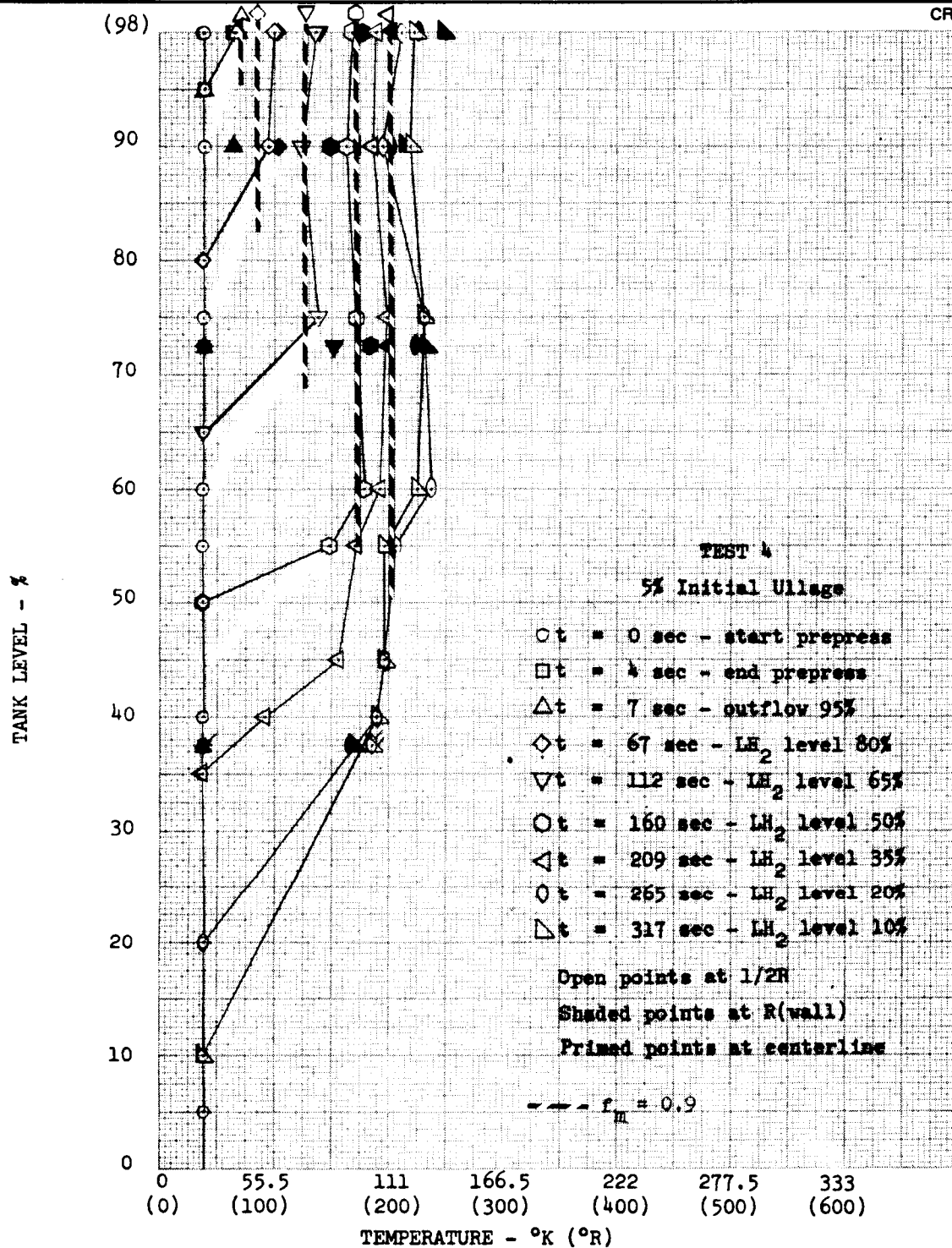Figure 39. Temperature Correlation for Test 1, NAS3-14381

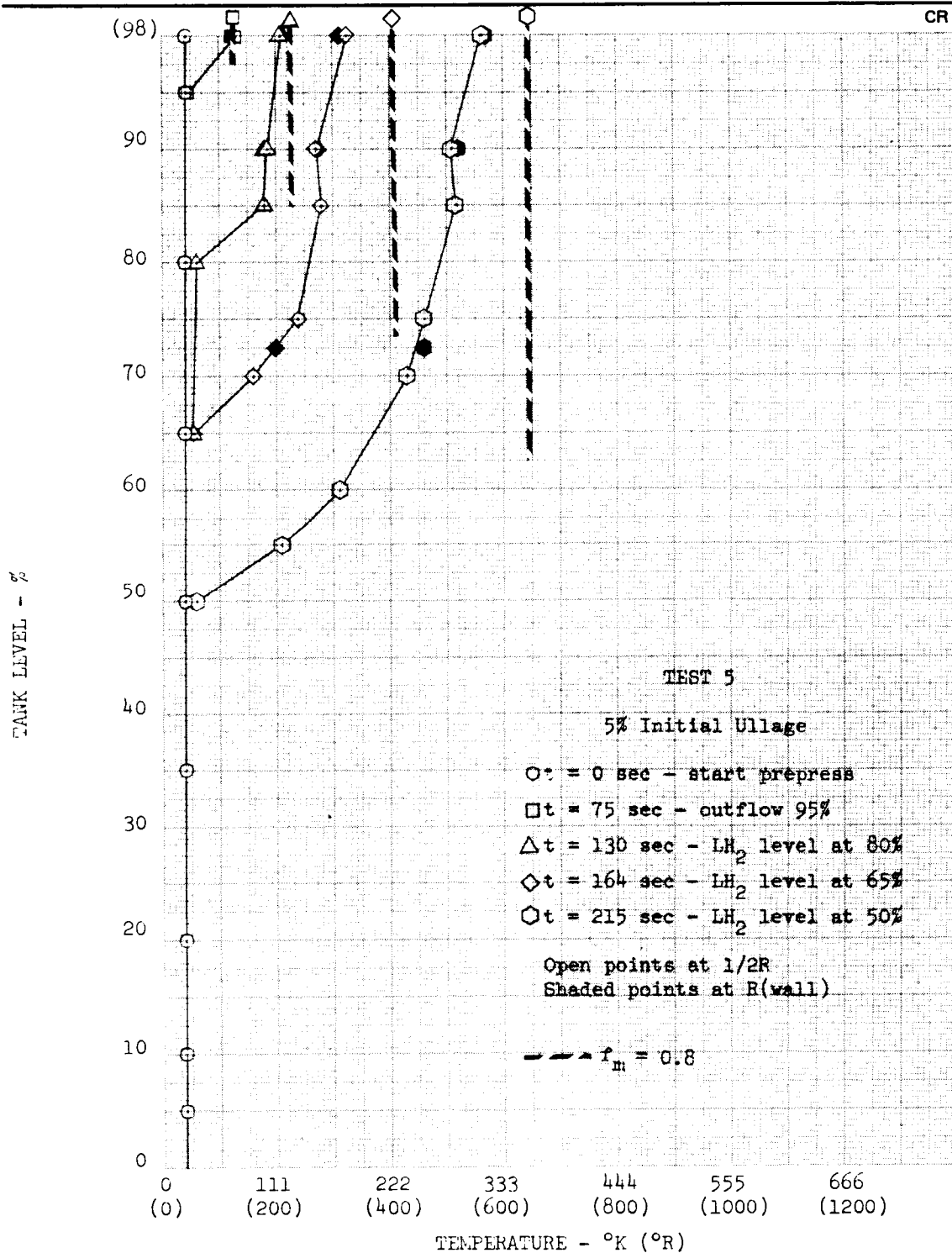Figure 40. Temperature Correlation for Test 4, NAS3-14381

103

Figure 41. Temperature Correlation for Test 5, NAS3-13306, Straight-Pipe

up at the interface, so that all heat input went to evaporation. Further, it was postulated that the evaporation would not necessarily depend on X_L because of the very short on-time fraction and very transient LH_2 penetration. It was assumed that evaporation would only depend on the available energy in the ullage, or simply as a fraction of q_c: Thus,

$$\dot{q}_g = 0.25\, q_c$$
$$\dot{q}_L = 0 \tag{25}$$

was the assumed correlation which, together with $f_m = 0.9$, gave good agreement with temperature history, GF_2 usage, and evaporation for Test 7, as described in Reference 2. Because of the similarity of Test 5 from this program to the previous Test 7, the same correlation was used, together with $f_m = 1.0$ and the NAR injector model. This gave fair agreement, and conservatively predicted the temperature history, as shown in Figure 42. However, the GF_2 usage prediction was high by 38 percent—2.22 kg (4.898 lb) compared to the observed 1.612 kg (3.552 lb). The data in Figure 42 indicated that the flow characteristics of the injector were changing during the test—note that the prediction first leads, then lags, then again leads the data. It was thought that while the injector was being damaged by overheating, it operated at a slightly different O/F ratio and equilibrium temperature. Assuming an O/F ratio of 30 and T_J equal to 1,390 °K (2,500 °R) gave good final temperature correlation, as shown in Figure 43, but the GF_2 usage was still predicted too high (see Table 7) and unexplained anomalies still existed during the test (for t = 192, 321, 499, and 585 seconds).

Again Test 7 from NAS3-13306 was analyzed with the new heat transfer mechanization, and with the Equation (25) interface model, and gave excellent correlation, as shown in Figure 44. The GF_2 usage comparisons, current and previous, are shown in Table 8.
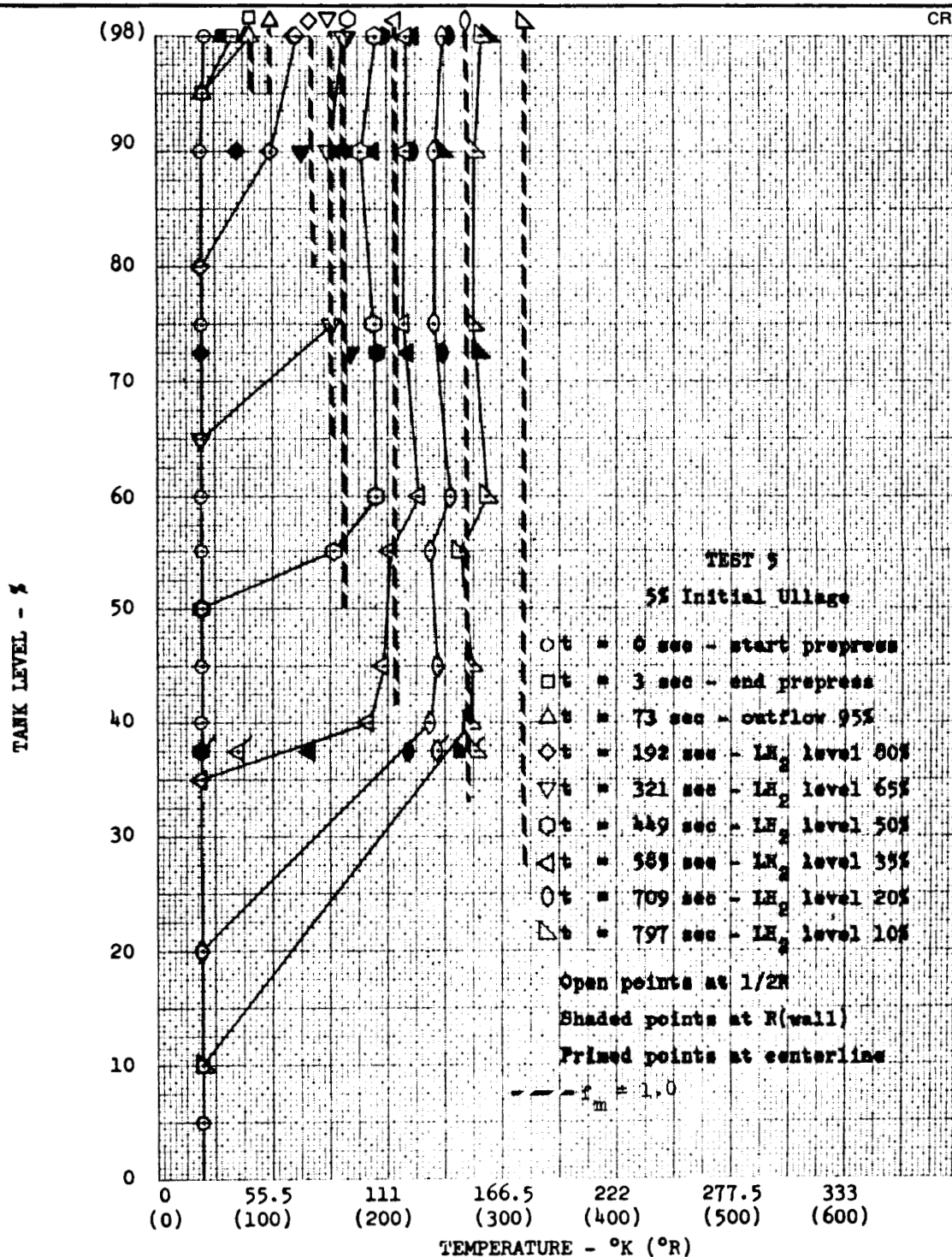
Figure 42. Temperature Correlation for Test 5, NAS3-14381

106
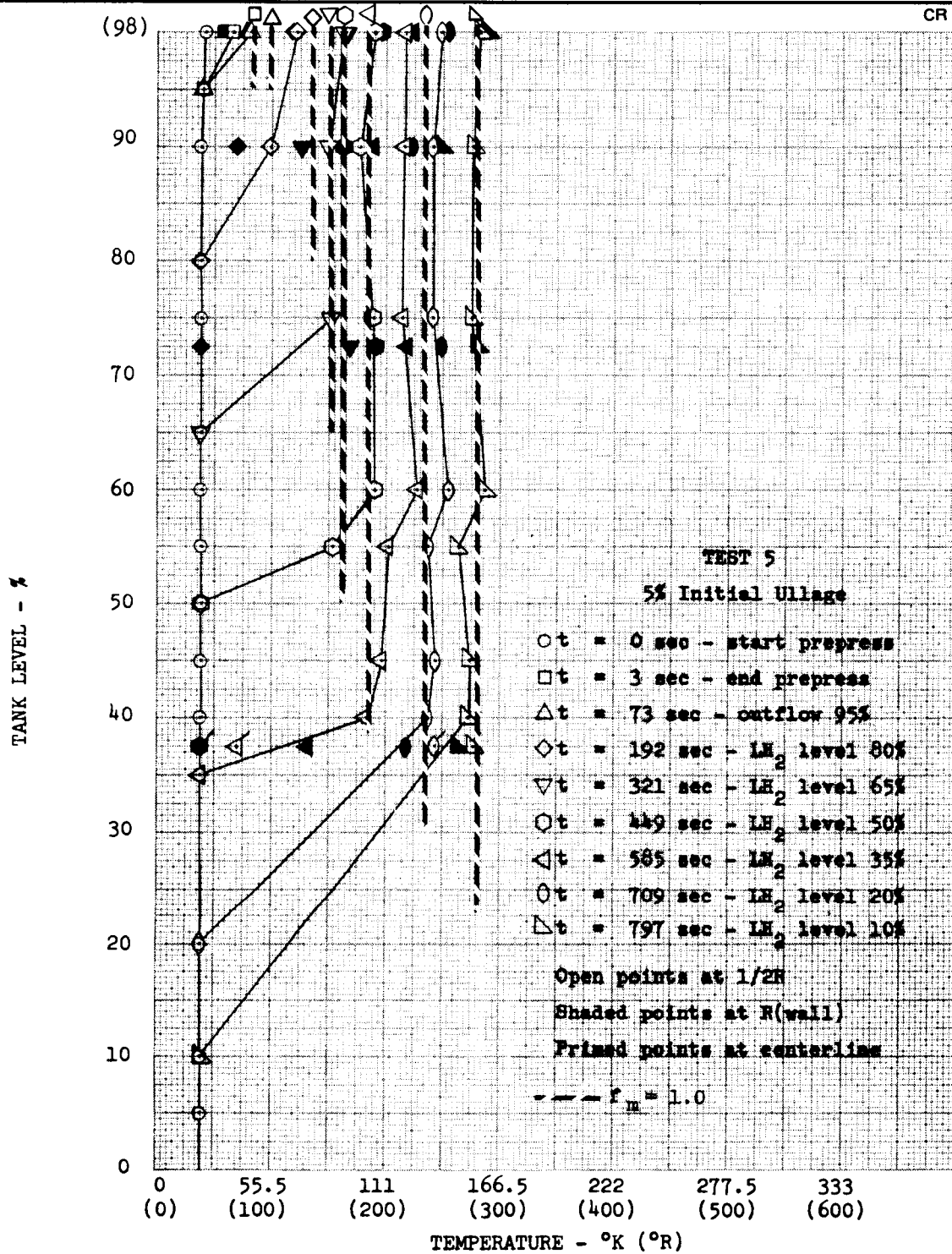
Figure 43. Temperature Correlation for Test 5, NAS3-14381, (O/F = 30, T_j = 1390°K (2500°R))

107
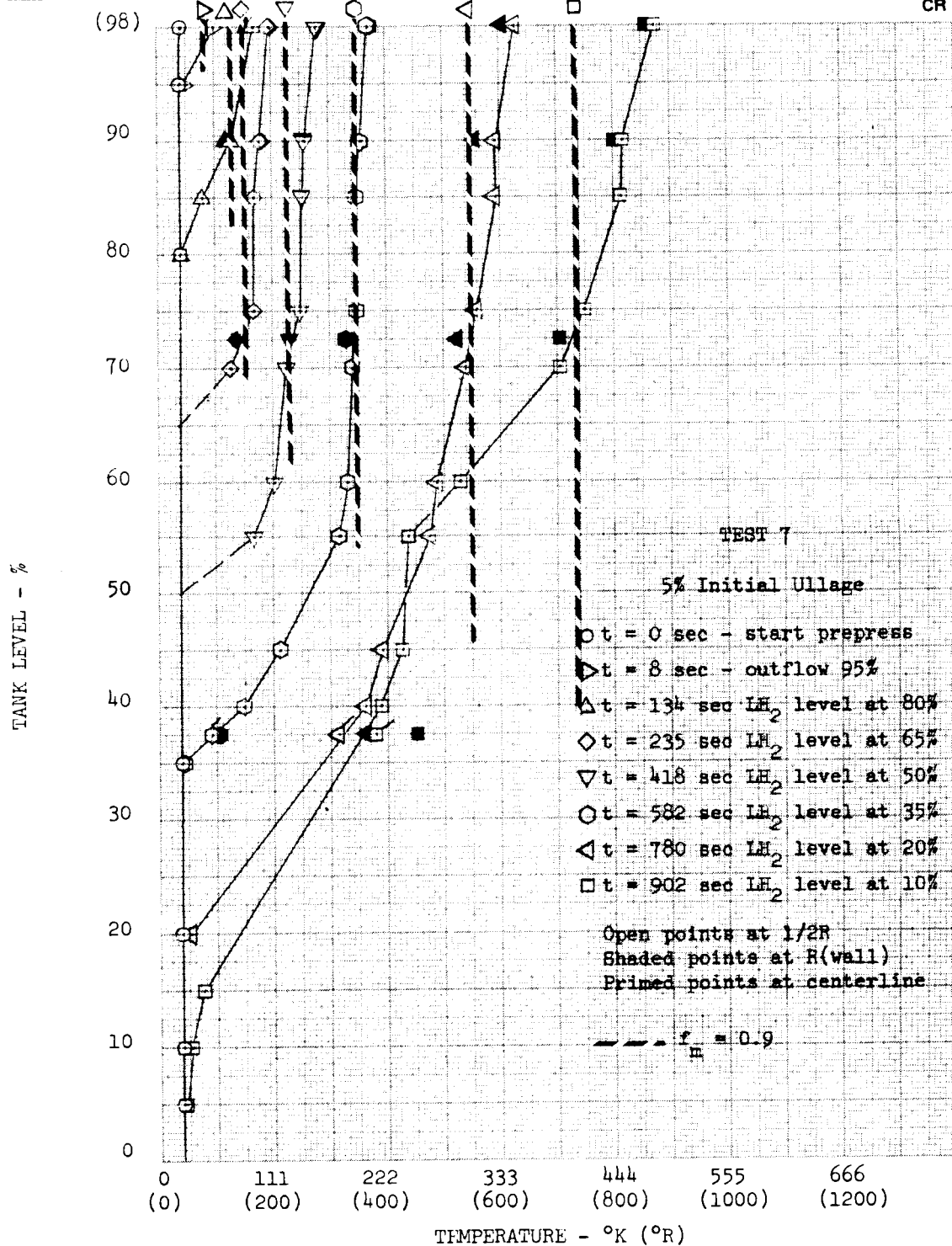
Figure 44. Temperature Correlation for Test 7, NAS3-13306, Straight-Pipe

The evaporated mass was also determined and is discussed in the next subsection.

Ullage Gas Mass and Tank Enthalpy Balance

An ullage mass balance and ullage gas and tank wall enthalpy balance was computed for each test. The ullage mass was calculated from the measured pressure and local temperature conditions measured at the sensor locations; the temperature was assumed to vary linearly between the measured points. When conditions in the ullage changed slowly, the temperature sensors were able to respond adequately, and the mass balance gave reasonable results. However, when the ullage temperatures changed rapidly, as during large ullage prepressurization, the response lag of the platinum temperature sensors gave erroneous results for the mass balance. Under these conditions, the ullage was actually warmer than the sensors were recording, so that the mass computed from the "colder" temperatures was larger than the actual mass. This effect also occasionally occurred due to temperature extrapolation caused by missing sensors, especially near the LH_2 interface. However, for the large ullage tests, the ullage mass stayed constant within 8 percent or less, which confirmed that ullage mass addition did not occur, as was predicted by the analysis.

The mass balances for the small ullage cases gave generally good results because of slower changes in temperature. These are shown in Table 9 and compared with the predicted evaporation.

As was the case for the tests under Contract NAS3-13306, the enthalpy balances were rather imprecise, because of temperature sensor lag and the requirement for linear interpolation between a relatively few wall temperature sensors.

Table 9

MASS BALANCES, 5-PERCENT ULLAGE

Test	Time	Ullage Mass Computed From Temperature Data		Predicted Ullage Mass	
		(kg)	(lb)	(kg)	(lb)
1	0	2.55	5.627	2.55	5.627
	4	4.55	10.013	4.92	10.834
	51	12.55	27.650	11.79	25.990
	99	12.30	27.061	12.72	28.040
	146	11.97	26.378	12.84	28.344
4	0	2.42	5.336	2.42	5.336
	4	4.63	10.198	5.05	11.135
	7	4.28	9.422	5.51	12.139
	67	9.25	20.408	11.12	24.558
	112	11.00	24.229	12.10	26.666
	160	11.10	24.449	12.25	26.980
	209	11.60	25.586	12.25	27.001
	265	(13.46)	(29.668)	*	*
	317	(13.43)	(29.593)	*	*
5	0	2.60	5.724	2.60	5.724
	3	3.19	7.024	2.80	6.186
	73	2.78	6.126	2.80	6.186
	192	6.09	13.410	4.35	9.577
	321	6.74	14.852	6.20	13.662
	449	7.09	15.609	8.05	17.738
	585	7.80	17.171	8.96	19.768
	709	(9.85)	(21.680)	8.96	19.768
	797	(10.67)	(23.533)	8.96	19.768

*Correlation not completed because of test interruption.
Parenthetical values based on linear interpolation due to missing temperature sensors.

Table 10 shows the comparison between the predicted evaporation for Tests 5 and 7 from NAS3-13306 using the current and previous correlations. Note that the evaporation for Test 5 is somewhat under-predicted by the current correlation; this accounts for the increased temperature shown in Figure 41.

ANALYSIS MODIFICATIONS

The jet pump injector capability was added to the computer analysis by incorporating Equation (20) for the calculation of the jet-exit velocity. This velocity is a function of two new input quantities, the jet pump O/F ratio and the average jet-exit temperature. The pumped hydrogen mass flow rate (determined by the O/F ratio and the GF_2 flow rate) is removed from the bottom of the tank as liquid and added to the mixed ullage region. The conventional straight-pipe injector is used as before in the program when a zero is input for the O/F ratio.

Additional pressure regulator options were added to the program as follows: 1) constant delivery pressure; 2) delivery pressure a specified multiple of the tank pressure; 3) delivery pressure specified by an input time-variable table; 4) option 3 switching to option 1 at the end of prepressurization; and 5) option 3 switching to option 2 at the end of prepressurization.

The revised relationship for the equivalent forced convection heat transfer velocity U_{fo} is

$$U_{fo} = .06 \, U_{Jo} \tag{26}$$

During the GF_2 valve off-times, the last computed value of the forced convection heat transfer coefficient increment from the previous injector on-time is added to the calculated free-convection coefficient;

Table 10

COMPARISON OF OBSERVED AND PREDICTED
ULLAGE MASS FROM NAS3-13306

Test	Time (sec)	Ullage Mass Computed from Temperature Data (kg)	(lb)	Previously Predicted Ullage Mass (kg)	(lb)	Currently Predicted Ullage Mass (kg)	(lb)
5	0	2.566	5.652	2.566	5.652	2.566	5.652
	75	3.366	7.415	4.700	10.340	3.255	7.175
	130	5.450	11.995	5.746	12.649	4.790	10.559
	164	6.662	14.688	5.830	12.840	4.970	10.957
	215	5.000	11.098	5.882	12.962	4.996	11.014
7	0	2.757	6.073	2.757	6.073	2.757	6.073
	8	2.822	6.216	2.797	6.159	2.914	6.425
	134	4.740	10.435	4.052	8.926	4.147	9.142
	235	5.494	12.097	5.608	12.355	5.775	12.732
	418	5.540	12.202	5.820	12.817	5.963	13.146
	582	5.650	12.455	5.875	12.934	5.963	13.146
	780	5.547	12.209	5.925	13.055	5.963	13.146
	902	6.830	15.044	5.947	13.090	5.963	13.146

this is in contrast to the previous model which added forced convection only when the injector was flowing GF_2. As previously, the forced convection heat transfer affects only the mixed ullage region. However, the mixed ullage region is retained during the injector off-time at the last computed value of the mixing depth from the previous injector on-time; this is in contrast to the previous model in which the subdivision of the entire ullage into nodes was permitted to occur during the injector off-times. The revised interface heat transfer relationship is given by Equation (24). This equation is used in the program in the same manner as the previous relationship [Equation (23)].

MTI SYSTEM CONSIDERATIONS

The first stage preheating and the second stage H_2 aspiration which occurs with the NAR injector contribute to increased penetration, mixing, evaporation, and reduced ullage gas temperatures and GF_2 consumption. However, the injector as designed to pump LH_2 would require a regulator, a larger valve, and a vacuum-jacketed LH_2 feed line. If the injector were redesigned to effectively aspirate GH_2, the heavy vacuum-jacketed line could be eliminated, but the injector regulator and larger valve, if flight-weight, could add perhaps 3.2 kg (7.0 lb) to the system weight; at the same time, for complete expulsion in a 28.3-m^3 ($1,000\text{-ft}^3$) tank, perhaps 3.2 kg (7.0 lb) of GF_2 would be saved, compared to the nonoptimized straight-pipe system tested under Contract NAS3-13306. In the previous program, an advanced Centaur vehicle MTI system was designed and analyzed. Because of the low g-field during pressurization, a diffuser-type injector was used, but excellent penetration, mixing, low GF_2 usage, and cold ullage temperatures were obtained.

Injectant penetration is clearly the most important parameter in obtaining good MTI pressurization performance, and through suitable selection of injection characteristics, the MTI system can be designed to deliver whatever level of performance is desired.

CONCLUSIONS

The conclusions from this comprehensive analytical and experimental program are as follows:

A. A unique jet-pump injector was designed and fabricated by North American Rockwell-Rocketdyne (NAR), and tested in the 28.3-m^3 ($1,000$-ft^3) flight-weight LH_2 test tank system used in Contract NAS3-13306. The MTI control and injection system was modified with the addition of a specially designed proportional GF_2 pressure regulator, enlarged injector valve, and vacuum-jacketed injector LH_2 feed line, and performed in a nominal fashion, controlling the tank pressure to within 0.69×10^4 N/m^2 (1.0 psia) under essentially all conditions.

B. The NAR injector was able to jet-pump LH_2 only under steady-state conditions when completely chilled (with a full LH_2 tank). During large ullage tests and during all cyclic operation of the MTI system, the injector pumped only H_2 vapor, which resulted in damage to the LH_2 pumping annulus from overheating.

C. The first stage preheating of the GF_2 injectant, and H_2 vapor pumping, resulted in increased jet penetration and ullage mixing for the NAR injector, which gave improved MTI pressurization performance (reduced ullage temperatures and GF_2 consumption) compared to that of a nonoptimum straight-pipe injector tested under Contract NAS3-13306.

D. The MTI pressurization computer code, H819, was used successfully to correlate the data from the NAR injector tests with only minor modifications.

REFERENCES

1. E. C. Cady. An Investigation of Fluorine-Hydrogen Main Tank Injection Pressurization. NASA CR-72408, (DAC-62233), April 1968.

2. E. C. Cady and D. W. Kendle. Vehicle-Scale Investigation of a Fluorine-Hydrogen Main Tank Injection Pressurization System. NASA CR-72756, (MDC G0805), July 1970.

3. H. E. Barber. Hydrogen Tank Pressurizing Gas Injector. NASA CR-72998, (R-8713), October 1971.

4. W. H. Roudebush. An Analysis of the Problem of Tank Pressurization During Outflow. NASA TN D-2585, January 1965.

5. Fortran Program for the Analysis of a Single-Propellant Tank Pressurization System. Rocketdyne Report S&ID IDWA 5835, 15 June 1964.

6. D. W. Kendle. A Tank Pressurization Computer Program for Research Applications. DAC-63076, December 1968.

7. D. W. Kendle. Ullage Mixing Effects on Cryogenic Tank Pressurization. DAC-63168, March 1968.

8. J. Laufer. Turbulent Shear Flows of Variable Density. AIAA Journal, April 1969; Vol. 7, No. 4, P 706.

9. R. L. DeWitt, R. J. Stochl, and W. R. Johnson. Experimental Evaluation of Pressurant Gas Injectors During the Pressurized Discharge of Liquid Hydrogen. NASA TN D-3458, June 1966.

10. W. H. McAdams. Heat Transmission. McGraw-Hill Book Co., New York, 1954.

Appendix

DISTRIBUTION LIST FOR FINAL REPORT, NASA CR-120947

Recipient	Designee	No. Copies
National Aeronautics & Space Administration Lewis Research Center 21000 Brookpark Road Cleveland, Ohio 44135		
Attn: Contracting Officer, MS 500-313		1
E. A. Bourke MS 500-203		5
J. W. Gregory 500-203		1
Technology Utilization Office, MS 3-16		1
AFSC Liaison Office, 501-3		2
Library		2
Office of Reliability & Quality Assurance, MS 500-111		1
E. M. Krawczonek MS 500-209		1
E. A. Edelman, Project Manager MS 501-6		3
R. J. Stochl, MS 500-204		1
R. L. Dewitt, MS 500-204		1
A. J. Stofan, MS 500-103		1
W. R. Dunbar, MS 500-106		1
Don A. Hart RPD Office of Aeronautics & Space Technology NASA Headquarters Washington, D. C. 20546		2
Frank W. Stephenson, Jr. RPI Office of Aeronautics & Space Technology NASA Headquarters Washington, D. C. 20546		2
Director, Launch Vehicles & Propulsion, SV Office of Space Science & Applications NASA Headquarters Washington, D. C. 20546		1

Recipient	Designee	No. Copies
Chief, Environmental Factors & Aerodynamics Code RV-1 Office of Advanced Research & Technology NASA Headquarters Washington, D.C. 20546		1
Chief, Space Vehicles Structures Office of Advanced Research & Technology NASA Headquarters Washington, D.C. 20546		1
Director, Advanced Manned Missions, MT Office of Manned Space Flight NASA Headquarters Washington, D.C. 20546		1
NASA Scientific & Technical Information Facility P.O. Box 33 College Park, Maryland 20740		2
Director, Technology Utilization Division Office of Technology Utilization NASA Headquarters Washington, D.C. 20546		1
National Aeronautics & Space Administration Ames Research Center Moffett Field, California 94035 Attn: Library	Hans M. Mark Missile Analysis Division	1
National Aeronautics & Space Administration Flight Research Center P.O. Box 273 Edwards, California 93523 Attn: Library		1
National Aeronautics & Space Administration Goddard Space Flight Center Greenbelt, Maryland 20771 Attn: Library	Merland L. Moseson, Code 620	1

Recipient	Designee	No. Copies
National Technical Information Service Springfield, Virginia 22151		30
National Aeronautics & Space Administration John F. Kennedy Space Center Cocoa Beach, Florida 32931 Attn: Library	Dr. Kurt H. Debus	1
National Aeronautics & Space Administration Langley Research Center Langley Station Hampton, Virginia 23365 Attn: Library	E. Cortwright Director	1
National Aeronautics & Space Administration Manned Spacecraft Center Houston, Texas 77001 Attn: Library	J. G. Thiobodaux, Jr. Chief, Propulsion & Power Division	1
National Aeronautics & Space Administration George C. Marshall Space Flight Center Huntsville, Alabama 35812 Attn: Library	Hans G. Paul James Thomas	1
Jet Propulsion Laboratory 4800 Oak Grove Drive Pasadena, California 91103 Attn: Library	J. Blumrich Henry Burlage, Jr.	1
Defense Documentation Center Cameron Station Building 5 5010 Duke Street Alexandria, Virginia 22314 Attn: TISIA		1
Office of the Director of Defense Research & Engineering Washington, D.C. 20301 Attn: Office of Asst. Dir. (Chem. Technology)		1
RTD (RTNP) Bolling Air Force Base Washington, D.C. 20332		1

Recipient	Designee	No. Copies
Arnold Engineering Development Center Air Force Systems Command Tullahoma, Tennessee 37389 Attn: Library	Dr. H. K. Doetsch	1
Advanced Research Projects Agency Washington, D. C. 20525 Attn: Library		1
Aeronautical Systems Division Air Force Systems Command Wright-Patterson Air Force Base, Dayton, Ohio Attn: Library		1
Air Force Missile Test Center Patrick Air Force Base, Florida Attn: Library	L. J. Ullian	1
Air Force Systems Command Andrews Air Force Base Washington, D. C. 20332 Attn: Library	Capt. S. W. Bowen SCLT	1
Air Force Rocket Propulsion Laboratory (RPR) Edwards, California 93523 Attn: Library		1
Air Force FTC (FTAT-2) Edwards Air Force Base, California 93523 Attn: Library	Donald Ross	1
Air Force Office of Scientific Research Washington, D. C. 20333 Attn: Library	SREP Dr. J. F. Masi	1
Space & Missile Systems Organization Air Force Unit Post Office Los Angeles, California 90045 Attn: Technical Data Center		1
Office of Research Analyses (OAR) Holloman Air Force Base, New Mexico Attn: Library 88330 RRRD		1
U. S. Air Force Washington, D. C. Attn: Library	Col. C. K. Stambaugh Code AFRST	1

Recipient	Designee	No. Copies
Commanding Officer U.S. Army Research Office (Durham) Box CM, Duke Station Durham, North Carolina 27706 Attn: Library		1
U.S. Army Missile Command Redstone Scientific Information Center Redstone Arsenal, Alabama 35808 Attn: Document Section	Dr. W. Wharton	1
Bureau of Naval Weapons Department of the Navy Washington, D.C. Attn: Library	J. Kay Code RTMS-41	1
Commander U.S. Naval Missile Center Point Mugu, California 93041 Attn: Technical Library		1
Commander U.S. Naval Weapons Center China Lake, California 93557 Attn: Library		1
Commanding Officer Naval Research Branch Office 1030 E. Green Street Pasadena, California 91101 Attn: Library		1
Director (Code 6180) U.S. Naval Research Laboratory Washington, D.C. 20390 Attn: Library	H.W. Carhart J. M. Krafft	1
Picatinny Arsenal Dover, New Jersey 07801 Attn: Library	I. Forsten	1
Air Force Aero Propulsion Laboratory Research & Technology Division Air Force Systems Command United States Air Force Wright-Patterson AFB, Ohio 45433 Attn: ARPR (Library)	R. Quigley C. M. Donaldson	1

Recipient	Designee	No. Copies
Electronics Division Aerojet-General Corporation P.O. Box 296 Azusa, California 91703 Attn: Library	W. L. Rogers	1
Space Division Aerojet-General Corporation 9200 East Flair Drive El Monte, California 91734 Attn: Library	S. Machlawski	1
Aerojet Ordnance and Manufacturing Aerojet-General Corporation 11711 South Woodruff Avenue Fullerton, California 90241 Attn: Library		1
Aerojet Liquid Rocket Company P.O. Box 13222 Sacramento, California 95813 Attn: Technical Library 2484-2015A	R. Stiff	1
Aeronutronic Division of Philco Ford Corp. Ford Road Newport Beach, California 92663 Attn: Technical Information Department	Dr. L. H. Linder	1
Aerospace Corporation 2400 E. El Segundo Blvd. Los Angeles, California 90045 Attn: Library-Documents	J. G. Wilder	1
Arthur D. Little, Inc. 20 Acorn Park Cambridge, Massachusetts 02140 Attn: Library	A.C. Tobey	1
ARO, Incorporated Arnold Engineering Development Center Arnold AF Station, Tennessee 37389 Attn: Library		1
Battelle Memorial Institute 505 King Avenue Columbus, Ohio 43201 Attn: Report Library, Room 6A		1

Recipient	Designee	No. Copies
Beech Aircraft Corporation Boulder Facility Box 631 Boulder, Colorado Attn: Library	Douglas Pope	1
Bell Aerosystems, Inc. Box 1 Buffalo, New York 14240 Attn: Library	W. M. Smith	1
Bendix Systems Division Bendix Corporation 3300 Plymouth Street Ann Arbor, Michigan Attn: Library	John M. Brueger	1
Bell comm 955 L'Enfant Plaza, S.W. Washington, D.C. Attn: Library	H. S. London	1
Boeing Company Space Division P. O. Box 868 Seattle, Washington 98124 Attn: Library	J. D. Alexander C. F. Tiffany	1
Boeing Company 1625 K Street, N.W. Washington, D.C. 20006		1
Chemical Propulsion Information Agency Applied Physics Laboratory 8621 Georgia Avenue Silver Spring, Maryland 20910	Tom Reedy	1
Chrysler Corporation Missile Division P.O. Box 2628 Detroit, Michigan Attn: Library	John Gates	1
Chrysler Corporation Space Division P.O. Box 29200 New Orleans, Louisiana 70129 Attn: Librarian		1

Recipient	Designee	No. Copies
Curtiss-Wright Corporation Wright Aeronautical Division Woodridge, New Jersey Attn: Library	G. Kelley	1
University of Denver Denver Research Institute P.O. Box 10127 Denver, Colorado 80210 Attn: Security Office		1
Fairchild Stratos Corporation Aircraft Missiles Division Hagerstown, Maryland Attn: Library		1
Reseach Center Fairchild Hiller Corporation Germantown, Maryland Attn: Library	Ralph Hall	1
Republic Aviation Fairchild Hiller Corporation Farmington, Long Island New York		1
General Dynamics/Convair P.O. Box 1128 San Diego, California 92112 Attn: Library	Frank Dore	1
Missiles and Space Systems Center General Electric Company Valley Forge Space Technology Center P.O. Box 8555 Philadelphia, Pa. 19101 Attn: Library		1
Grumman Aircraft Engineering Corporation Bethpage, Long Island, New York Attn: Library	Joseph Gavin	1
Hercules Powder Company Allegheny Ballistics Laboratory P.O. Box 210 Cumberland, Maryland 21501 Attn: Library		1

Recipient	Designee	No. Copies
Honeywell, Inc. Aerospace Division 2600 Ridgeway Road Minneapolis, Minnesota Attn: Library		1
IIT Research Institute Technology Center Chicago, Illinois 60616 Attn: Library	C. K. Hersh	1
Kidde Aerospace Division Walter Kidde & Company, Inc. 567 Main Street Belleville, New Jersey 07109	R. J. Hanville	1
Ling-Temco-Vought Corporation P.O. Box 5907 Dallas, Texas 75222 Attn: Library		1
Lockheed Missiles and Space Company P.O. Box 504 Sunnyvale, California 94087 Attn: Library		1
Lockheed Propulsion Company P.O. Box 111 Redlands, California 92374 Attn: Library	H. L. Thackwell	1
Marquardt Corporation 16555 Saticoy Street Box 2013 - South Annex Van Nuys, California 91409	L. R. Bell Jr.	1
Martin-Marietta Corporation (Baltimore Division) Baltimore, Maryland 21203 Attn: Library		1
Denver Division Martin-Marietta Corporation P.O. Box 179 Denver, Colorado 80201 Attn: Library	Dr. Morganthaler	1

Recipient	Designee	No. Copies
Orlando Division Martin-Marietta Corporation Box 5827 Orlando, Florida Attn: Library	J. Fern	1
Western Division McDonnell Douglas Astronautics 5301 Bolsa Ave. Huntington Beach, California 92647 Attn: Library	R. W. Hallet G. W. Burge P. Klevatt	1
McDonnell Douglas Aircraft Corporation P.O. Box 516 Lambert Field, Missouri 63166 Attn: Library	R. A. Herzmark	1
Rocketdyne Division North American Rockwell, Inc. 6633 Canoga Avenue Canoga Park, California 91304 Attn: Library, Department 596-306	R. R. J. Thompson S. F. Jacobellis	1
Space & Information Systems Division North American Rockwell 12214 Lakewood Blvd. Downey, California Attn: Library		1
Northrop Space Laboratories 3401 West Broadway Hawthorne, California Attn: Library	Dr. William Howard	1
Purdue University Lafayette, Indiana 47907 Attn: Library (Technical)	Dr. Bruce Reese	1
Rocket Research Corporation Willow Road at 116th Street Redmond, Washington 98052 Attn: Library	F. McCullough, Jr.	1
Stanford Research Institute 333 Ravenswood Avenue Menlo Park, California 94025 Attn: Library	Dr. Gerald Marksman	1

Recipient	Designee	No. Copies
Thiokol Chemical Corporation Redstone Division Huntsville, Alabama Attn: Library	John Goodloe	1
TRW Systems, Inc. 1 Space Park Redondo Beach, California 90278 Attn: Tech. Lib. Doc. Acquisitions	D. H. Lee	1
TRW TAPCO Division 23555 Euclid Avenue Cleveland, Ohio 44117	P. T. Angell	1
United Aircraft Corporation Corporation Library 400 Main Street East Hartford, Connecticut 06108 Attn: Library		1
United Aircraft Corporation Pratt & Whitney Division Florida Research & Development Center P.O. Box 2691 West Palm Beach, Florida 33402 Attn: Library	R. J. Coar Dr. Schmitke	1
United Aircraft Corporation United Technology Center P.O. Box 358 Sunnyvale, California 94038 Attn: Library	Dr. David Altman	1
Vickers Incorporated Box 302 Troy, Michigan		1
Vought Astronautics Box 5907 Dallas, Texas Attn: Library		1